Time Domain Fast-Multipole Translation for Ambisonics

Diploma thesis

Ralf
Baumgartner

Supervision: DI. Dr. Franz Zotter
Assessor: o.Univ.-Prof. Mag. DI. Dr. Robert Höldrich

Graz, June 8, 2011

kunst uni graz

institut für elektronische musik und akustik

Abstract

Representation and reproduction of sound fields is a dedicated goal in electro acoustics and acoustics. There arise more and more possibilities to make sound sources and their emitted acoustic fields audible in a realistic way especially due to modern sound reproduction methods like Ambisonics and Wave Field Synthesis. One important aspect of this field of research is the auralization of directional sound sources. If such a source moves and rotates in space, the resulting tonal changes can be described as proper translation terms. In Ambisonics these operations are expressed as filter matrices.

The aim of this work is the implementation and stabilization of these filter matrices in the time domain with regard to real time applications. The implementation of these translation filters could pave the way to further applications for broad band acoustic sound field simulations.

Thus the displacement of sound sources is stated in this thesis as a matrix, composed by nearly stable and time discrete IIR-filters, which are determined analytically directly out of the theoretical basics. The emerging filters are designed for playback of multi channel directivity data of sound sources with a multi channel Ambisonics surround loudspeaker setup. Additionally, strategies for translation of incident acoustic fields in combination with possibilities for stabilization of the developed filters are a part of this work.

Zusammenfassung

Die Beschreibung und Reproduktion von Schallfeldern ist das erklärte Ziel in Akustik und Elektroakustik. Vor allem durch moderne Reproduktionsverfahren wie Ambisonics und Wellenfeldsynthese ergeben sich immer mehr Möglichkeiten, Schallquellen und deren emittierte Felder realitätsnah hörbar zu machen. Ein wichtiger Aspekt innerhalb dieser Bestrebungen ist die Auralisierung von gerichteten Schallquellen. Bewegt oder dreht sich eine solche Quelle im Raum, können die resultierenden Unterschiede im Klangbild durch geeignete Verschiebungsvorschriften nachgebildet werden. In Ambisonics werden diese Operationen mit Hilfe von Filtermatrizen durchgeführt.

Im Hinblick auf eine Echtzeitrealisierung ist es Ziel dieser Arbeit, diese Filtermatrizen im Zeitbereich zu implementieren und zu stabilisieren. Von diesen Verschiebungsvorschriften erwartet man sich zukünftige Anwendungen bei der breitbandigen Simulation akustischer Schallfelder.

So beschreibt diese Arbeit die Verschiebung von Schallquellen als eine Matrix aus beinahe stabilen, zeitdiskreten IIR-Filtern, die direkt aus den theoretischen Zusammenhängen hergeleitet werden. Diese Filter sind für eine Wiedergabe mehrkanaliger, holografischer Aufnahmen von Schallquellen mit einem mehrkanaligen Ambisonics Surround-Lautsprechersystem entworfen. Als Teil der Arbeit wird zusätzlich auf Verschiebungsstrategien für einfallenden Schall und Betrachtungen zur Stabilisierung der entworfenen Filterstrukturen eingegangen.

Acknowledgements

This thesis states the end of an intense and exciting time. Throughout the years of study there were a lot of people who made this time possible and who shared their knowledge with me. Thus I want to grab the chance to thank these people for their help.

Especially I want to thank Franz Zotter for being a superb advisor of this thesis who always had a sympathetic ear for all kind of questions and problems. His competence and enthusiasm were and are a perpetual motivation.

Furthermore I want to thank my parents Anita and Richard for their encouragement and support throughout the years and for making all the things in my live possible. Thank you Robert.

Thank you Dorothea for your love, patience and support.

Thanks to my friends and fellow students for a terrific time. I hope we'll stay in touch!

Thank You!

Contents

1 Introduction **1**

1.1 Radial Steering Filters 1

1.2 Motivation 2

1.3 Preview of thesis 3

2 Wave Field Description in Spherical Coordinates **4**

2.1 The Helmholtz Equation 4

2.2 Spherical Wave Expansion 5

2.2.1 Spectra and Spherical Basis Functions 11

2.3 Vector and Matrix Notation 11

2.4 Synoptic View 14

3 Coordinate Transforms **18**

3.1 Re-expansion over Spherical Basis Functions 18

3.2 Rotation 22

3.2.1 Rotation Coefficients 23

3.3 Coaxial Translation 26

3.3.1 Coaxial Translation Coefficients 26

3.4 Truncation of Expansion 31

4 Coaxial Translation in Time Domain **33**

4.1 Singular to Regular Translation 33

4.1.1 Combination of Translation and Distance Coding Filters 35

4.1.2 Single Pole Compensation 39

4.1.3 Integration of Radial Steering Filters 40

4.1.4 Parameter Optimization 41
4.2 Singular to Singular or Regular to Regular Translations 45
4.2.1 Moving Average Approach 45
4.2.2 Time Reversal Approach 48

5 Conclusion and Outlook **52**
5.1 Time Domain Simulation 52
5.2 Future Work 54

A Derivation of Zero Order Spherical Bessel Filter in Z-Domain **55**

B Spherical Bessel Filter **56**

C Corrected Impulse Invariance Method Applied on Hankel Filters **63**

D Spherical Bessel Filter in z-Domain **65**

1 Introduction

The perception of natural sound sources is dependent on the orientation and the distance between the source and the listener as well as on the interaction of the emitted sound wave with the surroundings. Thus the resulting sound impression for the listener is strongly conditioned by the frequency dependent directivity patterns of the source.

As a consequence, to record and, if necessary, to reproduce the emitted acoustic field of a sound source it is obvious, that every radiation direction has to be taken into account. For instance a live played musical instrument in an arbitrary room has got completely different properties than the same instrument recorded by one microphone and played back with a loudspeaker in the same surrounding. Even if the microphone and the loudspeaker do not introduce timbral changes and are both oriented towards the listener, the complex frequency dependent directivity patterns of the instrument can not be covered adequately so that the room responses might differ tremendously between the live situation and the reproduced one.

Therefore, several recording and reproduction methods with microphone and loudspeaker arrays were developed recently. Especially for natural sound sources like musical instruments, the usage of spherical geometries seems most appropriate to describe the radiation and propagation of acoustic fields. Hence, this thesis is limited to solutions and applications in spherical coordinates. The required mathematical basics are stated in a variety of literatur e.g. [Wil99], [GD04] and [Zot09].

For the purpose of recording emitted fields a spherical microphone array was developed in the master thesis of Fabian Hohl [Hoh09]. Peter Plessas investistigated and evaluated several designes of microphone arrays for recording and decomposition of incident fields [Ple10]. Michael Kerscher made a compact, spherical loudspeaker array for the reproduction of recorded sources with the associated directivity patterns [Ker10]. Related efforts can be found in [Pol07]. For the reproduction of surrounding sound scenes Zmölnig derived in his master thesis design methods for the installation of live sound reinforcement applications like the "Cube" at the Institute of Electronic Music and Acoustic (Graz) [Zmo00]. Moreover, further studies in periphonic sound field reproduction methods for binaural synthesis were carried out in [Son03] and [MN02].

1.1 Radial Steering Filters

In order to reproduce a certain directivity pattern at an arbitrary radius with one of the referred loudspeaker arrays, one has to compensate the changes of the acoustic field due to the radial propagation away from the source.

Pomberger has realized this compensation in his master thesis [Pom08] in the z-domain. The results are nearly stable discrete time domain filters, so that the signals of each loudspeaker in the array can be filtered appropriately to synthesize the desired pattern at the given distance.

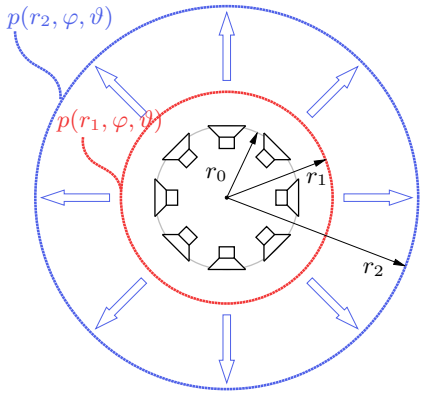

Figure 1 – Compact spherical loudspeaker array for synthesizing pressure patterns. A distinct directivity pattern at r_1 can be projected to r_2 by filtering the driving signals of the speakers by radial steering filters (cf. [Pom08]).

Generally with these, so-called, "radial steering filters" or "holography filters", it is possible to calculate an acoustic field at an arbitrary radius r_2 with the knowledge of the properties of the field at another radius r_1 as illustrated in figure 1.

1.2 Motivation

For realistic reproduction of acoustic sound fields with loudspeaker arrays or by binaural synthesis there are no possibilities up to now to realize movements and rotations (around arbitrary axes) of virtual sound sources or effects of shadowing and reflection by virtual objects placed between the source and the listener in real time. The derivation of the required time domain filters to instantiate these processes is the main issue in this work and will thereby continue the research of Menzies, who studied the basic behaviour of these filters in frequency domain [Men07].

The achieved filters will not only be useful for sound field reproduction as mentioned above. Boundary element methods, which are used so far for intricate sound field simulations will be able to be replaced with new simulation methods in time domain with the help of these filters. Main advantages over conventional numerical methods, which are carried out in the frequency domain, of so-called "Fast Multipole Methods" in time domain are an expected reduction of computing time and resources as well as the fact of an inherent broad band simulation.

1.3 Preview of thesis

Chapter 2 - Wave Field Description in Spherical Coordinates

Beginning with the general wave equation the decomposition of sound fields into angular and radial eigenfunctions in a spherical coordinate system will be briefly presented. Hereby, the eigenfunctions will be discussed which are solutions of the wave equation and their properties are shown. Concluding this chapter, a short overview of an ambisonic system described by the developed basis- or eigenfunctions will be given.

Chapter 3 - Coordinate Transforms

Based on Chapter 2, translations and rotations of an acoustic sound field, decomposed in the spherical basis functions, will be outlined and efficient calculation methods for both, displacement and rotation, will be presented. Moreover a valuation of the error, depending on the truncation order of the ideally infinite series of basis functions is provided.

Chapter 4 - Coaxial Translation in Time Domain

This chapter presents the time domain realizations of the derived translation methods. At first, a solution to implement the originally unstable translation filters for a singular to regular translation by a reasonable restructuring of the signal path and a parameter optimization will be given. Secondly different time domain realizations of regular to regular or singular to singular translations will be discussed.

Chapter 5 - Conclusion and Outlook

Finally, a short summary of the achievements in this work is given and a basic sound field simulation of a translated source in an Ambisonics sytem with the derived filters in time domain is presented. Morover an outview and perspectives for future applications will be given.

2 Wave Field Description in Spherical Coordinates

For a better understanding of translation methods this chapter provides a brief overview of the theoretical basics of sound field representation and the wave expansion in spherical coordinates. Due to the choice of spherical geometry most of real sound sources can be modeled more accurately than in other coordinate systems. The derivations mainly follow the explanations of [Wil99], [GD04] and [Zot09].

2.1 The Helmholtz Equation

In general the Helmholtz equation is used to describe potential fields. In acoustics, this partial differential equation of second order is defined in the frequency domain as

$$\nabla^2 p(\boldsymbol{r}) + k^2 p(\boldsymbol{r}) = -q(\boldsymbol{r}) \tag{2.1}$$

with $p(\boldsymbol{r})$ representing the potential field and k the wave number $k = \frac{\omega}{c}$. The right hand side of the term, $q(\boldsymbol{r})$, describes the spatial distribution of sources in the case of an inhomogenous field. If $q(\boldsymbol{r})$ is zero an homogenous field (source free) is given. The behavior of acoustic wave fields referred to pressure p and particle velocity v constitutes the solutions of the Helmholtz equation in the coordinate system. The transformation of cartesian (x, y, z) to the used spherical coordinate system (r, ϑ, φ) is given by

$$\boldsymbol{r} = \begin{pmatrix} x \\ y \\ z \end{pmatrix} = r\boldsymbol{\theta} = r \begin{pmatrix} \cos(\varphi)\sin(\vartheta) \\ \sin(\varphi)\sin(\vartheta) \\ \cos(\vartheta) \end{pmatrix}, \tag{2.2}$$

where the angles φ and ϑ are called azimuth and zenith angle and are limited to $0 \leq \varphi \leq 2\pi$ respectively $0 \leq \vartheta \leq \pi$.

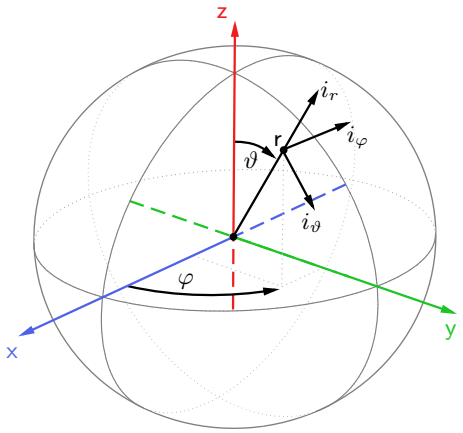

Figure 2 – Cartesian and spherical coordinate systems.

The vectors $\boldsymbol{i}_\varphi$,$\boldsymbol{i}_\vartheta$ and $\boldsymbol{i}_r$ are the orthonormal basis of the spherical coordinate system. Executing the Laplace operator $\triangle = \nabla^2$ of eq. (2.1) in consideration of spherical coordinates, the homogenous wave equation can be written as

$$\frac{1}{r^2}\frac{\partial}{\partial r}\Big(r^2\frac{\partial p}{\partial r}\Big) + \frac{1}{r^2\sin\vartheta}\frac{\partial}{\partial\vartheta}\Big(\sin\vartheta\frac{\partial p}{\partial\vartheta}\Big) + \frac{1}{r^2\sin^2(\vartheta)}\frac{\partial^2 p}{\partial\varphi^2} - \frac{1}{c^2}\frac{\partial^2 p}{\partial t^2} = 0\ . \tag{2.3}$$

Equation (2.3) can be solved with the product ansatz and separation of variables

$$p(\boldsymbol{r}) = R(kr)\Phi(\varphi)\Theta(\vartheta)T(t), \tag{2.4}$$

which leads to following decoupled differential terms:

$$\begin{pmatrix} \frac{\mathrm{d}^2}{\mathrm{d}(kr)^2}(kr)^2R(kr) + \big((kr^2) - n(n+1)\big)R(kr) \\ \frac{\mathrm{d}^2}{\mathrm{d}\varphi^2}\Phi(\varphi) + m^2\Phi(\varphi) \\ \frac{\mathrm{d}}{\mathrm{d}\mu}\big(\frac{1}{1-\mu^2}\frac{\mathrm{d}}{\mathrm{d}\mu}\Theta(\cos(\mu))\big) + \big(n(n+1) - \frac{m^2}{1-\mu^2}\big)\Theta(\cos(\mu)) \\ \frac{1}{c^2}\frac{\mathrm{d}^2T}{\mathrm{d}t^2} + k^2T \end{pmatrix} = \begin{pmatrix}0\\0\\0\\0\end{pmatrix}. \tag{2.5}$$

The time dependent solution can be obtained by

$$T(\omega) = Te^{i\omega t}. \tag{2.6}$$

The next sections review the different solutions of the angular and radial terms and their behavior.

2.2 Spherical Wave Expansion

On closer inspection of the differential equations (2.5), one can see
– a linear differential equation for Φ
– a Legendre associated one in Θ-direction
– and a Bessel differential equation for the radial components.
So the set of mathematical possibilities for solving the wave equation are

$$\begin{aligned}\Phi(\varphi) =& \Phi_m(\varphi) = \{\sin(m\varphi), \cos(m\varphi)|e^{\pm im\varphi}\},\\ \Theta(\vartheta) =& \Theta_n^m(\vartheta) = \{P_n^m(\mu), Q_n^m(\mu)\},\\ R(kr) =& R_n(kr) = \{j_n(kr), y_n(kr)|h_n^{(1)}(kr), h_n^{(2)}(kr)\}.\end{aligned}$$

In acoustics, not all of these functions are reasonable solutions of the problem. With realistic assumptions some of them can be rejected as illustrated in the following.

Azimuth angle:
For the azimuth the selection of the solution is arbitrarily. Thus one can describe the azimuth dependent characteristics in real or complex notation

$$\begin{aligned}\Phi(\varphi) &= \{\sin(m\varphi), \cos(m\varphi)|\cancel{e^{\pm im\varphi}}\}\\ &= \cancel{\{\sin(m\varphi), \cos(m\varphi)|}e^{\pm im\varphi}\}.\end{aligned}$$

With regard to the 2π-periodicity of $\Phi(\varphi)$, m must be an integer to maintain the required continuity.

Zenith angle:
For the elevation the Legendre functions of the second kind $Q_n^m(\mu)$ can be rejected because of their singularity at $\mu = \cos(\vartheta) = \pm 1$.

$$\Theta(\vartheta) = \Theta_n^m(\vartheta) = \{P_n^m(\mu), \cancel{Q_n^m(\mu)}\} \tag{2.7}$$

The residual functions can be calculated on the basis of unassociated Legendre polynomials $P_n(\mu) \stackrel{\text{def}}{=} P_n^0(\mu)$ which can be defined with the so called Rodrigues Formula:

$$P_n(\mu) = \frac{1}{2^n n!} \frac{\mathrm{d}^n}{\mathrm{d}\mu^n} (\mu^2 - 1)^n. \tag{2.8}$$

A noteworthy property of these orthogonal terms is

$$P_n(-\mu) = (-1)^n P_n(\mu). \tag{2.9}$$

Examples of the first five orders are depicted in figure (3). The associated functions

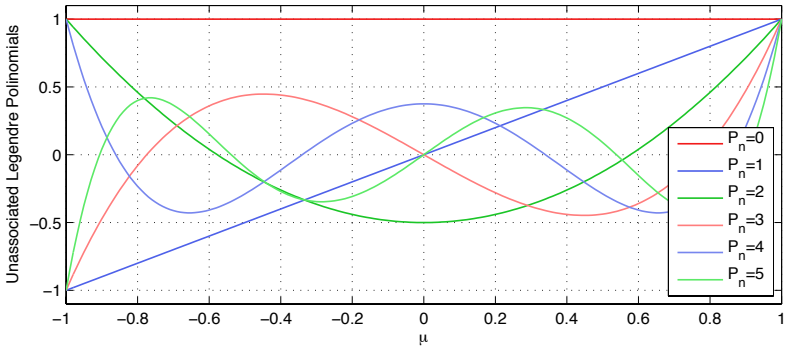

Figure 3 – Unassociated Legendre Polynomials up to the order $n = 5$.

are defined by two integers, order n and degree m and can be calculated initially by the formula

$$P_n^m(\mu) = (-1)^m (1 - \mu^2)^{m/2} \frac{\mathrm{d}^m}{\mathrm{d}\mu^m} P_n(\mu). \tag{2.10}$$

To avoid a divergency of the associated Legendre functions of the first kind, n has to be an integer, too. Moreover, it can be mentioned, that $P_n^m(\mu) = 0$ for $m > n$ if m and n are integers. In practice recurrence relations can be used to get higher order functions.

Some of them are stated below.

$$(2n+1)\mu P_n^m(\mu) = (n-m+1)P_{n+1}^m(\mu) + (n+m)P_{n-1}^m(\mu) \tag{2.11}$$

$$P_n^{m+2}(\mu) = -2(m+1)\frac{\mu}{\sqrt{1-\mu^2}}P_n^{m+1}(\mu) - (n-m)(n+m+1)P_n^m(\mu) \tag{2.12}$$

$$P_{n-1}^m(\mu) - P_{n+1}^m(\mu) = (2n+1)\sqrt{1-\mu^2}P_n^{m-1}(\mu) \tag{2.13}$$

$$P_{-n-1}^m(\mu) = P_n^m(\mu) \tag{2.14}$$

Spherical Harmonics:
For convenience, both angular solutions are combined in so-called spherical harmonics which depend on φ and ϑ. So the real or complex valued spherical harmonics with order n and degree m can be written as

$$Y_n^m(\boldsymbol{\theta}) \stackrel{\text{def}}{=} N_n^{|m|}\Theta_n^{|m|}(\vartheta)\Phi_m(\varphi) \tag{2.15}$$

$$= N_n^{|m|}P_n^{|m|}(\cos(\vartheta)) \begin{cases} \sin(m\varphi), \text{ for } m < 0\ , \\ \cos(m\varphi), \text{ for } m \geq 0\ , \end{cases} \quad \text{real valued}$$

$$\text{or}$$

$$e^{\pm im\varphi}, \quad \text{complex valued.}$$

They are zero for all $|m| \leq n$ because of the behavior of Legendre polynomials as mentioned above.

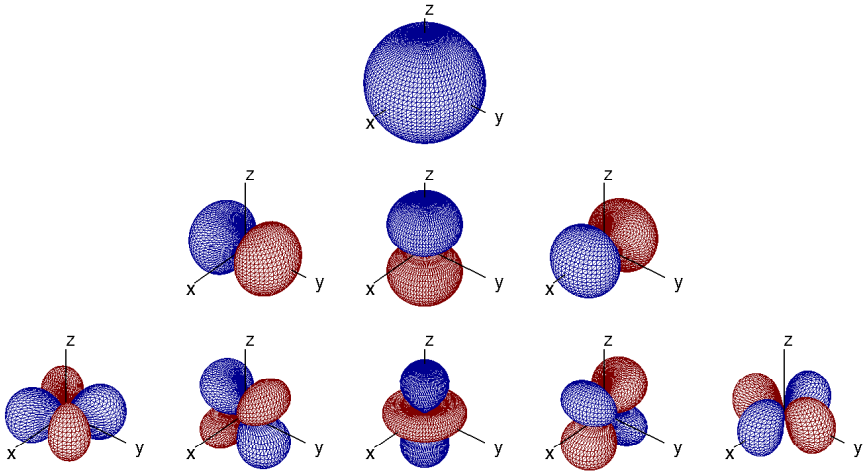

Figure 4 – Real valued spherical harmonics up to the order $n = 2$ ([Deb10]).

Scalar normalization constant:
With the used scalar normalization constant - dependent on the unit vector $\boldsymbol{\theta}$ - defined as [ZP11]

$$N_n^m = N_n^{|m|} := \sqrt{\frac{(2-\delta_m)}{4\pi}\frac{(n-|m|)!}{(n+|m|)!}}, \tag{2.16}$$

the spherical harmonics describe the complete angular part of the orthonormal basis of the spherical coordinate system and can be interpreted as spherical eigenfunctions or modes. Their orthogonality can be proofed by a product of Kronecker Deltas:

$$\int_{\mathbb{S}^2} Y_n^m(\boldsymbol{\theta}) Y_{n'}^{m'}(\boldsymbol{\theta})^* d\boldsymbol{\theta} = \delta_{nn'}\delta_{mm'}.$$

Spherical Bessel functions:
Different solutions of the Bessel differential equation for radial components of expanding acoustic wave fields are the spherical Bessel functions of the first kind

$$j_n(kr) \begin{cases} = (-1)^n (kr)^n \left(\frac{\mathsf{d}}{kr\mathsf{d}(kr)}\right)^n \frac{\sin(kr)}{kr} \\ = (\frac{\pi}{2kr})^{1/2} J_{n+1/2}(kr) \\ \approx \frac{(kr)^n}{(2n+1)!!}(1 - \frac{(kr)^2}{2(2n+3)} + ...) \end{cases} \tag{2.17}$$

and of the second kind, also called Neumann functions

$$y_n(kr) \begin{cases} = -(-1)^n (kr)^n \left(\frac{\mathsf{d}}{kr\mathsf{d}(kr)}\right)^n \frac{\cos(kr)}{kr} \\ = (\frac{\pi}{2kr})^{1/2} Y_{n+1/2}(kr) \\ \approx -\frac{(2n-1)!!}{(kr)^{n+1}}(1 - \frac{(kr)^2}{2(1-2n)} + ...). \end{cases} \tag{2.18}$$

J_n and Y_n are representing cylindrical harmonics also called cylindrical Bessel functions of first and second kind. The first few orders of these (j_n,y_n) functions are illustrated in fig. (5). Because of the singularity of $y_n(kr)$ for $kr = 0$, which is not reasonable in a practical point of view - there can not be any singularities in a homogenous field- these solutions can be rejected.

Spherical Hankel functions:
Moreover, the linear combination of the latter functions are solutions, too. They are called spherical Bessel functions of the third kind or Hankel functions of first and second kinds and are defined as

$$h_n^{(2)}(kr) \begin{cases} = h_n^{(1)*}(kr) \\ = j_n(kr) - iy_n(kr) \\ = (-i)^n \frac{e^{-ikr}}{(ikr)^{n+1}} \sum_{l=0}^{n} \frac{(n+l)!}{l!(n-l)!2^l}(ikr)^{n-l} \\ \approx \frac{1}{kr} \quad \text{for} \quad kr \gg \frac{n(n+1)}{2}. \end{cases} \tag{2.19}$$

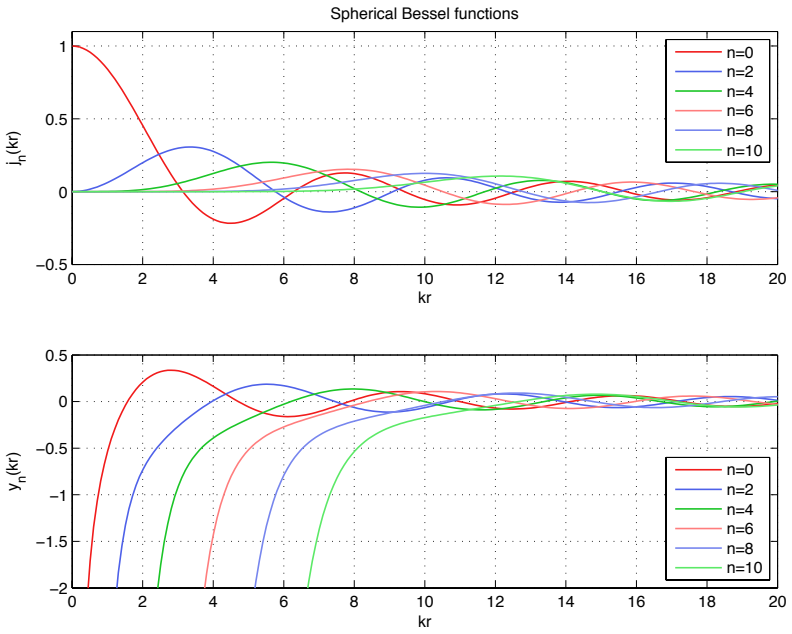

Figure 5 – Spherical Bessel functions $j_n(kr)$ and $y_n(kr)$

Regarding Sommerfeld's radiation condition

$$\lim_{r\to\infty}\left(-\frac{i\rho_0 cp(kr)}{\frac{\partial}{\partial(kr)}p(kr)}\right)=\rho_0 c, \tag{2.20}$$

$$\lim_{r\to\infty} r\left(\frac{\partial}{\partial(kr)}+ik\right)p(kr)=0, \tag{2.21}$$

which requires the impedance of a radiated wave field to converge to $z_0 = \rho_0 c$ at infinity, only the Hankel functions of the second kind are feasible terminations. Due to their singularity at $kr = 0$ and their regularity for exceeding arguments they represent all exterior or outgoing boundary problems. Some useful recurrence relations for calculating Bessel functions whatever kinds and for arbitrary arguments ζ denoted with $f_n(\zeta)$ can be given as

$$f_{n-1}(\zeta)+f_{n+1}(\zeta)=\frac{2n+1}{(\zeta)}f_n(\zeta), \tag{2.22}$$

$$nf_{n-1}(\zeta)-(n+1)f_{n+1}(\zeta)=(2n+1)f_n'(\zeta), \tag{2.23}$$

$$\frac{n+1}{(\zeta)}f_n(\zeta)+f_n'(\zeta)=f_{n-1}(\zeta), \tag{2.24}$$

$$\frac{n}{(\zeta)}f_n(\zeta)-f_n'(\zeta)=f_{n+1}(\zeta). \tag{2.25}$$

The prime specifies the first derivative with respect to the argument.

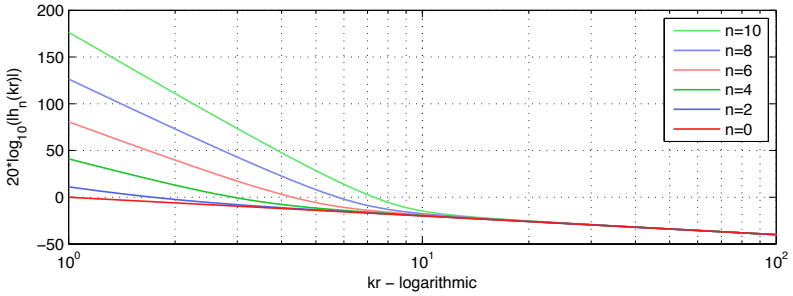

Figure 6 – Magnitude of spherical Hankel functions of the second kind $h_n^{(2)}(kr)$

Spherical wave spectrum:
As commonly done in signal processing, where time signals are analyzed and synthesized with a Fourier transform with the kernel $e^{\pm i\omega t}$, one can decompose every function on a sphere using a so-called spherical harmonics transform. So it is possible to specify - equivalent to a Fourier transform - an expansion with the kernel $Y_n^m(\boldsymbol{\theta})$ of a continuous distribution $g(\boldsymbol{\theta})$ on a unit sphere $\boldsymbol{\theta}$:

$$\mathcal{SHT}\{g(\boldsymbol{\theta})\} = \int_{\mathbb{S}^2} f(\boldsymbol{\theta}) Y_n^m(\boldsymbol{\theta}) d\boldsymbol{\theta} = \gamma_{nm}(\boldsymbol{\theta}), \tag{2.26}$$

$$\mathcal{ISHT}\{\gamma_{nm}(\boldsymbol{\theta})\} = \sum_{n=0}^{\infty} \sum_{m=-n}^{n} \gamma_{nm}(\boldsymbol{\theta}) Y_n^m(\boldsymbol{\theta}) = g(\boldsymbol{\theta}). \tag{2.27}$$

Spherical wave spectra found in the sound field are denoted as $\gamma_{nm}(\boldsymbol{\theta})$ when the sound pressure $p(\boldsymbol{\theta})$ is regarded and as $\nu_{nm}(\boldsymbol{\theta})$ when regarding sound particle velocity $v(\boldsymbol{\theta})$. Note that the spherical wave spectra $\psi_{nm}(\boldsymbol{\theta})$ and $\nu_{nm}(\boldsymbol{\theta})$ depend on the radial weighting by spherical Hankel and Bessel functions, which is due to the product ansatz. In fact, the spherical wave spectrum is composed of the product of the wave spectral coefficients and the radial solutions. The expanded sound pressure is

$$p(kr, \boldsymbol{\theta}) = \sum_{n=0}^{\infty} \sum_{m=-n}^{n} \psi_{nm}(kr, \boldsymbol{\theta}) Y_n^m(\boldsymbol{\theta}). \tag{2.28}$$

Wave spectrum:
These coefficients (here b_{nm} and c_{nm}) are denoted as wave spectra of the incident and radiating sound fields, which are expanded into the spherical wave spectrum of pressure and velocity using following expressions.

$$\psi_{nm}(kr) = b_{nm} j_n(kr) + c_{nm} h_n^{(2)}(kr) \tag{2.29}$$

$$\nu_{nm}(kr) = \frac{i}{\rho c}\left(b_{nm} j_n'(r) + c_{nm} h_n'^{(2)}(kr)\right) \tag{2.30}$$

2.2.1 Spectra and Spherical Basis Functions

Spherical basis functions are a combination of the radial weighting functions with the corresponding spherical harmonics. So a complete set of formulas and different descriptions of the $\mathcal{SHT}$ can be stated

$$\mathcal{SHT}\{p(kr,\boldsymbol{\theta})\} = \int_{\mathbb{S}^2} p(kr,\boldsymbol{\theta}) Y_n^m(\boldsymbol{\theta}) d\boldsymbol{\theta} = \psi(kr,\boldsymbol{\theta}), \tag{2.31}$$

$$p(kr,\boldsymbol{\theta}) = \sum_{n=0}^{\infty} \sum_{m=-n}^{n} [b_{nm} j_n(kr) + c_{nm} h_n^{(2)}(kr)] Y_n^m(\boldsymbol{\theta}) \tag{2.32}$$

$$= \sum_{n=0}^{\infty} \sum_{m=-n}^{n} [b_{nm} R_n^m(kr,\boldsymbol{\theta}) + c_{nm} S_n^m(kr,\boldsymbol{\theta})]. \tag{2.33}$$

The nomenclature of the basis functions $R_n^m(kr,\boldsymbol{\theta})$ and $S_n^m(kr,\boldsymbol{\theta})$ are because of their regular or singular behavior due to the characteristics of the involved Hankel and Bessel functions. R_n^m are thereby used for interior and S_n^m for exterior problems and fields.

2.3 Vector and Matrix Notation

For convenience, a vector and matrix notation of latter formulations can be established. Therefore the following conventions, according to [Zot09], are used:

Wave spectrum
Assume any wave spectrum $e_{nm} = \{b_{nm}|c_{nm}\}$, the coefficients $0 \leq n \leq N_t$ can be combined in a vector $\boldsymbol{e}_{N_t}$.

$$\boldsymbol{e}_{N_t} := \Big(e_{0,0} \ , \ e_{1,-1} \ , \ e_{1,0} \ , \ \ldots, \underbrace{e_{n,-n} \ , \ \ldots \ , \ e_{n,n}}_{2n+1} \ , \ \ldots \ , \ e_{N_t,N_t} \Big)^T \tag{2.34}$$

If $\boldsymbol{e}_{N_t}$ is independent of m the vector can be notated as follows (2.35).

$$\boldsymbol{e}_{N_t} := \Big(e_0 \ , \ e_1 \ , \ e_1 \ , \ \ldots, \underbrace{e_n \ , \ \ldots \ , \ e_n}_{2n+1} \ , \ \ldots \ , \ e_{N_t} \Big)^T \tag{2.35}$$

It can be useful to define a secondary coefficient vector for a specific m and all appendant n:

$$\boldsymbol{e}_{N_t}^m := \Big(e_{|m|,m} \ , \ e_{|m|+1,m} \ , \ e_{|m|+2,m} \ , \ \ldots \ , \ e_{N_t,m} \Big)^T. \tag{2.36}$$

Spherical Hankel and Bessel functions

At the beginning a vector of spherical Hankel or Bessel functions can be defined like in (2.34) as

$$\boldsymbol{j}_{N_t}(kr) = := \Big(j_0 \ , \ j_1 \ , \ j_1 \ , \ j_1 \ , \ \dots \ , \ \underbrace{j_n \ , \ \dots \ , \ j_n}_{2n+1} \ , \ \dots \ , \ j_{N_t}\Big)^T,$$

$$\boldsymbol{h}_{N_t}(kr) = := \Big(h_0 \ , \ h_1 \ , \ h_1 \ , \ h_1 \ , \ \dots \ , \ \underbrace{h_n \ , \ \dots \ , \ h_n}_{2n+1} \ , \ \dots \ , \ h_{N_t}\Big)^T. \tag{2.37}$$

The radial solutions can be embraced in diagonal matrices as

$$\boldsymbol{J}_{N_t}(kr) = diag\{\boldsymbol{j}_n(kr)\} := \begin{pmatrix} j_0(kr) & 0 & 0 & 0 & 0 & \cdots & 0 \\ 0 & j_1(kr) & 0 & 0 & 0 & \cdots & 0 \\ 0 & 0 & j_1(kr) & 0 & 0 & \cdots & 0 \\ 0 & 0 & 0 & j_1(kr) & 0 & \cdots & 0 \\ 0 & 0 & 0 & 0 & j_2(kr) & \cdots & 0 \\ \vdots & \vdots & \vdots & \vdots & \vdots & \ddots & \vdots \\ 0 & 0 & 0 & 0 & 0 & \cdots & j_{N_t}(kr) \end{pmatrix},$$

$$\boldsymbol{H}_{N_t}(kr) = diag\{\boldsymbol{h}_n(kr)\} := \begin{pmatrix} h_0(kr) & 0 & 0 & 0 & 0 & \cdots & 0 \\ 0 & h_1(kr) & 0 & 0 & 0 & \cdots & 0 \\ 0 & 0 & h_1(kr) & 0 & 0 & \cdots & 0 \\ 0 & 0 & 0 & h_1(kr) & 0 & \cdots & 0 \\ 0 & 0 & 0 & 0 & h_2(kr) & \cdots & 0 \\ \vdots & \vdots & \vdots & \vdots & \vdots & \ddots & \vdots \\ 0 & 0 & 0 & 0 & 0 & \cdots & h_{N_t}(kr) \end{pmatrix}. \tag{2.38}$$

Spherical Wave Spectrum

The resulting spherical wave spectra can be stated

$$\boldsymbol{\psi}_{N_t}(kr) = \boldsymbol{J}_{N_t}(kr)\boldsymbol{b}_{N_t} + \boldsymbol{H}_{N_t}(kr)\boldsymbol{c}_{N_t} = \begin{pmatrix} \boldsymbol{\psi}_{0,0}(kr) \\ \boldsymbol{\psi}_{1,-1}(kr) \\ \boldsymbol{\psi}_{1,0}(kr) \\ \vdots \\ \left.\begin{matrix} \boldsymbol{\psi}_{n,-n}(kr) \\ \vdots \\ \boldsymbol{\psi}_{n,n}(kr) \end{matrix}\right\} \ 2n+1 \\ \vdots \\ \boldsymbol{\psi}_{N_t,N_t}(kr) \end{pmatrix},$$

$$\boldsymbol{\nu}_{N_t}(kr) = \frac{\mathrm{i}}{\rho_0 c}\left(\boldsymbol{J}'_{N_t}(kr)\boldsymbol{b}_{N_t} + \boldsymbol{H}'_{N_t}(kr)\boldsymbol{c}_{N_t}\right) = \begin{pmatrix} \boldsymbol{\nu}_{0,0}(kr) \\ \boldsymbol{\nu}_{1,-1}(kr) \\ \boldsymbol{\nu}_{1,0}(kr) \\ \vdots \\ \left.\begin{matrix} \boldsymbol{\nu}_{n,-n}(kr) \\ \vdots \\ \boldsymbol{\nu}_{n,n}(kr) \end{matrix}\right\} 2n+1 \\ \vdots \\ \boldsymbol{\nu}_{N_t,N_t}(kr) \end{pmatrix}. \tag{2.39}$$

Spherical Harmonics

Spherical harmonics are written in vector notation as

$$\boldsymbol{y}_{N_t}(\boldsymbol{\theta}) := \begin{pmatrix} Y_0^0(\boldsymbol{\theta}) \\ Y_1^{-1}(\boldsymbol{\theta}) \\ Y_1^0(\boldsymbol{\theta}) \\ \vdots \\ \left.\begin{matrix} Y_n^{-n}(\boldsymbol{\theta}) \\ \vdots \\ Y_n^{-n}(\boldsymbol{\theta}) \end{matrix}\right\} 2n+1 \\ \vdots \\ Y_{N_t}^{N_t}(\boldsymbol{\theta}) \end{pmatrix}. \tag{2.40}$$

and for $l = 1, ..., L$ sampling nodes, the spherical harmonics vectors can be combined in a spherical harmonics matrix

$$\boldsymbol{Y}_{N_t} := \begin{pmatrix} \boldsymbol{y}_{N_t}^{(1)^T} \\ \boldsymbol{y}_{N_t 1}^{(2)^T} \\ \vdots \\ \boldsymbol{y}_{N_t}^{(L)^T} \end{pmatrix}. \tag{2.41}$$

2.4 Synoptic View

A brief overview of an Ambisonics system we deal with, from the sampling of a sound source to the auralization, is given and realizations in practice for $\mathcal{SHT}$ and $\mathcal{ISHT}$ are briefly introduced.

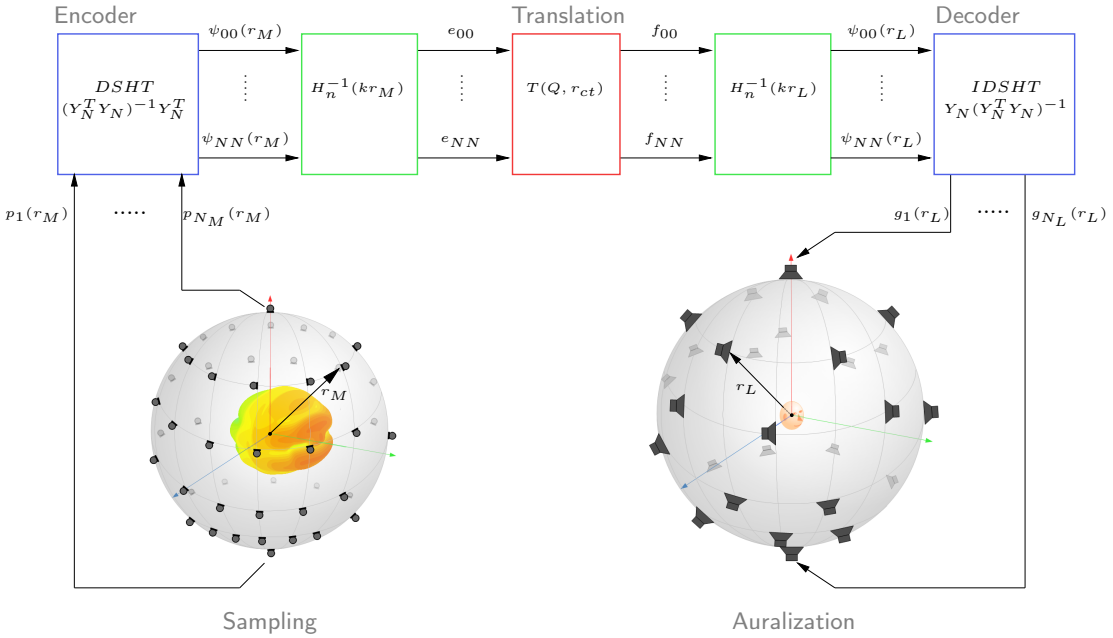

Figure 7 – Block diagram of the whole signal chain, with sampling a sound source, performing spherical harmonic transform, translation and rotation and finally a decoder for calculating driver functions for sound reinforcement.

Analyzing an emitted field:
To encode a natural sound source in ambisonic format (spherical wave spectra) a spatial sampled recording with a multitude of microphones located on a spherical surface has to be performed. In our case, a free outgoing field is desired, so one has to minimize reflections into the surface and thereby a superposition of incident and outgoing waves. With the assumption of an angular band limitation of the directivity of the source the discrete measured pressure distribution $\boldsymbol{p}_N$, defined as

$$\boldsymbol{p}_N := \begin{pmatrix} p(r_M, \varphi_1, \vartheta_1) \\ p(r_M, \varphi_2, \vartheta_2) \\ \vdots \\ p(r_M, \varphi_{N_M}, \vartheta_{N_M}) \end{pmatrix} \tag{2.42}$$

with r_M denoting the radius of the microphone array with the according angles φ_l and

ϑ_l, indexed by the sampling point number l, can be encoded in ambisonics by performing a $\mathcal{SHT}$ (2.26).

$$\boldsymbol{p}_N = \boldsymbol{Y}_N \boldsymbol{\psi}_N, \tag{2.43}$$

$$\boldsymbol{\psi}_N = \boldsymbol{Y}_N^{-1} \boldsymbol{p}_N. \tag{2.44}$$

Depending on the distribution and the number of used microphones (cf. different sampling strategies and spatial aliasing problems [Zot09, Wil99, Deb10]) the inversion of $\boldsymbol{Y}_N$ is not trivial. In almost all practical cases (disregarding hyperinterpolation with extremal sampling points), $\boldsymbol{Y}_N$ is a non-square matrix so that the inverse does not exist. As a consequence the pseudo or left inverse indexed by $\boldsymbol{Y}_N^\dagger$ of the matrix, in Ambisonics called Encoder, is applied. This relates an error minimizing problem [ZP11], matching the original and sampled wave spectra. $J(\boldsymbol{\psi}_N)$ denotes the cost or error function:

$$J(\boldsymbol{\psi}_N) = \|\boldsymbol{p_N} - \boldsymbol{Y}_N \boldsymbol{\psi}_N\|^2 \Rightarrow min, \tag{2.45}$$

$$\frac{\partial}{\partial \boldsymbol{\psi}_N^T} J(\boldsymbol{\psi}_N) = \boldsymbol{Y}_N^T \boldsymbol{p_N} - \boldsymbol{Y}_N^T \boldsymbol{Y}_N \boldsymbol{\psi}_N \stackrel{!}{=} 0, \tag{2.46}$$

$$\boldsymbol{\psi}_N = (\boldsymbol{Y}_N^T \boldsymbol{Y}_N)^{-1} \boldsymbol{Y}_N^T \boldsymbol{p}_N = \boldsymbol{Y}_N^\dagger \boldsymbol{p}_N. \tag{2.47}$$

After encoding and calculating the spherical wave spectrum, the coefficients $\boldsymbol{c}_N$ can be obtained by distance coding $\boldsymbol{H}_N^{-1}(kr)$ (2.48)

$$c_N = \boldsymbol{H}_N^{-1}(kr) \boldsymbol{\psi}_N. \tag{2.48}$$

Reproduction of an incident sound field:
To reproduce a sound field described by the expansion coefficients $\mathbf{f}_N$ for one or more listeners, loudspeakers (real or virtual) are placed on a spherical arrangement with the radius r_L and at discrete angles (φ_L, ϑ_L). For the calculation of the driving functions $\boldsymbol{g}_N$, defined as

$$\boldsymbol{g}_N := \begin{pmatrix} g(r_L, \varphi_1, \vartheta_1) \\ g(r_L, \varphi_2, \vartheta_2) \\ \vdots \\ g(r_L, \varphi_{N_L}, \vartheta_{N_L}) \end{pmatrix} \tag{2.49}$$

$$= (\boldsymbol{Y}_N^T)^{-1} \boldsymbol{\gamma}_N, \tag{2.50}$$

the speakers are modeled as point sources with unity gain. Thus the produced sound field can be described by the inhomogeneous Helmholtz equation with the source-strength distribution

$$\hat{q}(\varphi, \vartheta) = \begin{pmatrix} \delta(\varphi - \varphi_1)\delta(\vartheta - \vartheta_1) \\ \delta(\varphi - \varphi_2)\delta(\vartheta - \vartheta_2) \\ \vdots \\ \delta(\varphi - \varphi_{N_L})\delta(\vartheta - \vartheta_{N_L}) \end{pmatrix}^T \boldsymbol{g}_N. \tag{2.51}$$

The spherical harmonic transform yield

$$\hat{\Phi}_Q = \mathcal{SHT}\{\hat{q}(\varphi, \vartheta)\} = \mathbf{Y}_N^T \boldsymbol{g}_N, \tag{2.52}$$

and the according wave spectrum of the loudspeaker distribution can be given as

$$\hat{\mathbf{b}}_N = -ik\mathbf{H}_N \mathbf{Y}_N^T \boldsymbol{g}_N. \tag{2.53}$$

In Ambisonics, the task is now to match the wave spectra $\mathbf{f}_N$ and $\hat{\mathbf{b}}_Q$. So it yields the following driving functions for the loudspeakers of the Ambisonics system valid for $r < r_L$ as

$$\boldsymbol{g}_N = (\mathbf{Y}_N^T)^{-1} \mathbf{H}_N^{-1} \mathbf{f}_N. \tag{2.54}$$

However, this matching problem of band limited spectra has more than one solution. Because of the fact that trying to execute the $\mathcal{ISHT}$ for the synthesis of band limited spherical harmonics, no exact inverse of $\boldsymbol{Y}_N^T$ exists and the right inverse $(\boldsymbol{Y}_N^T)^\dagger$, in Ambisonics called Decoder, has to be applied.

As a consequence a minimum energy of the driving functions is additionally demanded to get a distinct solution [ZP11] (λ denotes so-called Lagrange multipliers):

$$\|\boldsymbol{g}\|^2 \Rightarrow min, \tag{2.55}$$

$$\boldsymbol{\gamma}_N \stackrel{!}{=} \boldsymbol{Y}_N^T \boldsymbol{g}, \tag{2.56}$$

$$J(\boldsymbol{g}, \boldsymbol{\lambda}) = \|\boldsymbol{g}\|^2 + (\boldsymbol{\gamma}_N^T - \boldsymbol{g}^T \boldsymbol{Y}_N)\boldsymbol{\lambda}, \tag{2.57}$$

and results in the right inverse

$$\boldsymbol{g} = \boldsymbol{Y}_N (\boldsymbol{Y}_N^T \boldsymbol{Y}_N)^{-1} \boldsymbol{\gamma}_N = (\boldsymbol{Y}_N^T)^\dagger \boldsymbol{\gamma}_N. \tag{2.58}$$

With the achieved driving functions for a distinct loudspeaker setup, real or virtual, any sound reinforcement application from public address to a binaural synthesis can be realized.

Reproduction of a directive source:
It suggests itself, that a reproduction of the analyzed emitted sound field of a directive source displaced at any location with an arbitrary orientation is desired.

This operation of rotating and translating a sound source out of the origin of the coordinate system can be interpreted as a coordinate transform. It should be possible to determine new expansion coefficients $\mathbf{f}_N$ of the transformed field with respect to the old and measured wave spectra $\mathbf{c}_N$ of the source. Therefor, these methods for the calculation of the new expansion coefficients have to be derived.

General formulations of this problem can be found in [Men07] for a frequency domain implementation. Nevertheless, in this work the involved filters for carrying out the translation are discussed much more in detail.

As a consequence, the analytical descriptions in chapter 3 for the rotation and the translation of acoustic fields lead to an efficient time domain implementation in chapter 4. Thereby, efficient calculation methods for these filters as well as their translation dependent frequency responses are presented.

3 Coordinate Transforms

So far, the solutions for the Helmholtz equation assumed a fixed reference frame and all descriptions were made with respective to the origin of the coordinate system. If the reference frame is changed or in other words a sound source is moved out of the center to another position in the coordinate system the different solutions discussed in chapter 2 can be expressed as linear combinations of elementary solutions in the new reference frame. This coordinate transform can be split up into rotation and translation methods and it is the basis for many sound field simulations in numerical acoustics and form the theoretical background for a real time application to move sound sources in an Ambisonics system. The intention of the following sections is to summarize the methods for describing sound fields of dislocated and rotated sound sources. To this end, recurrence relations and calculation methods for translating operations are given and the involved relationships are illustrated for a better understanding.

3.1 Re-expansion over Spherical Basis Functions

The wave field of an ideal point source, which is located at the coordinate system's origin and a translated counterpart are depicted in figure 8. As mentioned above, the

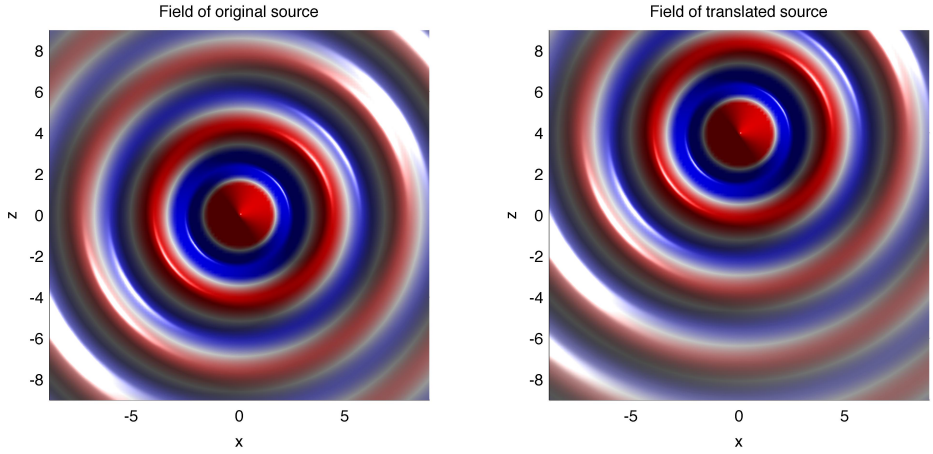

Figure 8 – Wave field of an ideal point source at the origin (left) and translated to $z = 4$ (right).

exclusively outgoing wave in the case of the original positioned monopole is described using only singular solutions and equals

$$p(k\boldsymbol{r}) = c_{0,0} S_0^0(k\boldsymbol{r}) = c_{0,0} h_0^{(2)}(k\boldsymbol{r}) Y_0^0(\boldsymbol{\theta}). \tag{3.1}$$

So the sum of elementary solutions can be simplified by setting the expansion coefficient $b_{nm} = 0$. Furthermore, the zero order spherical harmonic is enough to represent the angular characteristics of a point source located at the origin.

In case of a source dislocated from the origin to the point $\boldsymbol{r}'$, the reference frame and consequently also the wave spectra change. The expansion coefficients for the new position are determined from the wave spectra in the old reference frame and need to be calculated to describe the sound field.

Thus trying to express the displaced sound field $p(k\boldsymbol{r}')$ the problem arises that the involved basis functions of the source feature a singularity at $\boldsymbol{r} - \boldsymbol{r}' = 0$, so that the singular basis functions are not valid towards the origin. In this area ($\|\boldsymbol{r}\| < \|\boldsymbol{r}'\|$) the field has to become source free and must not hold Sommerfeld's radiation condition to enable the description of the field. The acoustic field beyond this area ($\|\boldsymbol{r}\| > \|\boldsymbol{r}'\|$) has to maintain the radiation condition. As a consequence, the emitted wave field of the translated source has to be divided into an outgoing and an incident field with respect to the new center of re-expansion or reference frame (fig. 9).

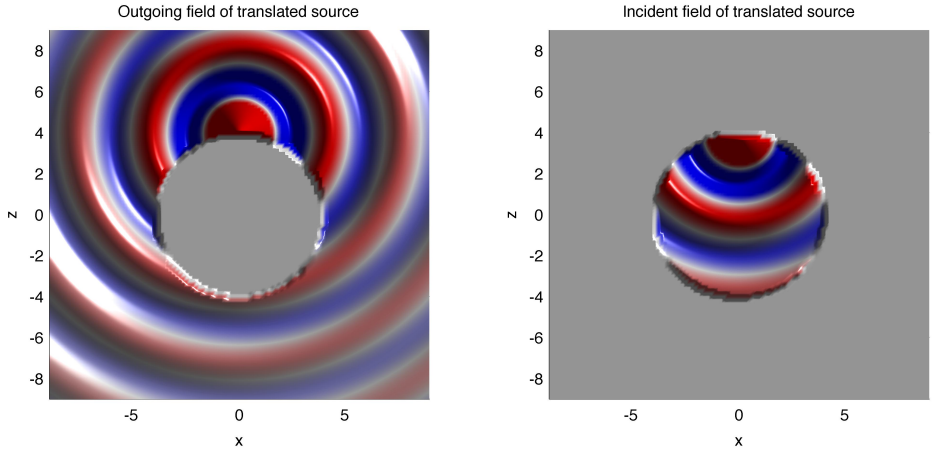

Figure 9 – Distinct expansions of outgoing and incident fields necessary to describe a displaced sound source.

The incoming field can be described by a sum of weighted regular basis functions whereas the outgoing field is represented as series of weighted singular basis functions. It is also obvious that more than one spherical harmonic (located at the center of re-expansion) are required to synthesize the angular characteristics of the wave field. For an example of a monopole the problem can be stated as

$$\begin{aligned} p(k\boldsymbol{r}) =& c_{0,0}|_{\boldsymbol{r}} S_0^0(k\boldsymbol{r}) \\ =& \sum_{n=0}^{\infty} \sum_{m=-n}^{n} \begin{cases} b_{nm}|_{\boldsymbol{r}'} R_n^m(k\boldsymbol{r}') \\ c_{nm}|_{\boldsymbol{r}'} S_n^m(k\boldsymbol{r}') \end{cases} = \boldsymbol{Y}_{N_t} \cdot \begin{cases} \boldsymbol{J}_{N_t} \boldsymbol{b}_{N_t} & \text{, for incident field,} \\ \boldsymbol{H}_{N_t} \boldsymbol{c}_{N_t} & \text{, for outgoing field.} \end{cases} \end{aligned} \tag{3.2}$$

with $\boldsymbol{r}$ representing the original and $\boldsymbol{r}'$ the translated reference frame.

To formulate the problem in an abstract way, we assume two centers of re-expansion $\boldsymbol{r_1}$ and $\boldsymbol{r}_2$ so that $\boldsymbol{r}_t = \boldsymbol{r}_2 - \boldsymbol{r}_1$ called translation vector. Due to the invariance of the wave

field $p(k\boldsymbol{r})$, which lies at the origin, its representation can be expanded at any center of re-expansion. Thereby, considering the prevailing constraints of source free fields and Sommerfeld's radiation condition are self-evident.

$$p(k\boldsymbol{r}) = \sum_{n=0}^{\infty}\sum_{m=-n}^{n}\begin{cases} b_{nm}|_{\boldsymbol{r_1}} R_n^m(k(\boldsymbol{r}-\boldsymbol{r}_1)), & \text{for } \|\boldsymbol{r}\| < \|\boldsymbol{r}_1\| \\ c_{nm}|_{\boldsymbol{r_1}} S_n^m(k(\boldsymbol{r}-\boldsymbol{r}_1)), & \text{for } \|\boldsymbol{r}\| > \|\boldsymbol{r}_1\| \end{cases} \tag{3.3}$$

$$= \sum_{n=0}^{\infty}\sum_{m=-n}^{n}\begin{cases} b_{nm}|_{\boldsymbol{r_2}} R_n^m(k(\boldsymbol{r}-\boldsymbol{r}_2)), & \text{for } \|\boldsymbol{r}\| < \|\boldsymbol{r}_2\| \\ c_{nm}|_{\boldsymbol{r_2}} S_n^m(k(\boldsymbol{r}-\boldsymbol{r}_2)), & \text{for } \|\boldsymbol{r}\| > \|\boldsymbol{r}_2\| \end{cases} \tag{3.4}$$

Changing positions or reference frames yield different linear combinations of basis functions with different coefficients (wave spectra). The relationship between these coefficients of different reference frames can be expressed by translation coefficients $T_{n'n}^{m'm}(k\boldsymbol{r}_t)$. Related to two reference frames, also called centers of re-expansion, the translation coefficients depend on the translation vector $\boldsymbol{r}_t$ as well as the order and degree (n and m) in the first and the corresponding ones (n' and m') in the second frame. Due to the orthogonality of the basis functions the addition theorem for the scalar wave equation equals

$$E_n^m(k(\boldsymbol{r}-\boldsymbol{r}_1)) = \sum_{n'=0}^{\infty}\sum_{m'=-n'}^{n'} T_{n'n}^{m'm}(k\boldsymbol{r}_t) F_{n'}^{m'}(k(\boldsymbol{r}-\boldsymbol{r}_2)). \tag{3.5}$$

For a general representation $E_n^m(k\boldsymbol{r})$ and $F_n^m(k\boldsymbol{r})$ are used for arbitrary singular or regular basis functions with their coefficients e_{nm} and f_{nm}. The dependencies on k of E_n^m, F_n^m and $T_{n'n}^{m'm}$ are omitted for convenience in the following formulations.

Consequently, it can be written

$$p(k\boldsymbol{r}) = \sum_{n=0}^{\infty}\sum_{m=-n}^{n} e_{nm}|_{\boldsymbol{r_1}} E_n^m(\boldsymbol{r}-\boldsymbol{r}_1) \tag{3.6}$$

$$= \sum_{n=0}^{\infty}\sum_{m=-n}^{n} e_{nm}|_{\boldsymbol{r_1}} \sum_{n'=0}^{\infty}\sum_{m'=-n'}^{n'} T_{n'n}^{m'm}(\boldsymbol{r}_t) F_{n'}^{m'}(\boldsymbol{r}-\boldsymbol{r}_2) \tag{3.7}$$

$$= \sum_{n'=0}^{\infty}\sum_{m'=-n'}^{n'} \Big[\sum_{n=0}^{\infty}\sum_{m=-n}^{n} e_{nm}|_{\boldsymbol{r_1}} T_{n'n}^{m'm}(\boldsymbol{r}_t)\Big] F_{n'}^{m'}(\boldsymbol{r}-\boldsymbol{r}_2) \tag{3.8}$$

$$= \sum_{n'=0}^{\infty}\sum_{m'=-n'}^{n'} f_{n'm'}|_{\boldsymbol{r_2}} F_{n'}^{m'}(\boldsymbol{r}-\boldsymbol{r}_2). \tag{3.9}$$

As a result, the relation of the expansion coefficients at one position, $e_{nm}|_{\boldsymbol{r_1}}$, to the ones at another point, $f_{n'm'}|_{\boldsymbol{r_2}}$, can be stated as

$$f_{n'm'}|_{\boldsymbol{r_2}} = \sum_{n=0}^{\infty}\sum_{m=-n}^{n} T_{n'n}^{m'm}(\boldsymbol{r}_t) e_{nm}|_{\boldsymbol{r_1}}. \tag{3.10}$$

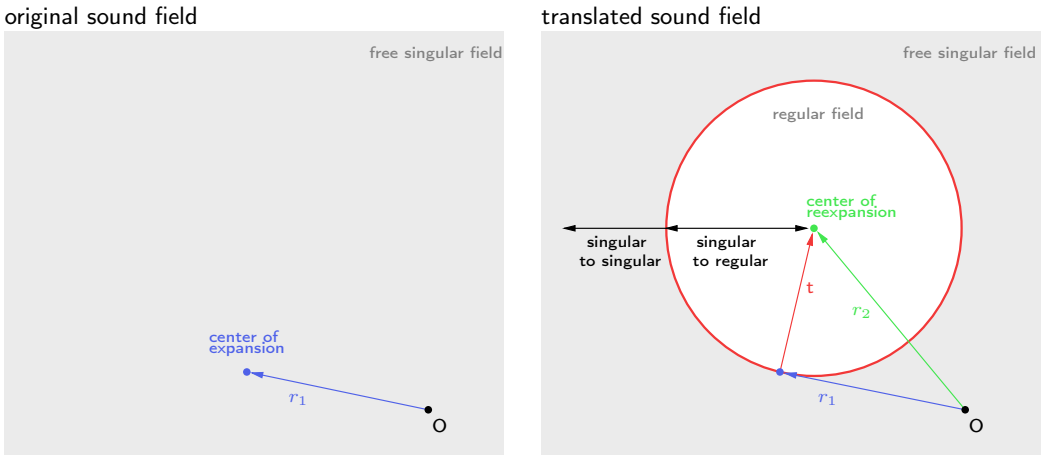

Figure 10 – Original sound field (left) and translated field with different translation modes labeled (right).

We can separate three different translation scenarios and areas:

1. Outgoing to incident fields (singular to regular)
   Due to the delocation of the reference frame, the original outgoing sound field, described by singular basis functions, changed to an incident field which has to be reexpanded over regular basis functions.

$$S_n^m(\boldsymbol{r}_1) = \sum_{n'=0}^{\infty} \sum_{m'=-n'}^{n'} T_{n'n}^{m'm}(\boldsymbol{r}_t) R_{n'}^{m'}(\boldsymbol{r}_2) \quad \text{for} \quad |\boldsymbol{r} - \boldsymbol{r}_2| < |\boldsymbol{r}_t| \tag{3.11}$$

   On the right hand side of figure 10, the white colored area inside the red circle represents the singular to regular domain.

2. Outgoing to outgoing fields (singular to singular)
   Outgoing sound fields remain outgoing or singular ones despite of translation (cf. fig. 10).

$$S_n^m(\boldsymbol{r}_1) = \sum_{n'=0}^{\infty} \sum_{m'=-n'}^{n'} T_{n'n}^{m'm}(\boldsymbol{r}_t) S_{n'}^{m'}(\boldsymbol{r}_2) \quad \text{for} \quad |\boldsymbol{r} - \boldsymbol{r}_2| > |\boldsymbol{r}_t| \tag{3.12}$$

3. Incident to incident fields (regular to regular)
   Incident sound fields and their regular basis functions in a finite domain can be reexpanded again in series of regular basis functions.

$$R_n^m(\boldsymbol{r}_1) = \sum_{n'=0}^{\infty} \sum_{m'=-n'}^{n'} T_{n'n}^{m'm}(\boldsymbol{r}_t) R_{n'}^{m'}(\boldsymbol{r}_2) \tag{3.13}$$

The residual combination regular to singular is not feasible because it would deduce that the regular field would radiate at infinity, which is not reasonable.

3.2 Rotation

A basic method of coordinate transforms is rotation of a reference frame to another direction. Based on equation (3.10) we can describe the rotation by recalculating the wave spectra. For further discussions we can assume the conservation of the radial behavior due to rotations around the center of expansion only. That implies, that regular basis functions remain regular and singular persist singular as well as the absolute values of vectors from the origin to any spatial point stay the same ($\|\boldsymbol{r}\| = \|\hat{\boldsymbol{r}}\|$).

In general, with $\boldsymbol{r} = (x, y, z)$ representing original and $\hat{\boldsymbol{r}} = (\hat{x}, \hat{y}, \hat{z})$ representing rotated orientation as well as e_n denoting spherical Bessel functions of any kind, it holds, that

$$\begin{aligned} E_n^m(\boldsymbol{r}) &= \sum_{n'=0}^{\infty} \sum_{m'=-n'}^{n'} T_{nn'}^{mm'}(Q) E_{n'}^{m'}(\hat{\boldsymbol{r}}) \\ &= \sum_{n'=0}^{\infty} \sum_{m'=-n'}^{n'} T_{nn'}^{mm'}(Q)\, e_{n'}(kr) Y_{n'}^{m'}(\hat{\boldsymbol{r}}) \\ &= \sum_{n'=0}^{\infty} e_{n'}(kr) \sum_{m'=-n'}^{n'} T_{nn'}^{mm'}(Q) Y_{n'}^{m'}(\hat{\boldsymbol{r}}). \end{aligned} \tag{3.14}$$

Because of the linear independency of Bessel and Hankel functions, it is not possible to express $e_n(kr)$ as a linear combination of functions with orders $n' \neq n$. Furthermore, taking the orthonormality of the spherical harmonics into account, the only possible and non-trivial solutions ($T_{n'n}^{m'm} \neq 0$) of eq. (3.14) can be achieved by setting $n' = n$. Consequently eq. (3.14) can be simplified to a finite sum written as

$$Y_n^m(\boldsymbol{r}) = \sum_{m'=-n'}^{n'} T_n^{mm'}(Q) Y_n^{m'}(\hat{\boldsymbol{r}}), \tag{3.15}$$

$$E_n^m(\boldsymbol{r}) = \sum_{m'=-n'}^{n'} T_n^{mm'}(Q) E_n^{m'}(\hat{\boldsymbol{r}}). \tag{3.16}$$

It can be seen, that wave spectra in rotated reference frames are related to each other by translation coefficients $T_n^{m'm}(Q)$. They are only dependent on the rotation matrix Q defined as

$$Q = \begin{bmatrix} i_{\hat{x}} \cdot i_x & i_{\hat{x}} \cdot i_y & i_{\hat{x}} \cdot i_z \\ i_{\hat{y}} \cdot i_x & i_{\hat{y}} \cdot i_y & i_{\hat{y}} \cdot i_z \\ i_{\hat{z}} \cdot i_x & i_{\hat{z}} \cdot i_y & i_{\hat{z}} \cdot i_z \end{bmatrix}, \tag{3.17}$$

so that

$$\hat{\boldsymbol{r}} = Q\boldsymbol{r}. \tag{3.18}$$

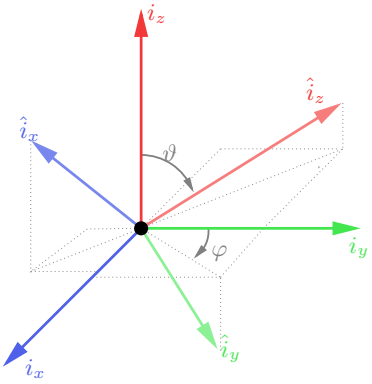

Figure 11 – Original and rotated coordinate system.

3.2.1 Rotation Coefficients

Complex valued SH - zyz-Rotation

In the case of complex valued spherical harmonics an arbitrary rotation Q can be divided into three operations, a rotation with the angle γ around the z-axis followed by a rotation around y-axis with the angle β and finally another rotation around z-axis with α. The calculation can be done efficiently using recurrence relations obtained from differentiation theorems for elementary solutions in spherical coordinates. The derivation of these relations are out of scope of this work but can be found in appropriate literature [GD04], [Zot09]

$$T_n^{m',0} = \sqrt{\frac{4\pi}{2n+1}} Y_n^{m'}(\boldsymbol{\theta}), \quad n = 0, 1, \ldots \quad m' = -n, \ldots, n, \tag{3.19}$$

$$T_n^{-m',-m}(Q) = (T_n^{m',m}(Q))^*, \quad n = 0, 1, \ldots \quad m' = -n, \ldots, n, \tag{3.20}$$

$$\begin{aligned} T_{n-1}^{m',m+1} = &\frac{e^{i\alpha}}{\zeta_{nm}} \Big(\frac{1}{2} [\zeta_n^{-m'-1} e^{i\gamma} (1 - \cos\beta) T_n^{m'+1,m} \\ &- \zeta_n^{m'-1} (1 + \cos\beta) e^{-i\gamma} T_n^{m'-1,m}] - \eta_{n-1}^{m'} \sin\beta T_n^{m',m} \Big). \end{aligned} \tag{3.21}$$

with the coefficients η_{nm} and ζ_{nm} equals

$$\eta_{nm} = \eta_{n|m|} = \sqrt{\frac{(n+1+|m|)(n+1-|m|)}{(2n+1)(2n+3)}} \quad \text{for} \quad n \geq |m|, \tag{3.22}$$

$$\zeta_{nm} = \begin{cases} \sqrt{\frac{(n-m-1)(n-m)}{(2n-1)(2n+1)}}, & \text{for } 0 \leq m \leq n, \\ -\sqrt{\frac{(n-m-1)(n-m)}{(2n-1)(2n+1)}}, & \text{for } -n \leq m \leq 0, \\ 0, & \text{for } |m| < n. \end{cases}$$

Complex valued SH - $zy_{\pi/2}zy_{\pi/2}z$-Rotation

For a more efficient implementation of the rotation method, a further decomposition can be used. Therefore an arbitrary rotation is divided into two basic methods, the rotation around z-axis and a fixed turn around y-axis with angle $\frac{\pi}{2}$. This yields

$$\hat{\boldsymbol{r}} = Q\boldsymbol{r} = Q_z(\alpha+\pi/2)Q_{y\frac{\pi}{2}}Q_z(\beta+\pi)Q_{y\frac{\pi}{2}}Q_z(\gamma+\pi/2)\boldsymbol{r}, \tag{3.23}$$

$$\Rightarrow T(Q) = T(Q_z)T_{Q_{y\frac{\pi}{2}}}T(Q_z)T_{Q_{y\frac{\pi}{2}}}T(Q_z). \tag{3.24}$$

The individual operations can be done on the basis of following relations:

$$T(Q_z(\gamma)) = \hat{\Phi}_m(\gamma)\delta_{n'n}\delta_{m'm}, \tag{3.25}$$

$$T(Q_{z\frac{\pi}{2}}) = \begin{pmatrix} 0 & -1 \\ 1 & 0 \end{pmatrix}^m \delta_{n'n}^{m'm}. \tag{3.26}$$

For the rotation operations around y-axis recurrence relations can be used, so that an initialization with

$$T_{nn}^{m'0}(Q_{y\frac{\pi}{2}})\boldsymbol{I} = \sqrt{\frac{4\pi}{2n+1}}\hat{Y}_n^{-m'}(0,\pi/2)\boldsymbol{I}, \tag{3.27}$$

is done before all other coefficients are calculated by the following recurrence and symmetry relations

$$\begin{aligned}\hat{T}_{n-1,n-1}^{m',m+1}(Q_{y\frac{\pi}{2}}) =& \frac{1}{2\zeta_{nm}}\big(\zeta_{n,m'-1}\hat{T}_{n,n}^{m'-1,m}(Q_{y\frac{\pi}{2}}) - \zeta_{n,-m'-1}\hat{T}_{n,n}^{m'+1,m}(Q_{y\frac{\pi}{2}}) \\ &+ 2\eta_{n-1,m'}\hat{T}_{n,n}^{m',m}(Q_{y\frac{\pi}{2}})\big),\end{aligned} \tag{3.28}$$

$$\hat{T}_{nn}^{m'm}(Q_{y\frac{\pi}{2}}) = (-1)^{m+m'}\hat{T}_{nn}^{m'm}(Q_{y\frac{\pi}{2}}^{-1}), \tag{3.29}$$

$$\hat{T}_{nn}^{m'm}(Q_{y\frac{\pi}{2}}) = (-1)^{n+m+m'}T_{nn}^{-m'm}(Q_{y\frac{\pi}{2}}). \tag{3.30}$$

Real valued SH - $zy_{\pi/2}zy_{\pi/2}z$-Rotation

In the case of real valued spherical harmonics the latter formulations can be rewritten as

$$T_{nn}^{m'0}(Q_{y\frac{\pi}{2}}) = \sqrt{\frac{4\pi}{2n+1}}\hat{Y}_n^{|m'|}(0,\pi/2), \tag{3.31}$$

$$\begin{aligned}\hat{T}_{n-1,n-1}^{m',m+1}(Q_{y\frac{\pi}{2}}) =& \frac{\sqrt{2-\delta_{m+1}}}{2\zeta_{nm}\sqrt{2-\delta_m}}\Bigg(\sqrt{2-\delta_{m'}}\big(\frac{\zeta_{n,m'-1}}{\sqrt{2-\delta_{m'-1}}}\hat{T}_{n,n}^{m'-1,m}(Q_{y\frac{\pi}{2}}) \\ &- \frac{\zeta_{n,-m'-1}}{\sqrt{2-\delta_{m'+1}}}\hat{T}_{n,n}^{m'+1,m}(Q_{y\frac{\pi}{2}})\big) + 2\eta_{n-1,m'}\hat{T}_{n,n}^{m',m}(Q_{y\frac{\pi}{2}})\Bigg),\end{aligned} \tag{3.32}$$

$$\hat{T}_{nn}^{m'm}(Q_{y\frac{\pi}{2}}) = (-1)^{m+m'}\hat{T}_{nn}^{-m'm}(Q_{y\frac{\pi}{2}}). \tag{3.33}$$

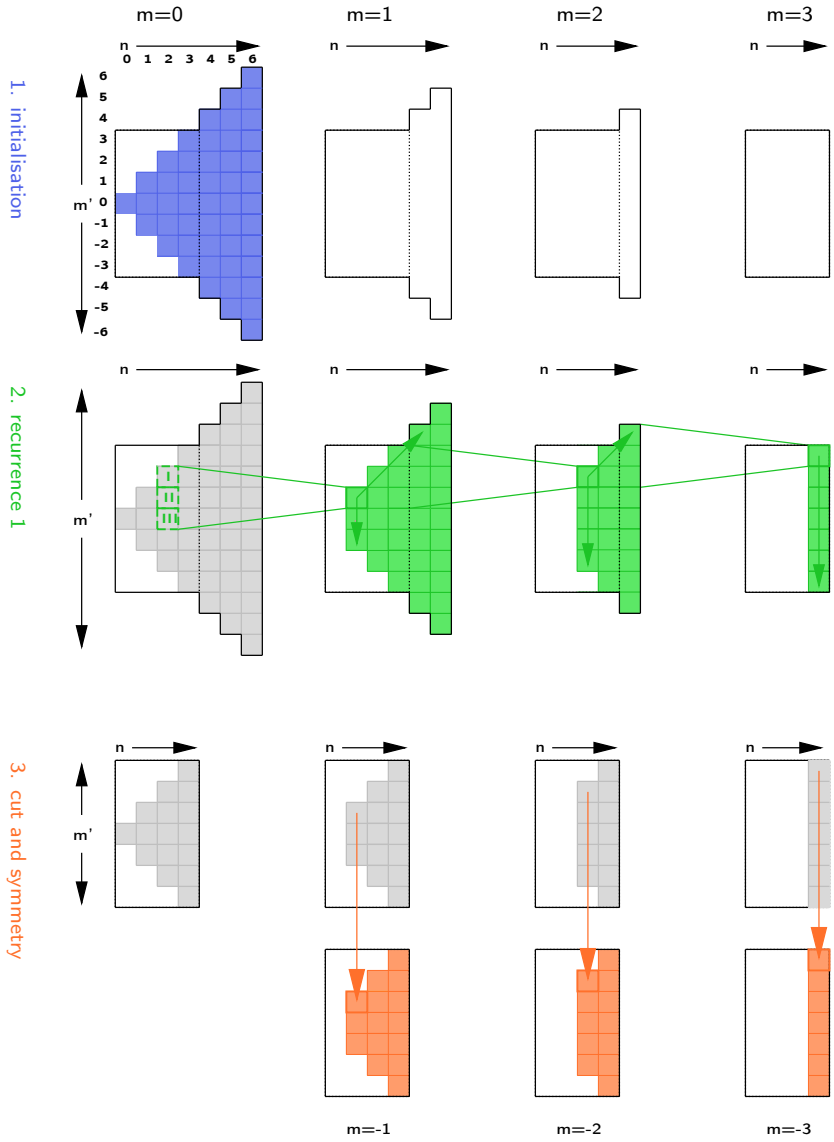

Figure 12 – Scheme of calculating rotation coefficients with recurrences and symmetry relations. After initialization with eq.(3.19) (alternatively (3.27) or (3.31)), recurrence relation eq.(3.21) (i.e. eq.(3.28) or (3.32)) is applied. Then symmetry relations eq.(3.20) (i.e. eq.(3.29),(3.30) or (3.33)) are obtained before the matrix is cropped to the desired dimensions. The arrows show the progressions of recurrences.

3.3 Coaxial Translation

For practical reasons, a further simplification is applied to translating methods. Assuming only a displacement in positive z-direction one can observe an independency of the basis functions on the polar angle φ concerning translations, so that $E_n^m(\boldsymbol{r}) \propto e^{im\varphi} \propto E_n^m(\boldsymbol{r} + r_{ct})$. This implies, that because of the orthogonality of $e^{im\varphi}$, $m = 0, \pm 1, \pm 2, ...$ each basis function of order m can only be expanded over basis functions with the same order. As a consequence, the translation coefficients are only dependent on the displacement distance and can be written as a linear combination of basis functions of order m. Due to $Y_n^m(\boldsymbol{\theta}) = 0$ for all $n < |m|$, the sum over n can be started at $|m|$

$$E_n^m(\boldsymbol{r} + r_{ct}) = \sum_{n'=|m|}^{\infty} T_{n'n}^m(r_{ct}) F_{n'}^m(\boldsymbol{r}). \tag{3.34}$$

To execute a full translation in an arbitrary direction, the operation can be split up into a rotation of the reference frame until the displacement can be performed only in the new z-direction. Afterwards the inverse rotation $\boldsymbol{Q}(\vartheta, \varphi, 0)^{-1} = \boldsymbol{Q}(0, -\vartheta, -\varphi)$ assures the right orientation [Zot09]

$$\begin{aligned} \boldsymbol{r'} =& \boldsymbol{r} + \boldsymbol{d}, && (3.35)\\ =& \boldsymbol{Q}(0, -\vartheta, -\varphi)[\boldsymbol{Q}(\vartheta, \varphi, 0)\boldsymbol{r} + \boldsymbol{r}_{r_{ct}}], && (3.36)\\ \boldsymbol{r}_t(\boldsymbol{r'}) =& \boldsymbol{r}_t(\boldsymbol{Q})\boldsymbol{r}_t(r_{ct})\boldsymbol{r}_t(\boldsymbol{Q}^{-1}). && (3.37) \end{aligned}$$

Figure (13) shows an example of the stepwise execution of the translation in an arbitrary direction.

3.3.1 Coaxial Translation Coefficients

The calculation of translation coefficients can be efficiently implemented with recurrence relations and symmetry properties which, can be stated as

$$\begin{aligned} \eta_{n-1,m} T_{n',n-1}^m - \eta_{n,m} T_{n',n+1}^m =& \eta_{n',m} T_{n'+1,n}^m - \eta_{n'-1,m} T_{n'-1,n}^m, && (3.38)\\ \zeta_{n,m} T_{n',n-1}^{m+1} - \zeta_{n+1,-m-1} T_{n',n+1}^{m+1} =& \zeta_{n'+1,m} T_{n'+1,n}^m - \zeta_{n,-m-1} T_{n'-1,n}^m, && (3.39)\\ T_{n',n}^m =& T_{n',n}^{-m} = T_{n'+1,n}^{|m|}. && (3.40) \end{aligned}$$

These relations can be derived by utilizing the derivation theorems, whose explanation lies outside the scope of this work (cf. [GD04]). Coefficients η_{nm} and ζ_{nm} can be calculated with eq. (3.22).

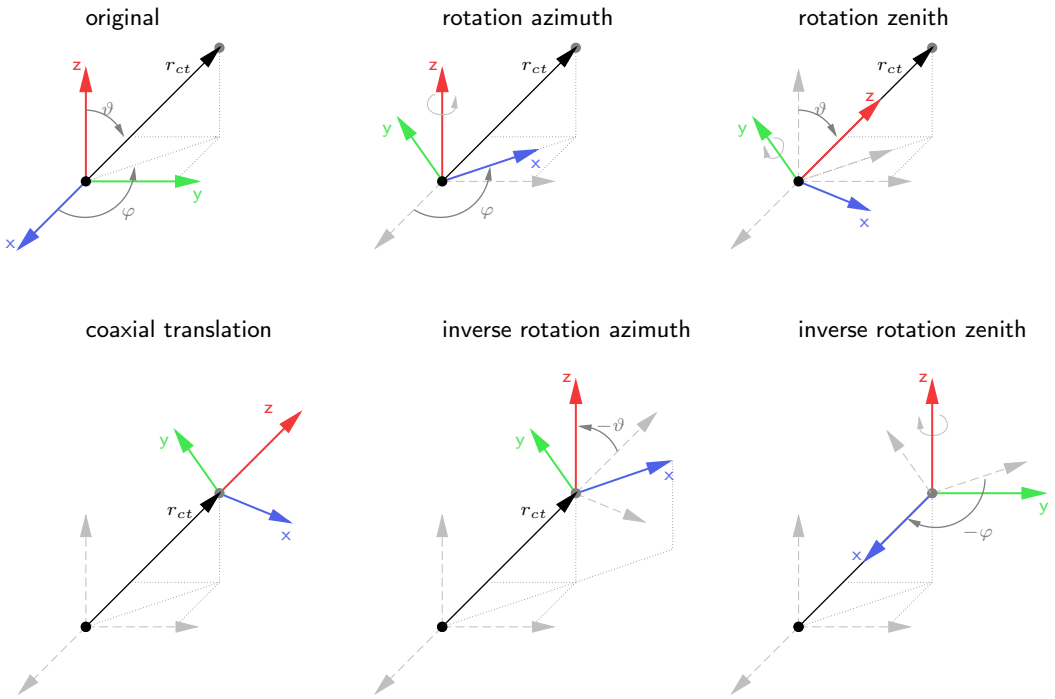

Figure 13 – Coaxial translation perform with zy-rotation, displacement in z direction and inverse yz-rotation to get the original orientation.

As a result, we obtain a 3D matrix $\boldsymbol{T}$ with the dimensions $dim\{\boldsymbol{T}\} = [Nt, Nt, Nt]$ and variable $[n', n, m]$. The calculation can be done in five steps to fill the matrix with its values (see fig. 14):

1. Initialization:
   Initial values for the first column ($m = 0$, $n = 0$, $\forall\ n'$) can be given, depending on the translation scenario, as

$$T^0_{n',0}(r_{ct}) = \sqrt{2n'+1} \begin{cases} h_{n'}(kr_{ct}), & \text{for singular to regular,} \\ j_{n'}(kr_{ct}), & \text{for singular to singular} \\ & \text{and regular to regular translation.} \end{cases} \tag{3.41}$$

   To enable performing recurrences for all required entries, the matrix has got needs to be as big as the dimensions $dim\{\boldsymbol{T}\} = [2Nt+1, Nt+1, Nt+1]$.

2. Initialize layers $m > 0$:
   Utilizing eq. (3.39) and omitting all terms $T^{m+1}_{n',n-1}$ which do not exist, the entries for $n = m$ and all $m \leq n' \leq 2Nt - m$ can be obtained.

3. Filling triangles:
   Using eq. (3.38) the triangle of the first layer for values between $n' \geq n$ and $n' \leq Nt - n$ can be calculated. Starting with $n = 0$, the value for $n < 0$ has to be omitted initially.

4. Symmetry properties:
   Eq. (3.40) uses the symmetry properties of the translation coefficients to complete the entries of the matrix for $n \geq m$ and $n' \geq m$.
5. Cutting matrix:
   The final step is to reduce the matrix to the desired dimensions $dim\{\boldsymbol{T}\} = [Nt, Nt, Nt]$

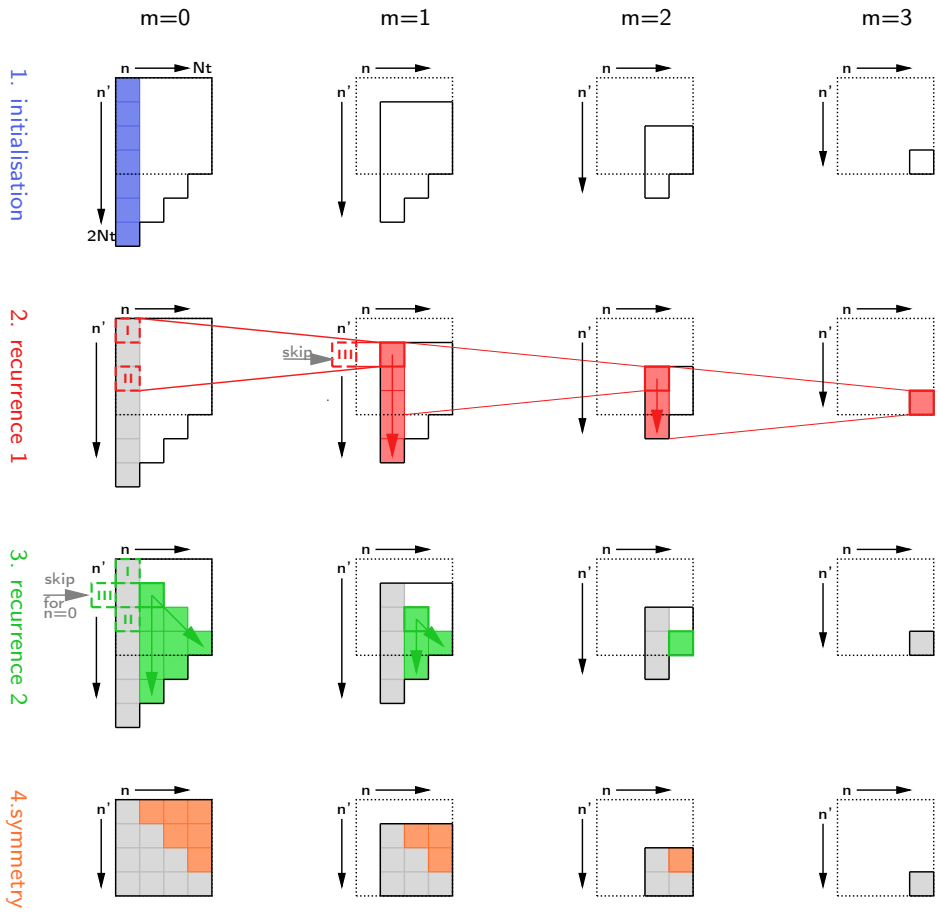

Figure 14 – Calculation scheme of translation coefficients with recurrence and symmetry relations. After initialisation with eq. (3.41), layers $m > 0$ are initialized with eq. (3.39) and filled using eq.(3.38). Before the matrix is cutted in desired dimensions, symmetry properties (3.39) are used to complete entries.

Taking a closer look at the resulting matrix, the maximal orders of inherent functions become obvious. Due to the recurrences employed, the matrix entries are a weighted

sum of spherical Hankel or Bessel functions. These are for the range $n' \geq n$

$$T^m_{n'n}(r_{ct}) = \sum_{l=n'}^{n+n'} q_l \begin{cases} h_{2l-n-n'}(kr_{ct}), & \text{for singular to regular,} \\ j_{2l-n-n'}(kr_{ct}), & \text{for singular to singular} \\ & \text{and regular to regular translation,} \end{cases} \tag{3.42}$$

where q_l denotes suitable weighting factors emanating a_{nm} and b_{nm} (eq.(3.22)) as well as the initial values. Entries for $0 \leq n' < n$ obtained by symmetry have an according representation. Let us define the maximum order included in each matrix entry $T^m_{n'n}$ as

$$d_{n'+n} := \max(deg\{T^m_{n'n}(r_{ct})\}) = n' + n. \tag{3.43}$$

The resulting structure of the matrix entries is symbolically illustrated in figure 15.

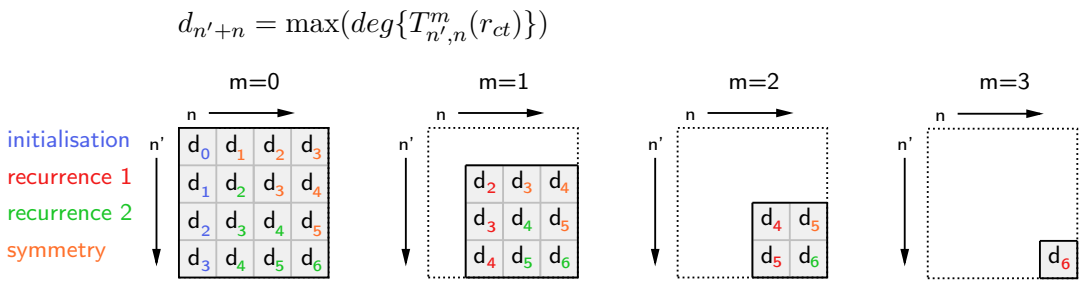

Figure 15 – Maximum order of spherical Bessel/Hankel functions in the translation matrix. The entries are labeled by color depending on their way of calculation.

The frequency responses of translation functions are dominated by the highest order of each matrix entry. This fact is crucial, especially regarding the magnitudes of spherical Hankel functions, as illustrated in fig. 6.

As an example, the resulting frequency responses for a translation by $r_{ct} = 1m$ is illustrated up to the order $N_t = 3$ in fig. 16. The impractically high dynamic ranges of up to more than 200dB at low frequencies reveal the main problem of time domain realizations of these filters and reflect the stability issues that are well separated in the frequency domain.

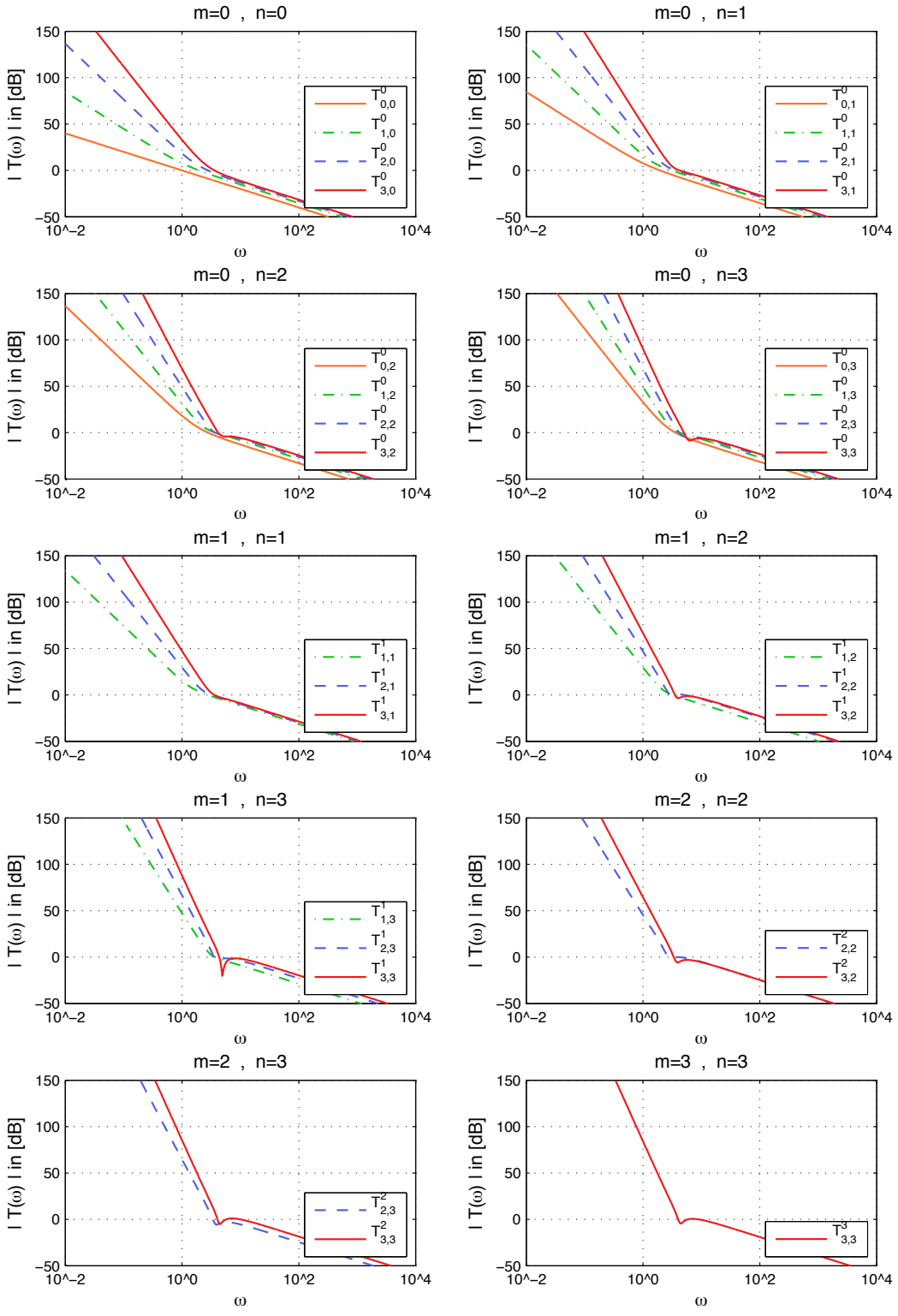

Figure 16 – Frequency responses of singular to regular translation filters of the orders up to $N_t = 3$ for $r_{ct} = 1m$.

3.4 Truncation of Expansion

For the considerations in the previous sections, the linear combination of the spherical basis functions where not limited to finite orders. In practice, a truncation of the sum over n has to be applied to enable computations and decompositions into spherical basis functions.

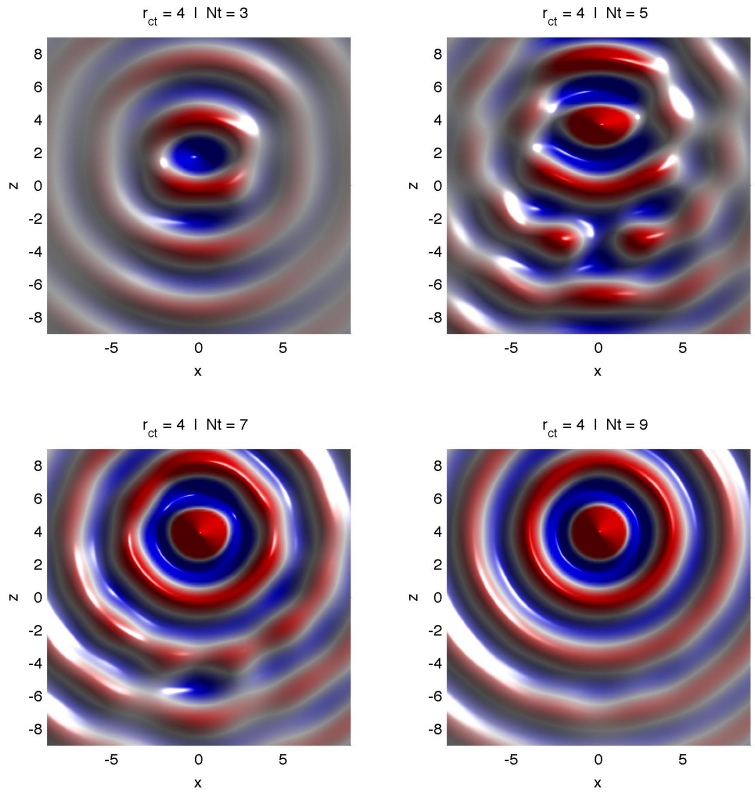

Figure 17 – Expansion over spherical basis functions of a translated monopole with truncation orders increasing from $N_t = 3$ to $N_t = 9$ ($f = 100Hz$,$k \approx 1.8$).

Due to the truncation of a wave spectrum, which is also referred to as a band limitation, an error is induced depending on the maximum order, denoted with $max(n) = N_t$. The wave spectrum can be written as the truncated sum, or briefly in a vector notation (cf. sec. 2.3)

$$\begin{aligned} p_{N_t}(kr) =& \sum_{n=0}^{N_t} \sum_{m=-n}^{n} [b_{nm}(r_1) R_n^m(k(r-r_1)) + c_{nm}(r_1) S_n^m(k(r-r_1))] \\ =& \boldsymbol{y}_{N_t}^T(\boldsymbol{\theta})[\boldsymbol{J}_{Nt}(kr)\boldsymbol{b}_{N_t} + \boldsymbol{H}_{N_t}(kr)\boldsymbol{c}_{N_t}]. \end{aligned} \tag{3.44}$$

The emerging error $\boldsymbol{\epsilon}_{N_t}$ is described by

$$\boldsymbol{\epsilon}_{N_t} = \boldsymbol{\psi}_{\infty}(kr) - \boldsymbol{\psi}_{N_t}(kr) \tag{3.45}$$

$$= \boldsymbol{J_{\infty}} \boldsymbol{b_{\infty}} - \boldsymbol{J_{N_t}} \boldsymbol{b_{N_t}} + \boldsymbol{H_{\infty}} \boldsymbol{c_{\infty}} - \boldsymbol{H_{N_t}} \boldsymbol{c_{N_t}}. \tag{3.46}$$

Translating sources consisting of higher order basis functions the produced error due to band limitation can become significant as shown in figures (17,18). As a rule-of-thumb, the required order of re-expansion for translating a sound source, can be given as ([GD04]):

$$N_t \geq N_{source} + k \cdot r_{ct}. \tag{3.47}$$

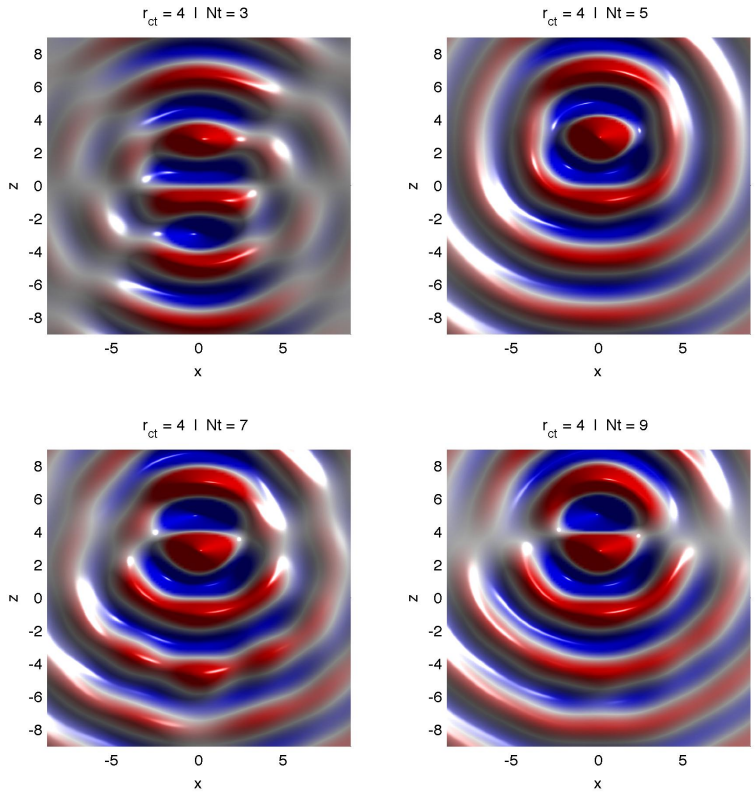

Figure 18 – Expansion over spherical basis functions of a translated dipole with increasing truncation orders from $N_t = 3$ up to $N_t = 9$ ($f = 100Hz$,$k \approx 1.8$). The translation order has to be $N_t \geq N_{source} + k \cdot r_{ct} = 1 + 1.8 \cdot 4 \approx 9$ for an appropriate sound field reproduction.

4 Coaxial Translation in Time Domain

The preceding chapter briefly discussed the theory of sound field representation in spherical coordinates and re-expansion after rotation and translation of the reference frames. It was asserted that acoustic wave fields can be characterized by linear combinations of spherical basis functions ($R_n^m(kr, \boldsymbol{\theta})$ and $S_n^m(kr, \boldsymbol{\theta})$) weighted by the according wave spectra ($b_{nm} \mid c_{nm}$).

Due to rotation and displacement of sound sources, or their reference frame, these coefficients (wave spectra) change. The relation between the wave spectra can be established by translation and rotation coefficients, which can be represented as matrices / tensors and thus provide the computational means of re-expansion.

For several reasons a time domain approach of the translation matrices, which were all stated in frequency domain, is eligible. For instance a time domain filter implementation of the translation matrix is desirable in real time applications of translated sound sources in Ambisonic playback systems as well as numerical sound field simulations, where multiple scattering can be modeled by feedback networks of translation filters.

Regarding an efficient time domain implementation of the system shown above (fig. 7), the radial terms $(j_n(kr)|h_n(kr))$ involved in the translating operations can be interpreted as IIR-filters. However their implementation requires a careful design to avoid instability.

In particular, the spherical Hankel functions are charakterized by a large dynamic range at small arguments, which is beyond a realistic IIR-filter implementation.

Despite high dynamic ranges and numerical inaccuracies are serious problems in the IIR-filter implementation, possible solutions can be discussed. As far as possible to resolve the following sections propose several strategies to obtain practical IIR-filter realizations.

4.1 Singular to Regular Translation

To consider the general behavior of singular to regular translation filters, the Laplace domain representation will be used because of its beneficial frequency scaling property.

For a singular to regular coaxial translation, the entries of the translation matrix are spherical Hankel functions. According to [Pom08], a Laplace domain representation of spherical Hankel functions can be derived as follows. Starting with the series notation in the frequency domain [GD04]

$$h_n(kr) = -i^n \frac{e^{-ikr}}{(ikr)^{n+1}} \sum_{l=0}^{n} \frac{(n+l)!}{l!(n-l)!2^l} (ikr)^{n-l}, \tag{4.1}$$

the relations

$$F(i\omega) = \mathcal{F}\{f(t)\} = \mathcal{L}\{(t)\}|_{s=i\omega} = F(s)|_{s=i\omega} \tag{4.2}$$

are used to transform $h_n(kr)$ by a substitution of $kr = \omega\Delta t$ and of $s = i\omega$ to

$$h_n(s\Delta t) = \frac{-i^n e^{s\Delta t}}{(s\Delta t)^{n+1}} \sum_{l=0}^{n} \frac{(n+l)!}{l!(n-l)!2^l} (s\Delta t)^{n-l}. \tag{4.3}$$

Δt denotes the time delay corresponding to the coaxial shift $\Delta t_{ct} = \frac{r_{ct}}{c}$ (c equals wave propagation speed). In an abbreviated form, and changing the summation index equals

$$h_n(s\Delta t) = -i^n e^{-s\Delta t} \frac{\sum_{k=0}^{n} \beta_n(k)(s\Delta t)^k}{(s\Delta t)^{n+1}}, \tag{4.4}$$

with the coefficients

$$\beta_n(k) = \frac{(2n-k-1)(2n-k)}{2(n-k)} \beta_{n-1}(k), \tag{4.5}$$

$$\beta_n(n) = 1, \qquad \forall n \geq 0. \tag{4.6}$$

Spherical Hankel functions have got $(n+1)$-multiple poles at $s = 0$ and a growing number of zeros for increasing function orders, as shown in Figure 19.

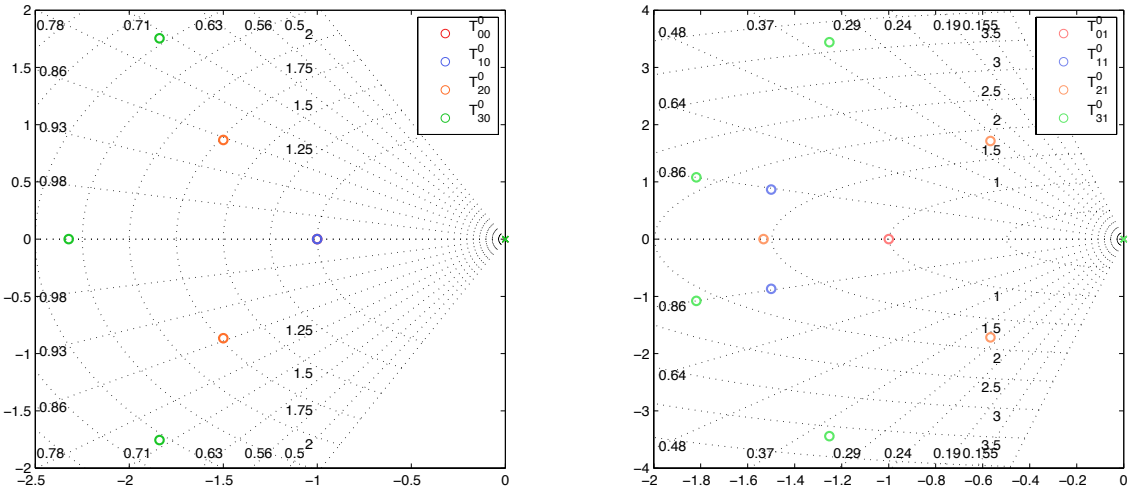

Figure 19 – Pole zero plots in Laplace domain for $T^m_{n'n}$ for all $n' = 0, ..., 3$, $n = 1, 2$ and $m = 0$ ($r_{ct} = 1$).

The fractional polynomials in eq. (4.4) has real-valued coefficients and thus allows linear factorization into real valued poles and zeros (denoted as α_r) or complex-conjugate paired written as $\alpha_c \pm i\omega_c$ (cf. [Pom08]).

The exact number and kinds of occurring zeros can be found with a root finding algorithm (e.g. Matlab's "roots.m"). The following regularity regarding the number of zeros of the numerator polynomial $n_{\alpha_r|\alpha_c \pm i\omega_c}$ can be stated as

$$n_{\alpha_r} = mod(n, 2), \qquad n_{\alpha_c \pm i\omega_c} = div(n, 2). \tag{4.7}$$

Figure 19 illustrates exemplarily the pole zero plots of the first eight translation filters.

For $n = m = 0$ and $n' = 0, ..., N_t$ the entries of the translation matrix are weighted $h_{n'}(s\Delta t)$. Due to recurrence relations the further entries (for $n \geq |m| > 0$) are weighted sums of different orders of spherical Hankel functions resp. filters. Their maximal numerator orders per entry are $d_{n'+n}$ as illustrated above (fig. 3.42).

Summing the different polynomials, the maximal order of the denominator remains the same and as a consequence every translation filter exhibits $(n+1)$-multiple poles at $s = 0$ and in general a sum of increasing number of zeros. Resulting frequency responses are illustrated in fig. 16.

4.1.1 Combination of Translation and Distance Coding Filters

As mentioned above (3.37), the coaxial translation can be split up into a rotation, followed by translation filtering and an inverse rotation.

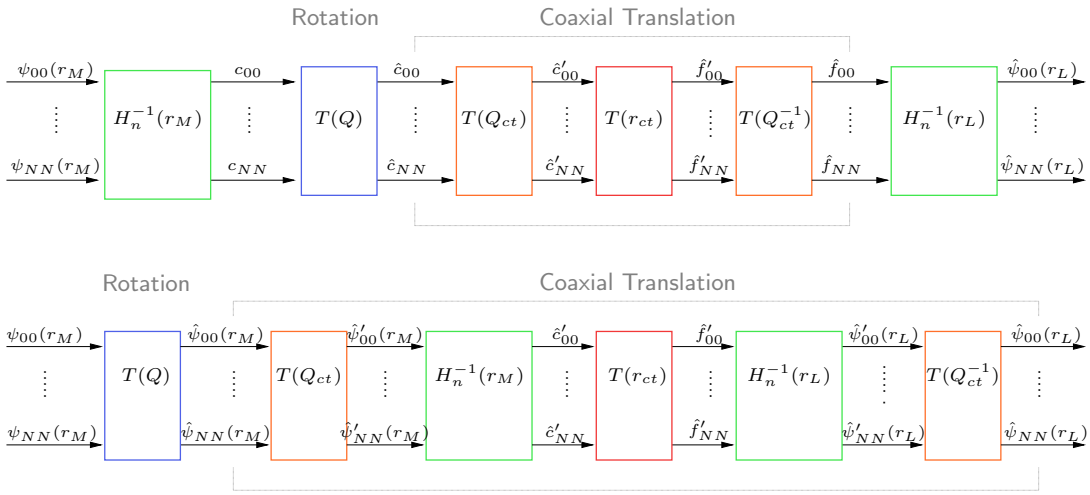

Figure 20 – Due to independence of $\boldsymbol{H}^{-1}(r_{M|L})$ with respect to m, these filter matrices can be relocated towards the translation matrix $\boldsymbol{T}(r_{ct})$ in order to stabilize the translation filters.

Because of the independency of rotation operations with respect to the order n like stated in equations (3.15) and (3.16), as well as the independency of spherical Hankel functions regarding degree m, it is possible to rearrange the operations of the system (fig. 7).

One can see, that the distance coding blocks $\boldsymbol{H}_N^{-1}(s\Delta t_{r_M}|s\Delta t_{r_L})$ can be positioned towards the translation filter matrix $T(s\Delta t_{r_{ct}})$. In figure 20, the original and the rearranged block diagrams are illustrated.

As a result of the rearrangement, the two distance coding filter matrices $\boldsymbol{H}_N^{-1}(s\Delta t_{r_M})$ and $\boldsymbol{H}_N^{-1}(s\Delta t_{r_L})$ can be implicated into the translation filter matrix, so that every matrix

entry is multiplied with two inverse spherical Hankel functions. In figure (21) the matrix multiplication with the involved function orders is shown symbolically.

Due to these multiplications, the frequency response of each translation filter, which is mainly conditioned by the highest involved function order, is compensated by the inverse characteristics of the according distance coding filters (in the following also called compensation filters), thus it is possible to reduce the demands on exorbitant dynamic ranges.

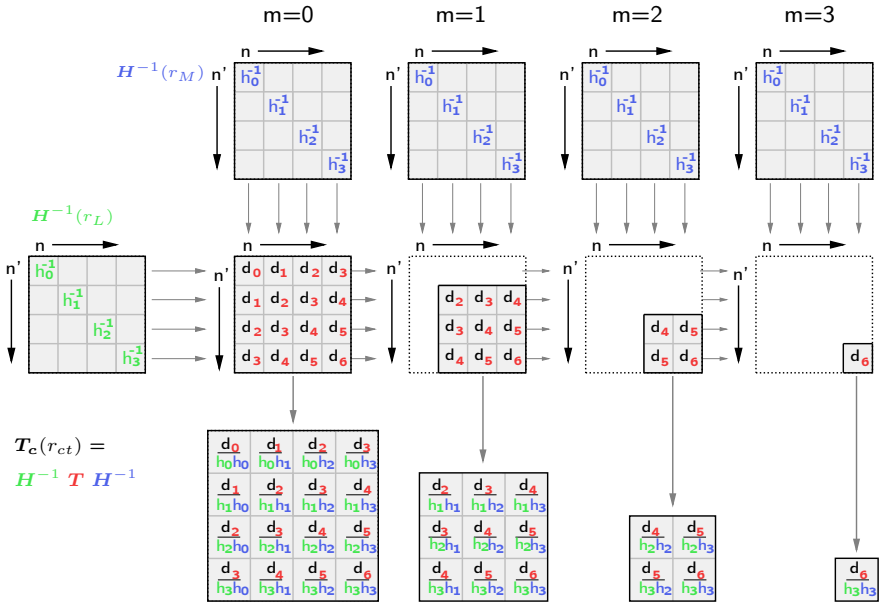

Figure 21 – Matrix multiplication of $\boldsymbol{T}(r_{ct})$ with $\boldsymbol{H}^{-1}(r_M)$ and $\boldsymbol{H}^{-1}(r_L)$. In $\boldsymbol{T}(r_{ct})$, the maximal order of involved spherical Hankel functions in each matrix entry is denoted.

A closer look at the behavior of a single spherical Hankel filter shows, that the frequency of each filters' near-/far-field intersection is dependent on the filter order and - as a scaling factor - the radius in the argument of the filter (4.8).

$$|h_n(kr)| \propto \begin{cases} \frac{(2n+1)!!}{(kr)^{n+1}} & \text{in the near-field for} \quad kr \ll 2 \\ \frac{1}{kr} & \text{in the far-field for} \quad kr \gg \frac{n(n+1)}{2} \end{cases} \tag{4.8}$$

Because of the frequency scaling property of the radii in the filter arguments, one can state that the frequency responses of the resulting, compensated translation filters are now dependent on the absolute displacement value r_{ct} and the radii r_M and r_L (i.e. the according time delays based on wave propagation $\Delta t_{r_M|r_L|r_{ct}}$) of the distance coding filters $\boldsymbol{H}_N^{-1}(s\Delta t_{r_M}|s\Delta t_{r_L})$ as can be seen in fig. 22. These facts are also reflected in the pole zero distributions of the involved filters. The positions of zeros of the translation filters are scaled in Laplace domain with the absolute displacement vector

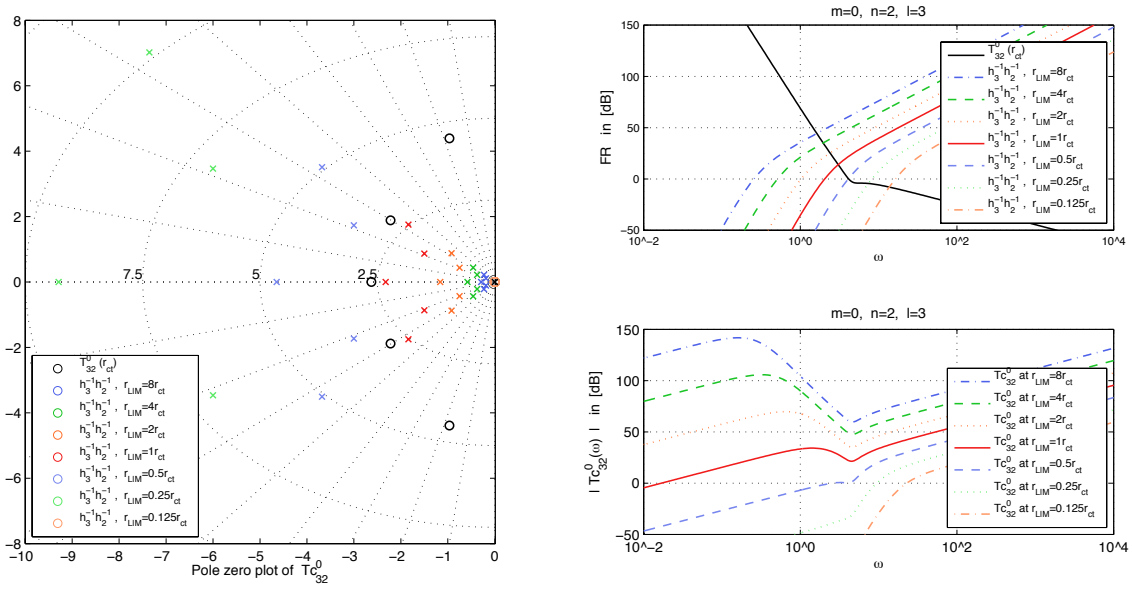

Figure 22 – Pole zero plots of a showcase translation filter T^0_{32} with dependent compensation filters scaled by different argument ratios on the left side. On the right hand side, each of the corresponding frequency responses (at the top) and the resulting compensated translation filters (at the bottom) for different value ratios are shown. The ratios are $r_{M|L} = r_{ct} \cdot 8, 4, 2, 1, 0.5, 0.25, 0.125$, $r_{ct} = 1m$.

r_{ct}. The occurring poles are located at the origin. The compensation filters behave complementarily, so that the locations of the poles are scaled by the values of $r_{M|L}$ and all zeros are placed at $s = 0$.

To achieve a minimum dynamic range, an optimum match of poles and zeros of translation and compensation filters is requested. Or in other words, the intersection frequencies of the involved filters (translation and compensation) has to be matched for an efficient and feasible implementation. Therefore, the scaling factors represented by the ratios of the parameters r_M, r_L and r_{ct} can be optimized. Figure 23 shows an example of frequency responses of compensated translation filters.

Finally it is apparent that all resulting compensation filters are proportional to ω. With a look at the Laplace domain representation of $h_n(s)$ it becomes clear, that this fact is caused by the multiplication of the two compensation filters, where two single zeros $\frac{1}{s}$ (inverted single poles) are always multiplied by one single pole (C.4).

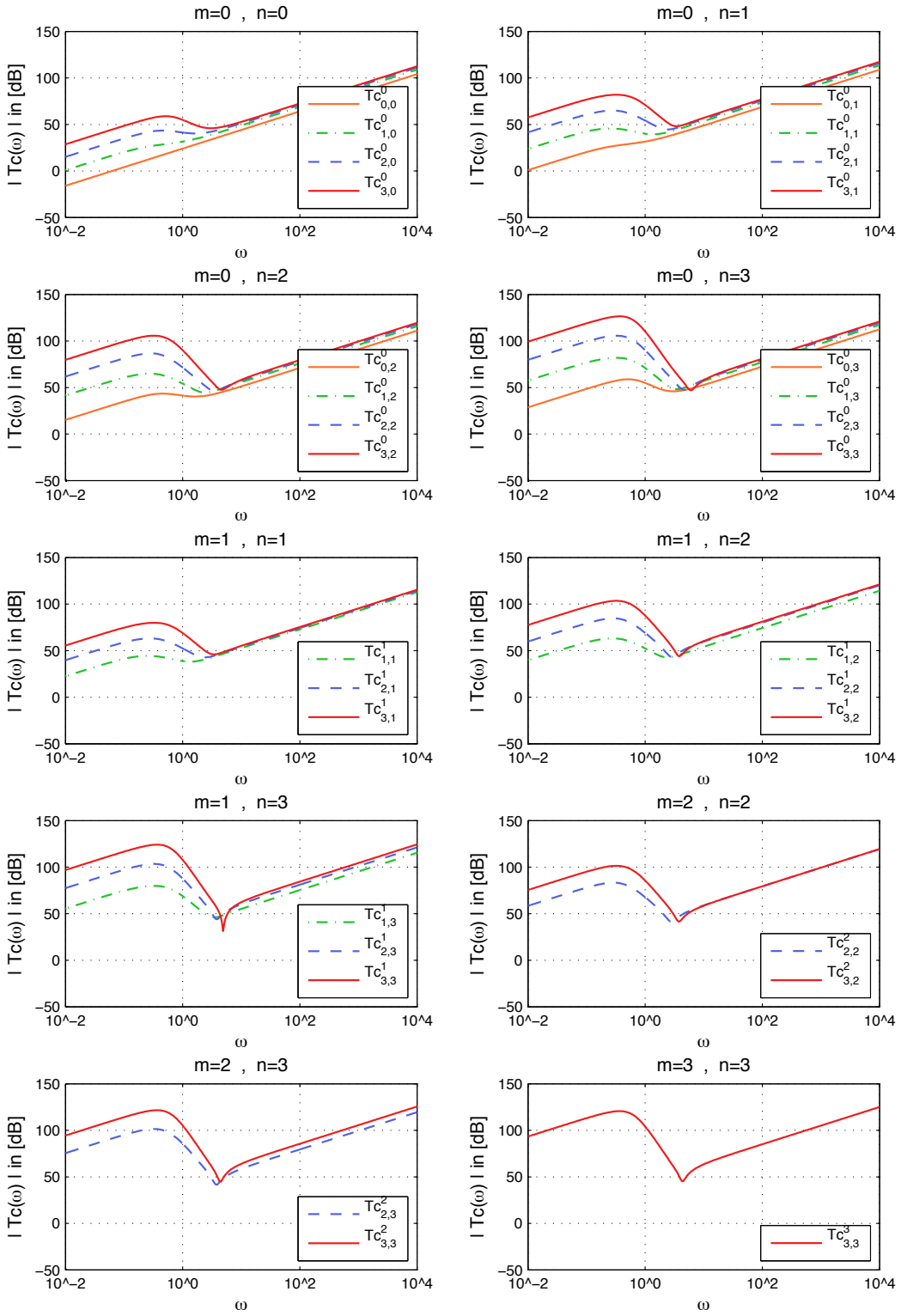

Figure 23 – Frequency responses of translation filters compensated with distance coding filters. In this example the values of the radii are $r_{ct} = 1m$, $r_M = r_L$ and $r_{M,L} = 4r_{ct}$.

4.1.2 Single Pole Compensation

The obtained compensated translation filters show a remaining ω-proportionality due to the compensation by distance coding blocks. The reason for this is the division by two Hankel functions which yields one zero too much in the characteristic polynomials of each filter, compared to a flat frequency response (cf. fig. 3.42).

All translation filters can be multiplied by $\frac{1}{s}$ to remove the proportionality from the translation matrix. The re-introduction of the filter operation can be more efficiently done in common for all resulting signals before or after the filter matrix. Resultant frequency responses are depicted in figure 24.

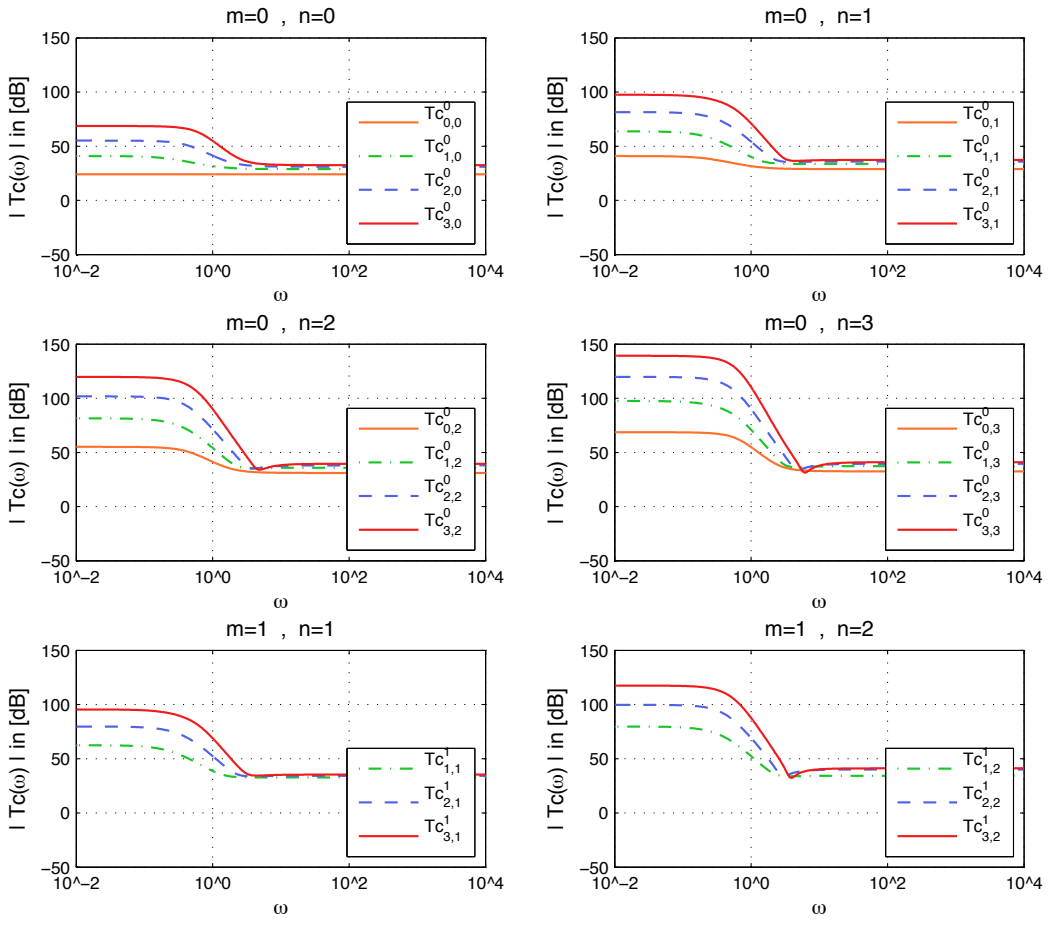

Figure 24 – Showcase frequency responses of the first few translation filters compensated with distance coding filters. The values of vectors are $r_{ct} = 1m$, $r_M = r_L = 4r_{ct}$. Furthermore, all translation filters were divided by s to simplify the translation filters.

All following considerations are done implicitly with the ω-slope pulled out of the translation filter matrix.

4.1.3 Integration of Radial Steering Filters

As we have seen in one of the latter sections, the resulting compensated coaxial translation filters are dependent on the translation vector r_{ct} and the radii of distance coding blocks $r_{M|L}$. To minimize the required dynamic range, a reasonable choice of the ratio of translation and compensation distances is desirable.

As can be seen exemplarily in fig. 25, the dynamic range can remarkably reduced by the choice of all vectors being the same length $r_{ct} = r_M = r_L = 1m$.

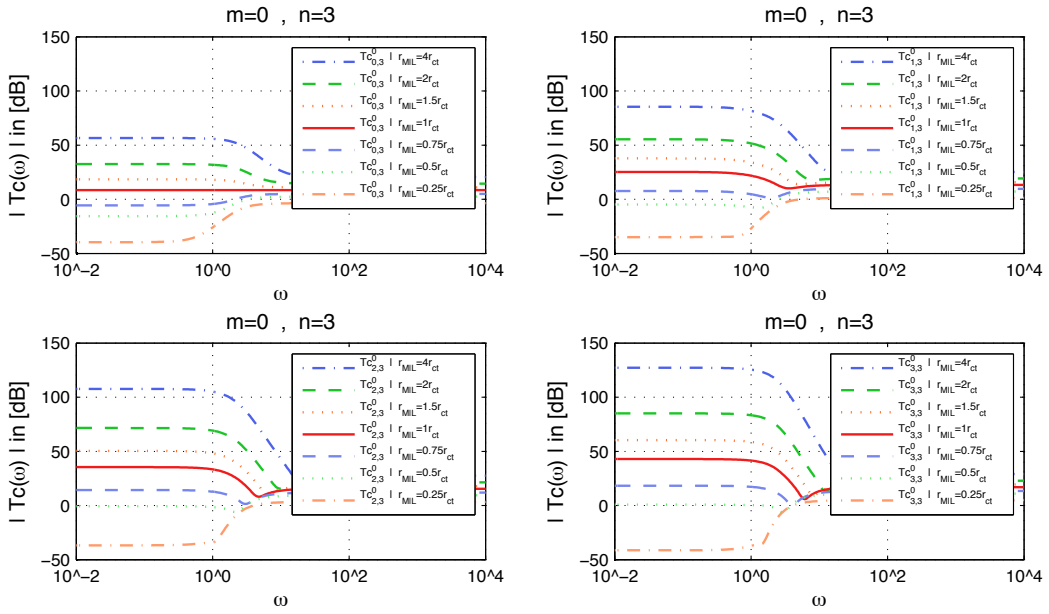

Figure 25 – Frequency responses of representatively compensated translation filters, each with different ratios $r_{M,L} = 4m, 2m, ..., 1m, ..., 0.25m$; $r_{ct} = 1m$.

To realize arbitrary parameter ratios for any displacements r_{ct}, radial steering filters as presented in sec. 1.1 can be used.

A spherical wave spectrum depending on the analysis radius r_M can be expanded by these RSFs to the arbitrary translation radius r_{ct} (eq. (4.9)) or to any other multiple radius of r_{ct}. The same procedure can be carried out at the synthesis side, thus the compensated translation filters can be scaled by the requested parameter ratio (eq. (4.10)).

$$\hat{\boldsymbol{\psi}}_N(r_{ct}) = diag\left\{\frac{h_n(r_{ct})}{h_n(r_M)}\right\}\hat{\boldsymbol{\psi}}_N(r_M) \tag{4.9}$$

$$\hat{\boldsymbol{\psi}}_N(r_L) = diag\left\{\frac{h_n(r_L)}{h_n(r_{ct})}\right\}\hat{\boldsymbol{\psi}}_N(r_{ct}) \tag{4.10}$$

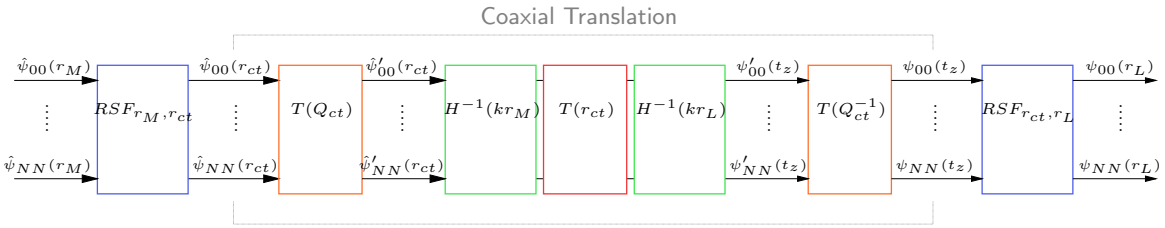

Figure 26 – With the usage of the radial steering filter, $\boldsymbol{H}^{-1}(r_{M|L})$ can be performed with $r_M = r_L = r_{ct}$ to assure a stabilization of modified translation matrix.

Thus, it is possible to set the ratios of scaling factors ($r_{ct|M|L}$) of the compensated coaxial translation filters for an arbitrary displacement to an optimum regarding the required dynamic range. The resulting block diagram is illustrated in fig. 26.

4.1.4 Parameter Optimization

The task of optimization depends very much on the particular goals and up to which function order the re-expansion is carried out.

A solution which is very easy to realize with the parameter ratio of $r_{ct} = r_{M|L}$, is illustrated above (fig. 25). Thereby, all filters for $m = 0, n = 0$ and all n' as well as matrix entries, which were obtained by symmetry properties of these entries ($m = 0, n' = 0$ and any n), consist of single weighted Hankel functions. As a consequence, the compensation filters exhibit the same near-/far-field intersection frequencies as the dependent compensation filters such that the resulting frequency responses are flat and have only constant gain factors. For all entries, consisting of a sum of Hankel filters (due to recurrences), the intersection frequencies of translation and compensation filters do not match any more and non-flat frequency responses with growing demands of dynamic ranges to higher orders are the result.

A more sophisticated approach is to use different parameter ratios for different function orders to reduce dynamic ranges at higher orders. With a closer look at figure 21, in combination with eq.(4.8), one can determine the scaling factors for the main diagonal of the compensated translation matrix regarding the different near-/far-field intersections of the corresponding filters. It yields

$$w_{scale} = \frac{((2d+1)!!)^{\frac{1}{d}}}{((2n_c+1)!!)^{\frac{1}{n_c}}}, \tag{4.11}$$

with d denoting the maximum involved filter order of the translation and n_c the involved function order of compensation filters. As can be seen in fig. 27, the dynamic range can be reduced tremendously for higher orders compared to an equal parameter ratio as shown above.

However, a regression in low orders can be observed due to an overcompensation, caused by too small arguments of the compensation filters. But in comparison to the advantages

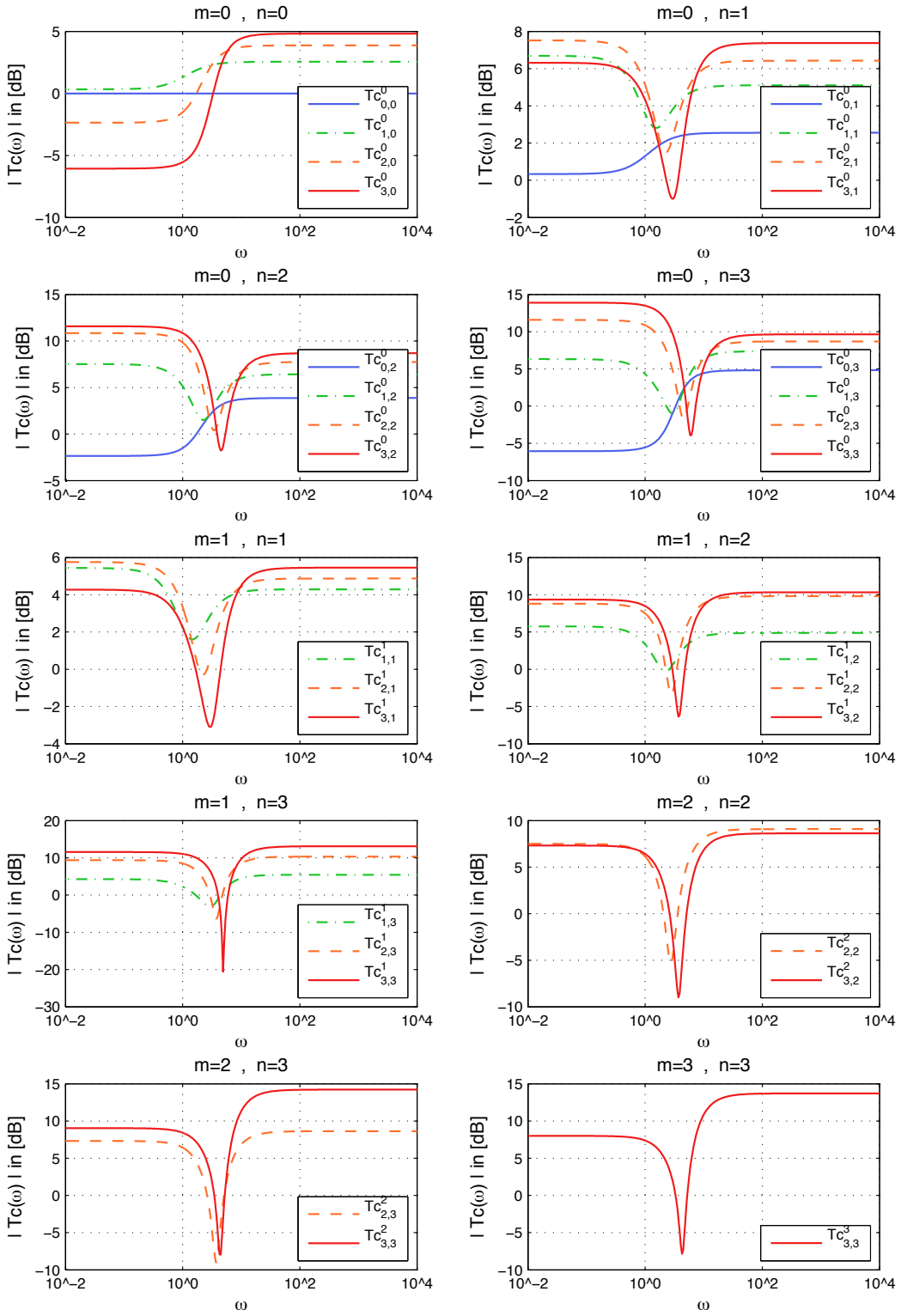

Figure 27 – Frequency responses of compensated translation filters. RSFs and thereby the compensation filters are scaled by eq.(4.11), which yields $r_{ct} = 1m = r_{M|L} \cdot [1, 1.2910, 1.4316, 1.5184]$.

achieved at higher orders without any further processing or filtering, this shortcoming is neglegible.

The drawback at low orders can be improved by an unequal scaling of analysis and synthesis side. Depending on the requirements that are set, various combinations can be implemented. For instance a ratio at the synthesis side of $r_{ct} = r_L$ and at the same time an increasing ratio for higher orders at the analysis side yield a better compensation of lower orders but fail at higher orders (fig. 28).

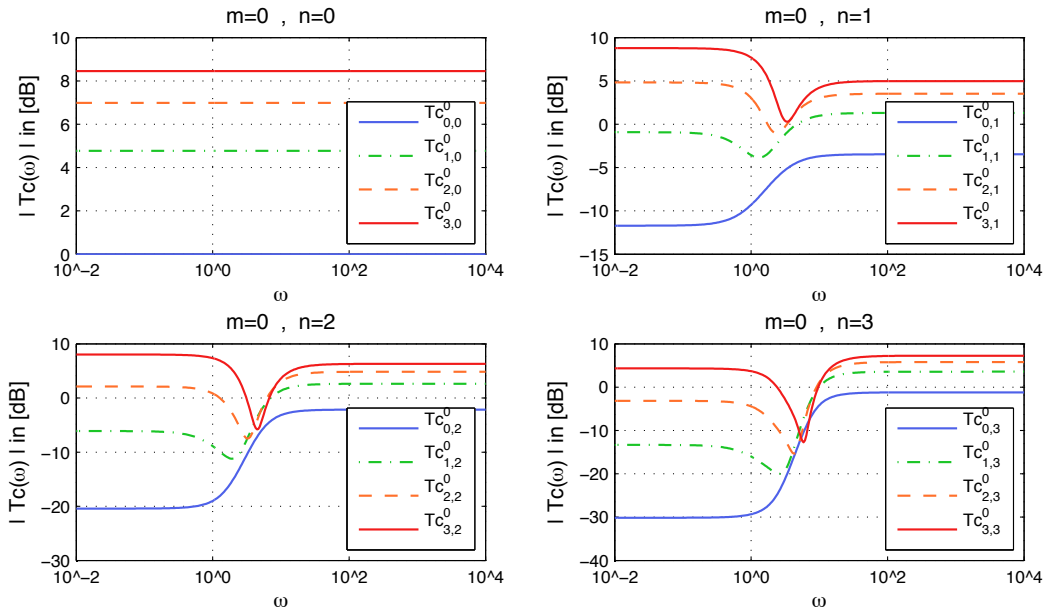

Figure 28 – Frequency responses of compensated translation filters. Compensation filters at synthesis side are parametrized with $r_{ct} = r_L$. RSFs and thereby the compensation filters at analysis side are scaled by eq.(4.11), which yields $r_{ct} = 1m = r_M \cdot [1, 2 \cdot 1.2910, 2 \cdot 1.4316, 2 \cdot 1.5184]$ with a doubling of higher order factors to counteract the under-compensation at the synthesis side.

A closer look at the frequency responses let suspect an optimal parameter ratio for each translation matrix entry, so that only a constant gain factor and for higher orders, normal and easy to realize peak/dip filters remain for each filter matrix entry. To implement such an individual parametrization, RSFs for each distinct matrix entry have to be applied to steer the spherical wave spectra dependent on m,n and n' to the required radii. After translation filtering this operation has to be carried out backwards for the synthesis side. As a consequence, the calculation costs due to the necessary matrix multiplications increase remarkably in comparison to the vector multiplication of the spherical wave spectra at the in- and outputs with the radial steering filters as illustrated in 21.

Due to the growing number of dependencies for translation filters of higher orders caused by the used recurrence relations, it is out of scope of this work to derive the general

optimum scaling factor for each individual translation matrix entry analytically, but for the first few filter orders, an empirically found optimum can be presented (fig. 29).

The scaling factors were determined as:

$$r_{ct} = 1m = r_{M|L} \cdot \begin{bmatrix} 1 & 1 & 1 & 1 \\ 1 & 1.41 & 1.442 & 1.4142 \\ 1 & 1.442 & 1.565 & 1.5848 \\ 1 & 1.4142 & 1.5848 & 1.651 \end{bmatrix} . \tag{4.12}$$

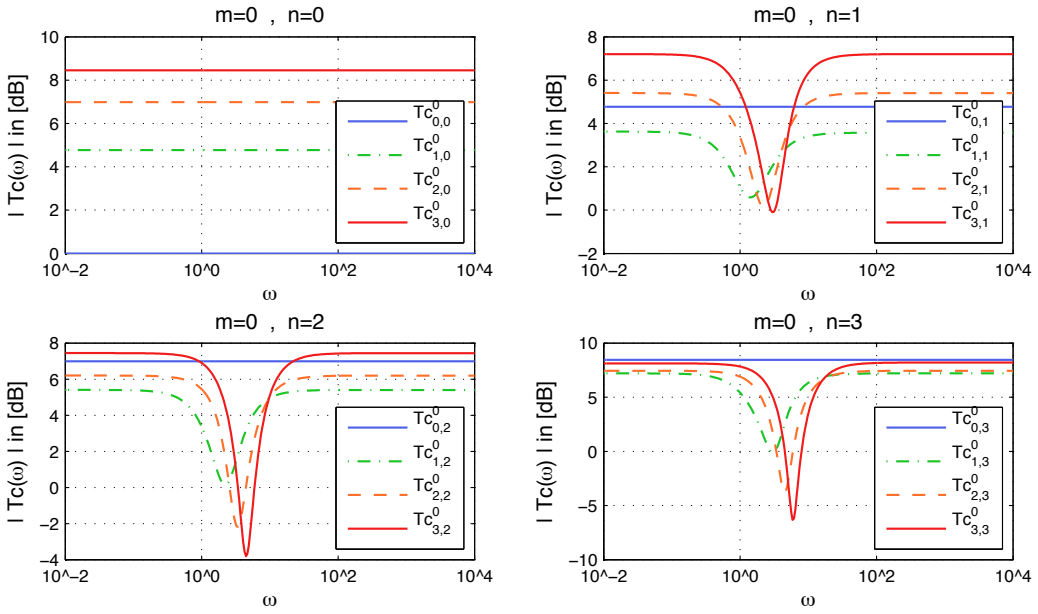

Figure 29 – Frequency responses of compensated translation filters. RSFs and thereby the compensation filters are scaled for each entry individually with the scaling factors stated in eq.(4.12).

Finally, the parameters of the peak/dip filters (bandwidth, center frequency and gain) can be implemented by a resulting biquad filter (cf. eq.(C.5)). The constant gain of each filter is dependent of the initialization factors (3.41) and constants of the recurrence relations (eq.(3.38),eq.(3.38)).

4.2 Singular to Singular or Regular to Regular Translations

The latter sections dealt with realizations of translating fields from outgoing to incoming ones (singular to regular). In the following, translations will be discussed, where the kinds of wave propagations or descriptions do not change, so that incoming persist incoming and outgoing remain outgoing fields. In sec. 3.3.1 we presented the basic structure of the translation matrix and its entries. It was mentioned, that for singular to singular or regular to regular translations, the entries of the translation matrix are weighted spherical Bessel functions of the first kind or weighted sums of them.

To realize discrete-time spherical Bessel filters implementing translations, one has to deal with yet other numerical problems. With a look at concrete formulations following the function definition of eq.(2.17), the first orders of spherical Bessel functions of the first kind can be written generally as [Wil99]

$$\begin{aligned} j_0(x) &= \frac{\sin x}{x}, \\ j_1(x) &= \frac{-\cos x}{x} + \frac{\sin x}{x^2}, \\ j_2(x) &= \frac{-\sin x}{x} - \frac{3\cos x}{x^2} + \frac{3\sin x}{x^3}, \\ j_3(x) &= \frac{\cos x}{x} - \frac{6\sin x}{x^2} - \frac{15\cos x}{x^3} + \frac{15\sin x}{x^4}. \end{aligned} \tag{4.13}$$

For small arguments and high function orders, the above exhibits a strong tendency towards divisions by zero and thereby an unstable behavior is the result. Moreover, a straight z-transform of spherical Bessel functions of higher orders, here defined in frequency domain, turns out to be complicated. In the following, possible realizations are discussed.

4.2.1 Moving Average Approach

For a straight forward implementation of time-domain spherical Bessel filters, each function order would have to be z-transformed by applying corrected impulse invariance method or a bilinear transform, which is not trivial especially for higher function orders. To do that in an easier and more efficient way, the recurrences (2.22) to (2.25) can be applied. With a closer look at the first few spherical Bessel function orders, one can see, that the zero order relates to a normal sinc function, here defined in frequency domain. Known from basic signal processing, a sinc function corresponds to a Fourier transform of a rectangular function, which can be interpreted as a moving average filter in the time domain. Thus initializing the recurrences with this moving average filter, further Bessel function filters can be obtained. The exact z-transform of the initializing MA can be found in appendix A.

The ideal impulse responses of the following filter orders would be alternating symmetrical (for even n and $n = 0$) and point symmetrical (for odd n) due to the sine and cosine

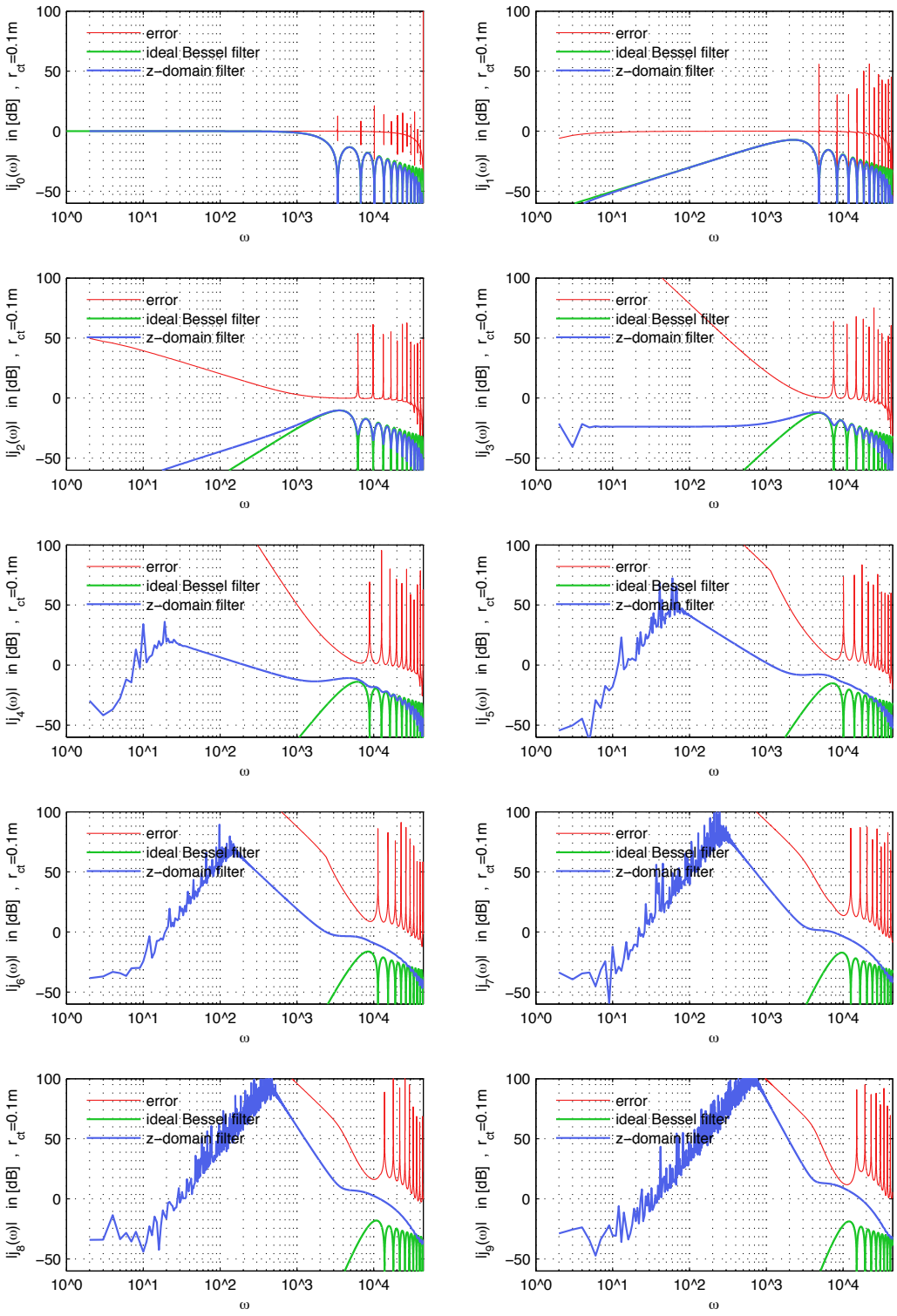

Figure 30 – Frequency responses of spherical Bessel filters of different orders calculated by (2.25) and a translation distance of $r_{ct} \approx 0.1m$ respectively $\Delta n = 13[sam]$.

terms in the frequency domain representation (4.13). $2\Delta n + n + 1$-zeros of the filter polynomials should be placed on the unit circle in the z-domain to reproduce the notches of the filters. Further zeros should compensate occurring poles in an appropriate way. The poles are ideally located at $z = 0$ and $z = 1$. The feasible resolution of translations Δr_{min} is dependent on the used sampling rate f_s and the according duration of one sample Δn, so that a resolution of

$$\Delta r_{min} = \frac{c}{f_s} = \frac{344}{44100} \frac{\frac{m}{sec}}{\frac{1}{sec}} \approx 0.0078m \tag{4.14}$$

with a sampling rate of $f_s = 44100Hz$ and an assumed wave propagation speed of $c = 344\frac{m}{s}$ can be employed. To realize differing translation radii, higher sampling rates or fractional delays have to be applied.

Three recurrence relations can be used for the calculations, eq. (2.22), (2.23) and (2.25). Different computation methods of these recurrences yield other numbers of poles and zeros as well as their distributions (especially around $z = 1$ and $z = -1$) and thereby, the performance regarding stability and precision of frequency responses are also different.

First option recurrence.
Using the recurrence relation (2.25) in z-domain, initialized with (A.12),

$$f_{n+1}(z) = \frac{nz}{(z-1)} f_n(z) - f'_n(z), \tag{4.15}$$

results in a generally good distribution of zeros at or near by the unit circle in z-domain. However for increasing filter orders, the zeros get departed away from the unit circle, so that the frequency responses are flattened more and more, and the compensation of poles and the overall gain get also worse. Moreover, the numerical problems occur at small frequencies caused by a multitude of poles around $z = 1$ and neighbored zeros. The impulse responses are unsuitable especially for higher orders (fig. 35). Resulting frequency responses, compared to the ideal ones are illustrated in fig. 30.

Second option recurrence.
The second possible recurrence

$$f_{n+1}(z) = \frac{n f_{n-1}(z) - (2n+1) f'_n(z)}{(n+1)}, \tag{4.16}$$

is also initialized with (A.12) and the first order function calculated by (2.23). Furthermore, differentiation is used for the computation again. The same number of poles as in the first case is the result. The number of zeros is generally larger than in the first realization, but they are placed more disadvantageous as can be seen in fig. 37. As a consequence, the overall gain at higher orders is even worse and the flatness of the frequency responses is comparable to the first implementation (fig. 36).

Third option recurrence.
Using the last possible recurrence relation (2.22)

$$f_{n+1}(z) = \frac{(2n+1)z}{(z-1)} f_n(z) - f_{n-1}(z), \tag{4.17}$$

initialized with (A.12) and the first order function (2.25), it is possible to avoid numerical problems at low frequencies that affected the other recurrences due to multitude of poles near $z = 1$ generated by differentiation, fig. 39. Despite the improved stability the frequency matching is inferior to the other recurrences (fig. 38).

All of the implementations possess inaccuracies regarding the match of notch frequencies as well as distinct problems at small arguments. Especially the resulting distribution of the poles and zeros around $z = 1$ is complicated. Particularly considering the results of the first and second recurrence, the issue is strongly pronounced.

4.2.2 Time Reversal Approach

Another possibility to realize a discrete time-domain spherical Bessel filter of the first kind is to use the spherical Hankel functions and filters. As discussed in sec. 2.2, the Bessel function can be written as the real part of the corresponding Hankel function. Consequently, the z-domain representation can be expressed as

$$\begin{aligned} j_n(z) =& \mathcal{Z}\{\mathcal{R}\{h_n(s)^{(2)|(1)}\}\} && (4.18)\\ =& \mathcal{Z}\{\frac{1}{2}[h_n(s) + h_n^*(s)]\} && (4.19)\\ =& \frac{1}{2}\Big(\mathcal{Z}\{h_n(s)\} + \mathcal{Z}\{h_n^*(s)\}\Big) && (4.20)\\ =& \frac{1}{2}\Big(\mathcal{Z}\{h_n(s)\} + \mathcal{Z}\{h_n(s)\}^*\Big). && (4.21) \end{aligned}$$

Considering the complex conjugate, used in eq.(4.18) and assuming real valued filter coefficients, it can be asserted that $\mathcal{Z}\{h_n(s)\}^*$ is the time reversal of $\mathcal{Z}\{h_n(s)\}$.

$$\begin{aligned} X^*(z) &= \sum_{n=-\infty}^{\infty} (x[n]z^{-n})^* = \sum_{n=-\infty}^{\infty} x^*[n]z^n && (4.22)\\ &= \sum_{n=-\infty}^{\infty} x^*[n]z^n = \sum_{n=-\infty}^{\infty} x^*[-n]z^{-n}. && (4.23) \end{aligned}$$

With this the z-transform $j_n(z)$ can be calculated analytically by complex conjugate Hankel filters representing the time reversals in z-domain. The derivation is carried out in appendix D and the results for this implementation can be seen exemplarily in the following frequency responses (fig. 31). A complete set of frequency responses can be found in the appendix (fig. 40).

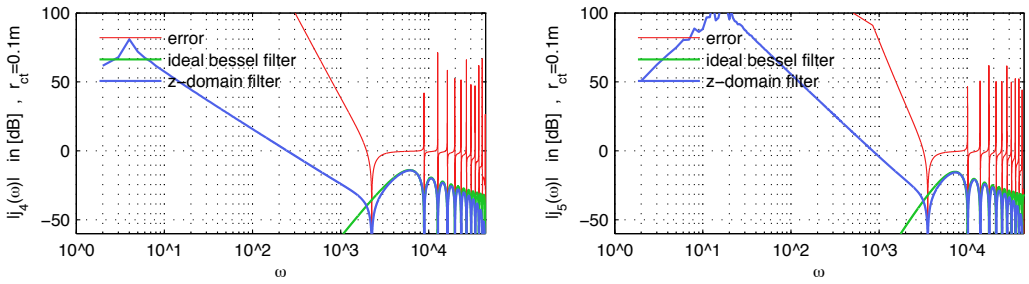

Figure 31 – Frequency responses of spherical Bessel filters of fourth and fifth order calculated with usage of the time reversal approach. The translation distance is $r_{ct} \approx 0.1m$ respectively $\Delta n = 13[sam]$.

Obviously this kind of implementation is much more accurate in terms of frequency response match and the reproduction of the depth of occurring notches compared to the recurrence implementations. However, it shows a more unstable behavior for small arguments because of the multitude of poles around $z = 1$ (cf. fig.32).

This problem can be solved by low cut filters or compensations as described in sec. 4.1.1. Considering the high pass filter solution, the error and the numerical problems can be minimized by a low cut filtering with a filter order

$$n_{hp} = 2(n - 1), \tag{4.24}$$

where n denotes the Bessel filter order and n_{hp} denotes the according low cut filter order. The cut-off-frequency can be set to the corresponding frequency of the zero which is closest to $z = 1$. Resulting frequency responses are illustrated below (fig. 33).

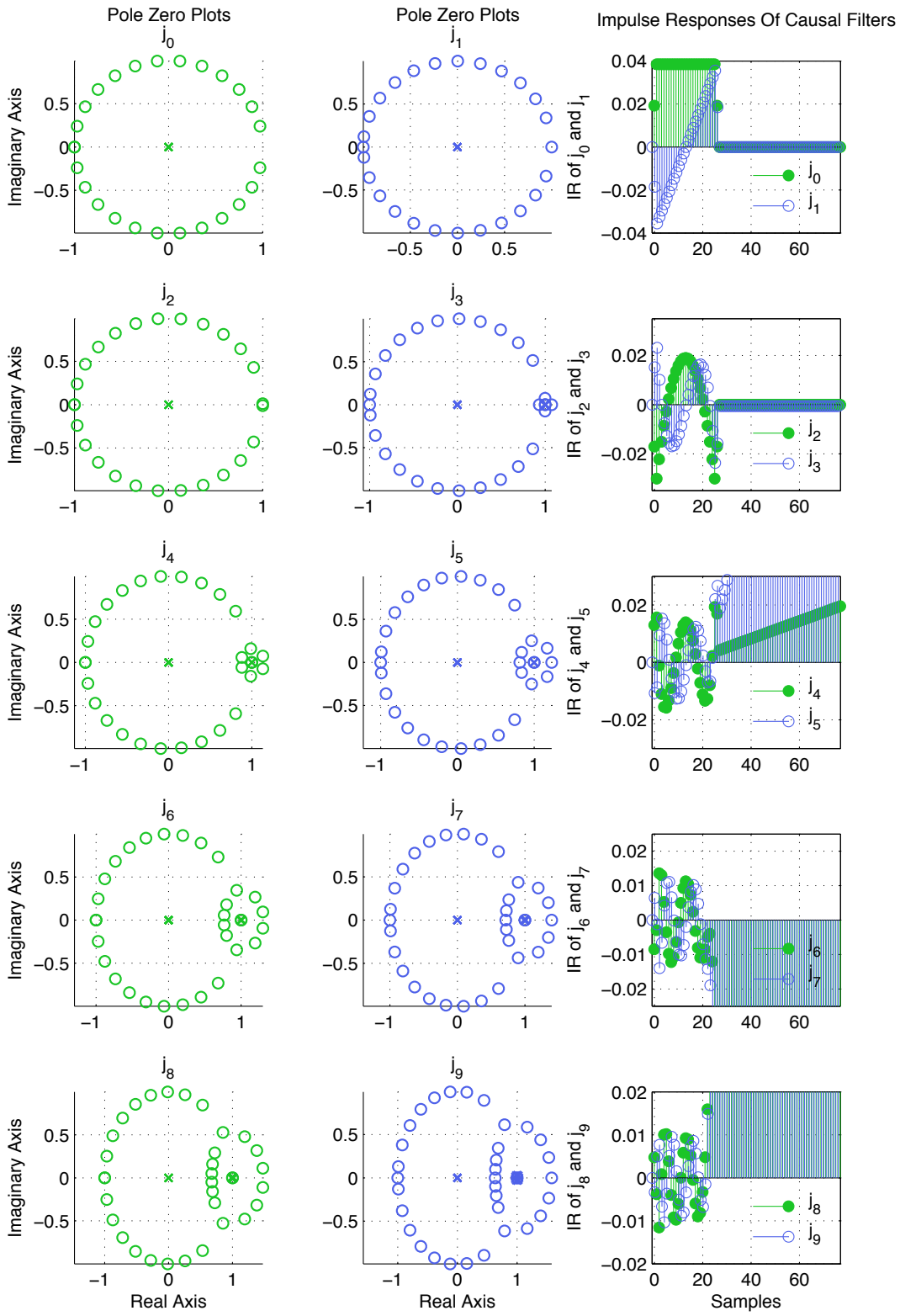

Figure 32 – Impulse responses and corresponding pole zero plots of spherical Bessel filters of different orders calculated by using the time-reversal representation of spherical Hankel filters ($r_{ct} \approx 0.1m$).

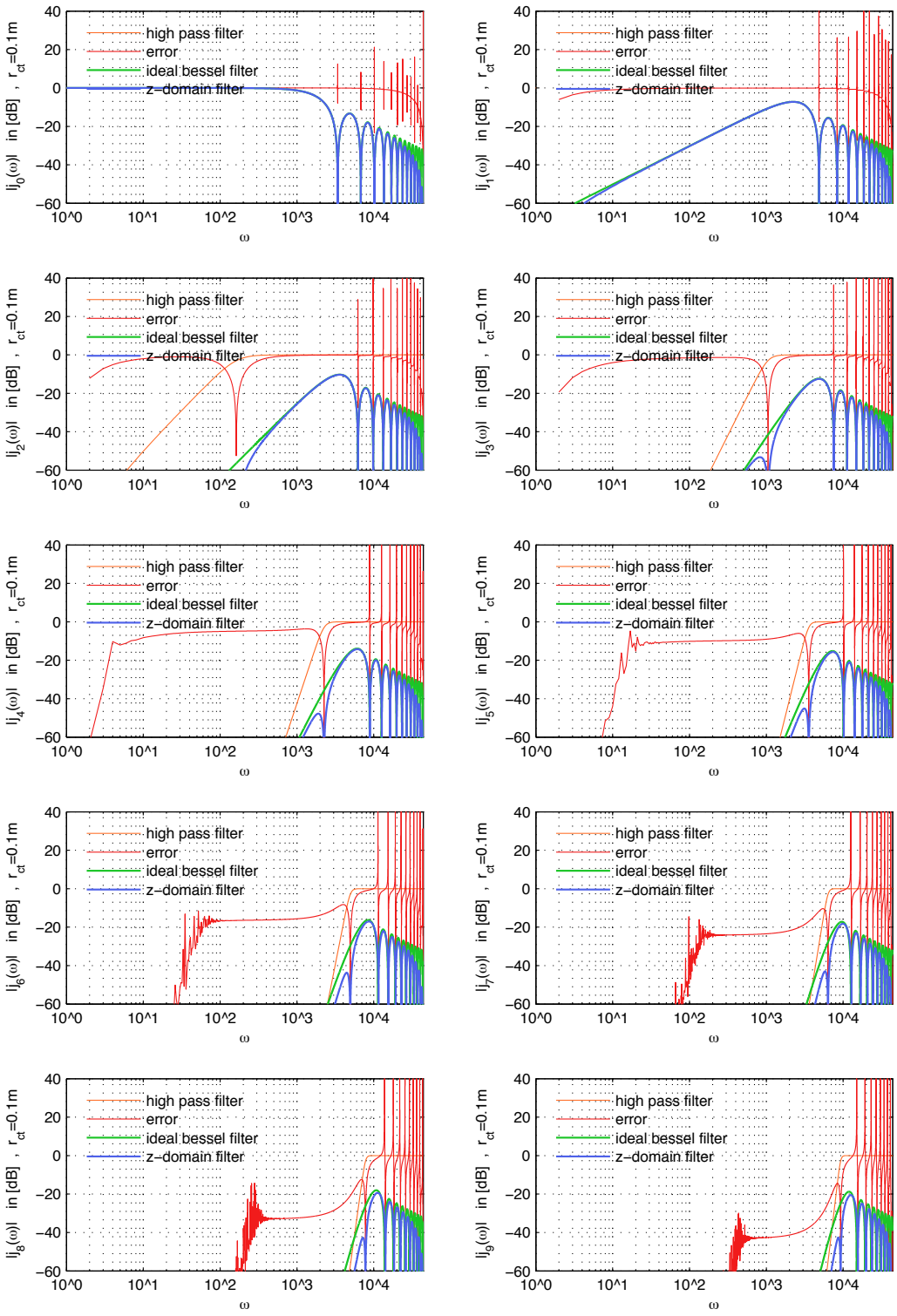

Figure 33 – Frequency responses of spherical Bessel filters of different orders calculated with usage of the time reversal Hankel function. The translation distance is $r_{ct} \approx 0.1m$ respectively $\Delta n = 13[sam]$. All filters were low cut and thereby stabilized.

5 Conclusion and Outlook

In this thesis, implementation methods for translating acoustic sound fields in spherical coordinates with discrete time domain IIR-filters were investigated .

Thereby it was found, that within an Ambisonics system, the very high dynamic ranges of spherical Hankel filters used for translations, where outgoing fields become incoming ones, can be compensated basically by restructuring of the signal path. In doing so, the distance compensations are considered inside the translation filter matrix with a beneficial stability effect. As a result, each translation filter can be compensated by two inverse spherical Hankel filters according to the distance coding blocks. The ratio of the obtained distances (translation distance and radii of microphone and loudspeaker arrays) is acting as a scaling factor for the compensation. We have seen that (almost) arbitrary ratios can be realized by usage of radial steering filters. The ratio where all distances are the same ($r_M = r_L = r_{ct}$) is the easiest implementation. To improve the compensation, different ratios according to the involved function orders can be employed. Although an optimal scaling factor that is individual for each translation matrix entry is possible, the analytical derivation of these factors remains to be done in future work. This would enable to reduce the translation filters to basic peak-dip-filters and constant gain factors as illustrated in 4.1.4.

Translations, that leave outgoing fields outgoing or incident fields incident, the spherical Bessel functions are required. Implementing these functions as discrete time domain filters, it was ascertained, that an implementation with spherical Hankel filters and their time reversal in combination with high pass filters achieve the best results in accuracy and numerical stability.

5.1 Time Domain Simulation

A simple time-domain simulation using the derived IIR-filters can be presented to conclude the achievements of this thesis. In this showcase, an Ambisonics system as illustrated in fig. 2.4 is used.

Thus, the original sources are assumed to be an ideal monopole and quadrupole recorded with a spherical microphone array with a radius of $r_M = 1m$. In this example the sources should be translated from the origin of the coordinate system to $z = 1$, so that $r_M = r_{ct} = 1m$. For the sound field reproduction an Ambisonics system with 204 virtual loudspeakers located on a spherical surface with the radius $r_L = r_{ct} = 1m$ is employed. Consequently, the assumption of a compensation scaling factor of one ($\frac{r_{ct}}{r_M r_L} = 1$) is maintained. For an optimal distribution, the exact positions of the virtual sound sources (loudspeakers) are determined by a so-called "t-design" (cf. [Zot09]). The simulation is carried out exactly as described in sec. 2.4 with a sampling rate of $f_s = 22050Hz$, so that a spatial resolution of $\Delta r_{min} \approx 15.6mm$ can be achieved. As a result, the following pictures show an impulse responses of the loudspeaker system respective to time.

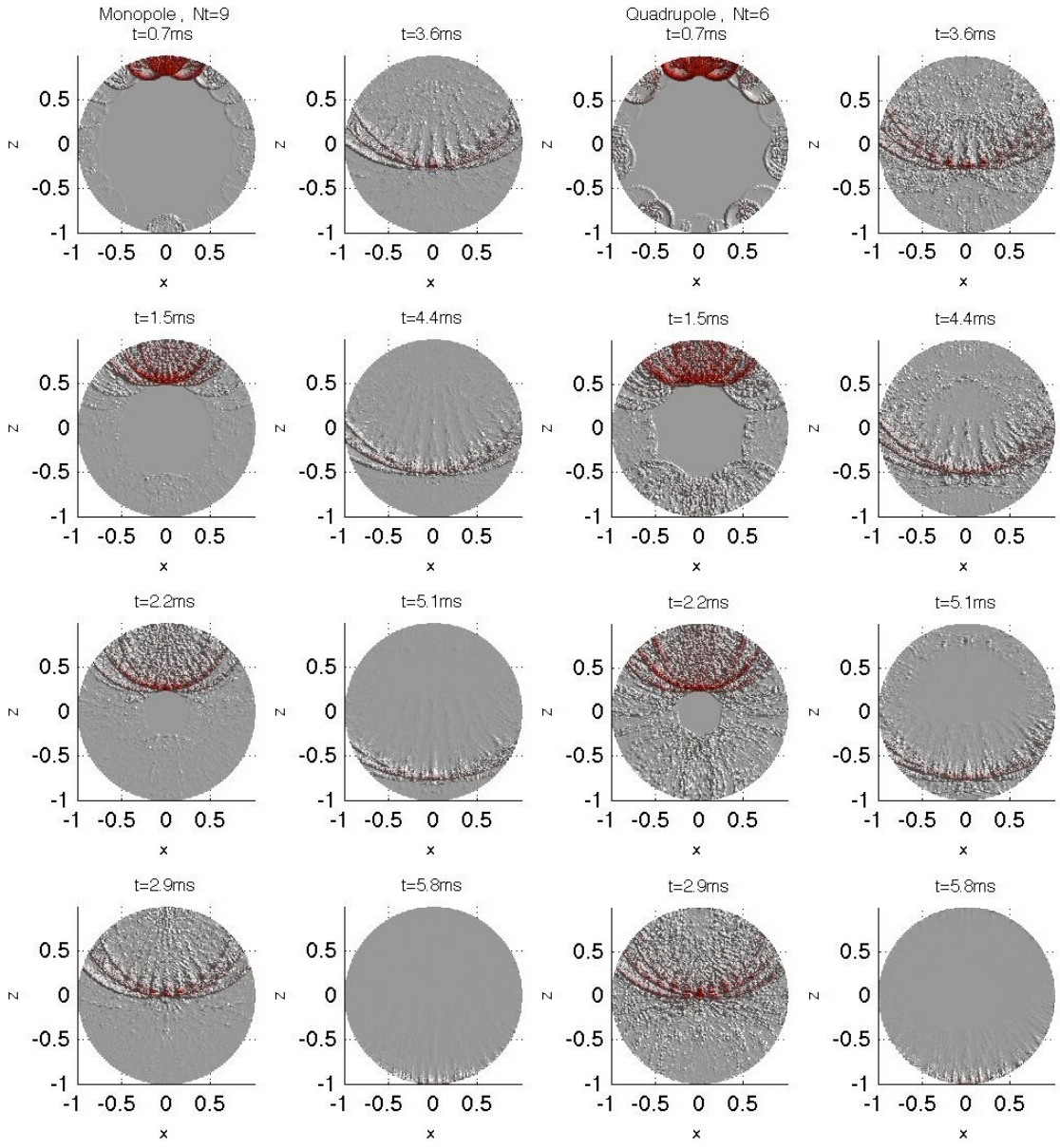

Figure 34 – Impulse response respective to time of the Ambisonics system with 204 virtual loudspeaker and a monopole (on the left hand side) and a quadrupole (on the right hand side) each translated to $z = 1$. The order of truncation is $N_t = 9$ for the monopole and $N_t = 6$ for the quadrupole.

As shown in fig. 34, the translation filters are able to reproduce the wave front at least around the center of the coordinate system. However, an increasing error arise with decreasing wave lengths (cf. 3.47). Thus, the higher the frequency, the smaller is the sweet area, where the reproduced sound field matches the desired one. Moreover, the infinite impulse responses and their decay of the involved spherical Hankel filters for

translation can be seen as well as spatial aliasing (depending on angular resolution of the loudspeaker setup) become manifest in the multitude of wave fronts.

5.2 Future Work

On the one hand, the computational efficient implementation of these translation methods in real-time applications will be a future task. This will enable an auralization of sound source movements for sound reinforcement systems as well as the implementation of shadowing and reflection effects caused by objects in the sound field.

On the other hand the implementations are seminal in the fields of numerical acoustics. Conventional boundary element methods will be able to be replaced by time domain applications in the future. Thus, computational costs for complex simulation scenarios could be decreased as well as the inherent broad-band simulation constitutes a clear advantage over conventional numerical methods. Especially in acoustics, where we deal with a large range of wave lengths, interaction effects of sound waves with objects can be described much more accurately by broad band simulations.

A Derivation of Zero Order Spherical Bessel Filter in Z-Domain

Calculating z-domain representation of spherical Bessel function zero order

Inverse Fourier transform:

$$j_0(kr) = \frac{sin(kr)}{kr} = \frac{sin(\omega\Delta t)}{\omega\Delta t} \tag{A.1}$$

$$= \frac{1}{\omega\Delta t} sin(\omega\Delta t) = \frac{1}{2i\omega\Delta t}(e^{i\omega\Delta t} - e^{-\omega\Delta t}) \tag{A.2}$$

$$= \frac{1}{2\Delta t}\int_{-\Delta t}^{\Delta t} e^{-i\omega t}dt = \frac{1}{2\Delta t}\int_{-\infty}^{\infty} \Pi_{\Delta t} e^{-i\omega t}dt \tag{A.3}$$

Discretization:

$$\Pi_{\Delta t}(t) = \frac{1}{2\Delta t}\begin{cases} 1 & , \|t\| < \Delta t \\ \frac{1}{2} & , \|t\| = \Delta t \\ 0 & , \|t\| > \Delta t \end{cases} \tag{A.4}$$

$$\Pi[n] = \Pi_{\Delta t}(t) \sum_{n=-\infty}^{\infty} \delta(t - nT_s) \tag{A.5}$$

$$\Pi_{\Delta n}[n] = \frac{1}{2\Delta n}\begin{cases} 1 & , \|n\| < \Delta n \\ \frac{1}{2} & , \|n\| = \Delta n \\ 0 & , \|n\| > \Delta n \end{cases} \tag{A.6}$$

$$\Pi_{\Delta n}(z) = \sum_{n=-\infty}^{\infty} \Pi[n] z^{-n} = j_0(z) \tag{A.7}$$

z-Transform (CIIM):

$$\Pi_{\Delta n}[n] = \frac{1}{2\Delta n}\Big(Tu[n+\Delta n] - \frac{T}{2}\delta[n+\Delta n]\Big) - \frac{1}{2\Delta n}\Big(Tu[n-\Delta n] - \frac{T}{2}\delta[n-\Delta n]\Big) \tag{A.8}$$

$$\updownarrow\mathcal{Z}$$

$$j_0(z) = \frac{1}{2\Delta n}\Big(\frac{T}{2}\frac{1+z^{-1}}{1-z^{-1}}\Big)z^{\Delta n} - \frac{1}{2\Delta n}\Big(\frac{T}{2}\frac{1+z^{-1}}{1-z^{-1}}\Big)z^{-\Delta n} \tag{A.9}$$

$$= \frac{1}{2\Delta n}\Big(\frac{T}{2}\frac{1+z^{-1}}{1-z^{-1}}\Big)(z^{\Delta n} - z^{-\Delta n}) \tag{A.10}$$

$$= \frac{T}{4\Delta n}\Big(\frac{z^{\Delta n} + z^{\Delta n-1} - z^{-\Delta n} - z^{-\Delta n-1}}{1-z^{-1}}\Big) \tag{A.11}$$

$$= \frac{T}{4\Delta n}\Big(\frac{z^{2\Delta n+1} + z^{2\Delta n} - z - 1}{z^{\Delta n+1} - z^{\Delta n}}\Big) \tag{A.12}$$

B Spherical Bessel Filter

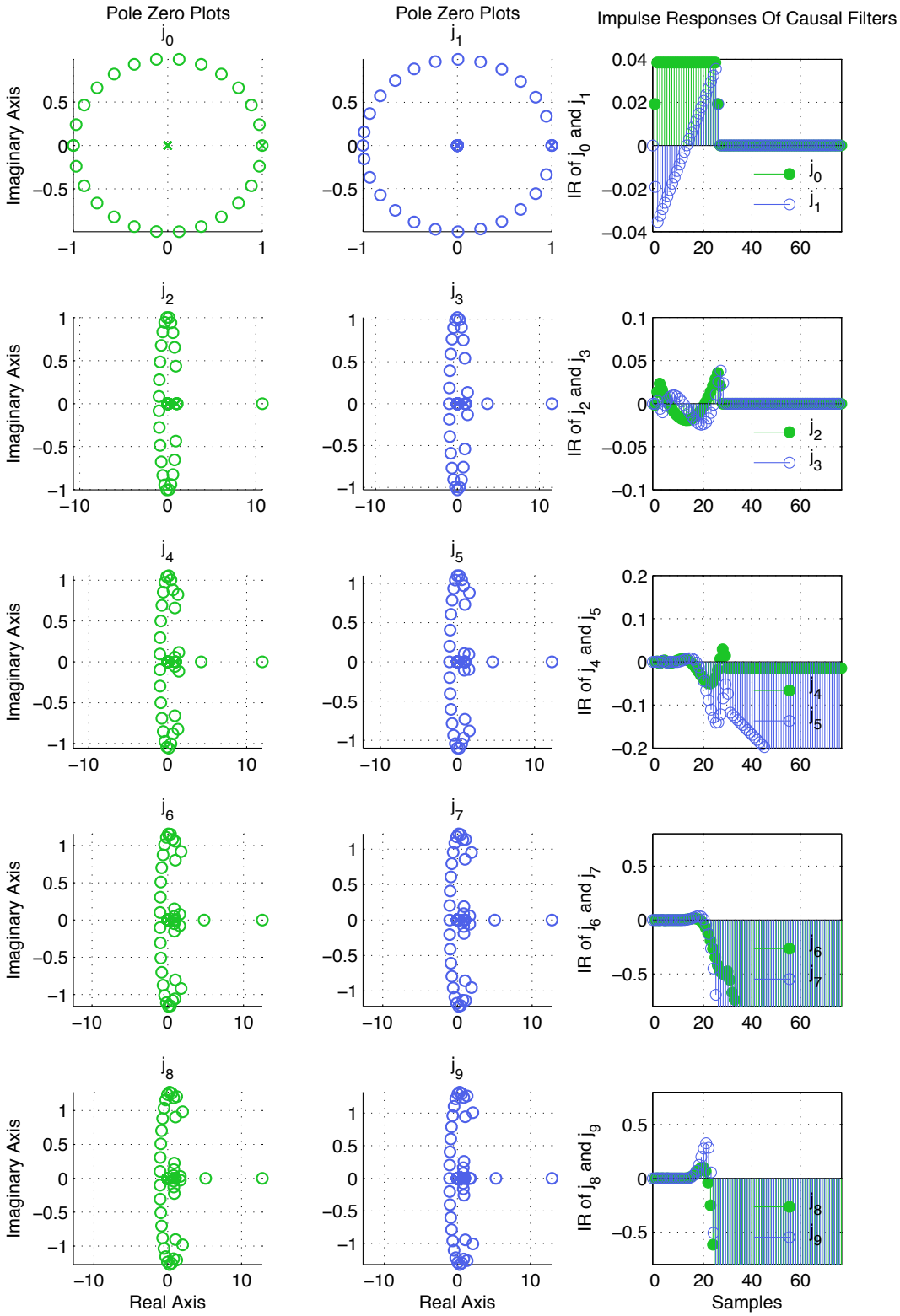

Figure 35 – Impulse responses and corresponding pole zero plots of spherical Bessel filters of different orders calculated by the first recurrence realtion (2.25) and a translation distance of $r_{ct} = 0.1m$ respectively $\Delta n = 13[sam]$.

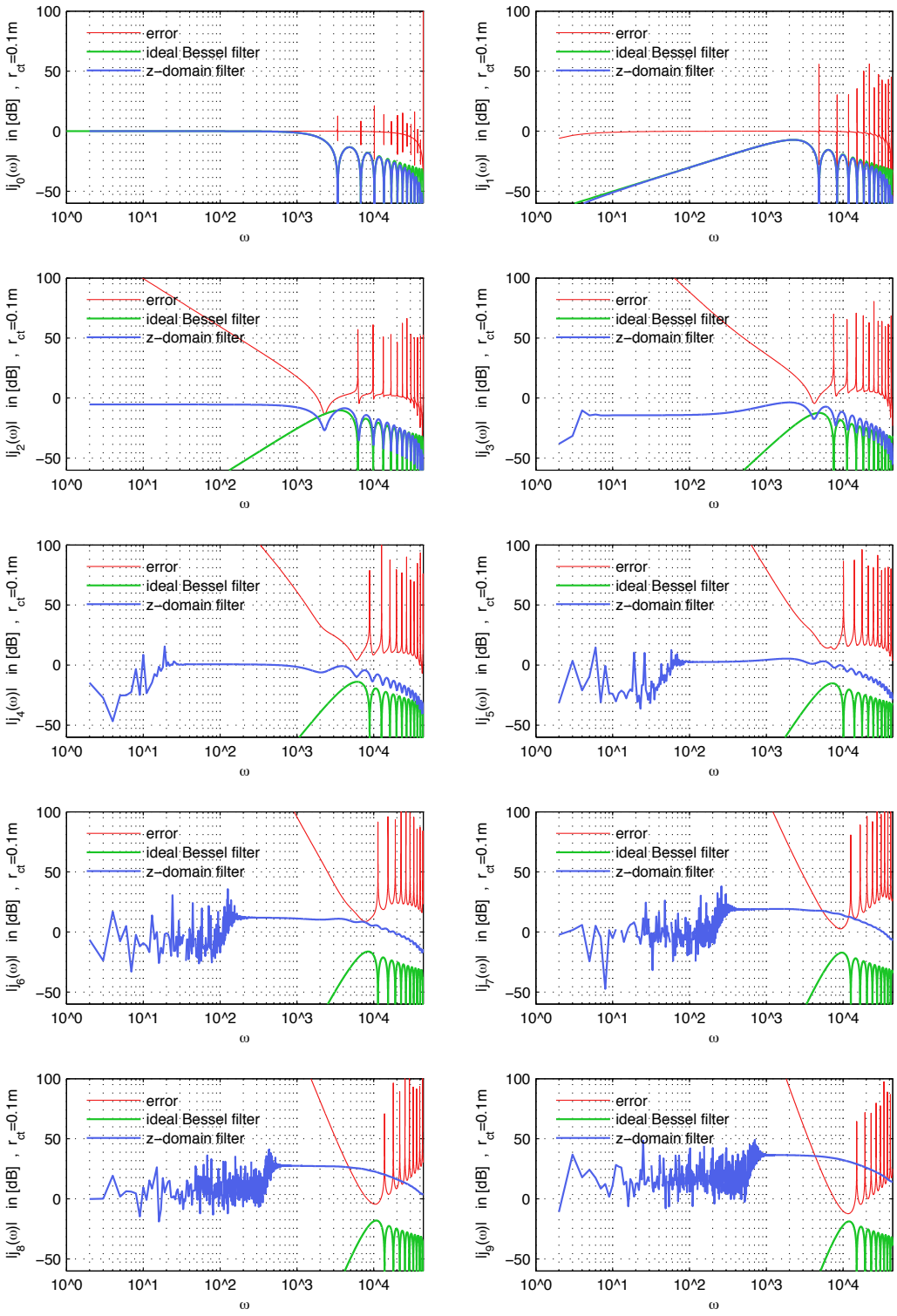

Figure 36 – Frequency responses of spherical Bessel filters of different orders calculated by the second recurrence relation (2.23) and a translation distance of $r_{ct} \approx 0.1m$ respectively $\Delta n = 13[sam]$.

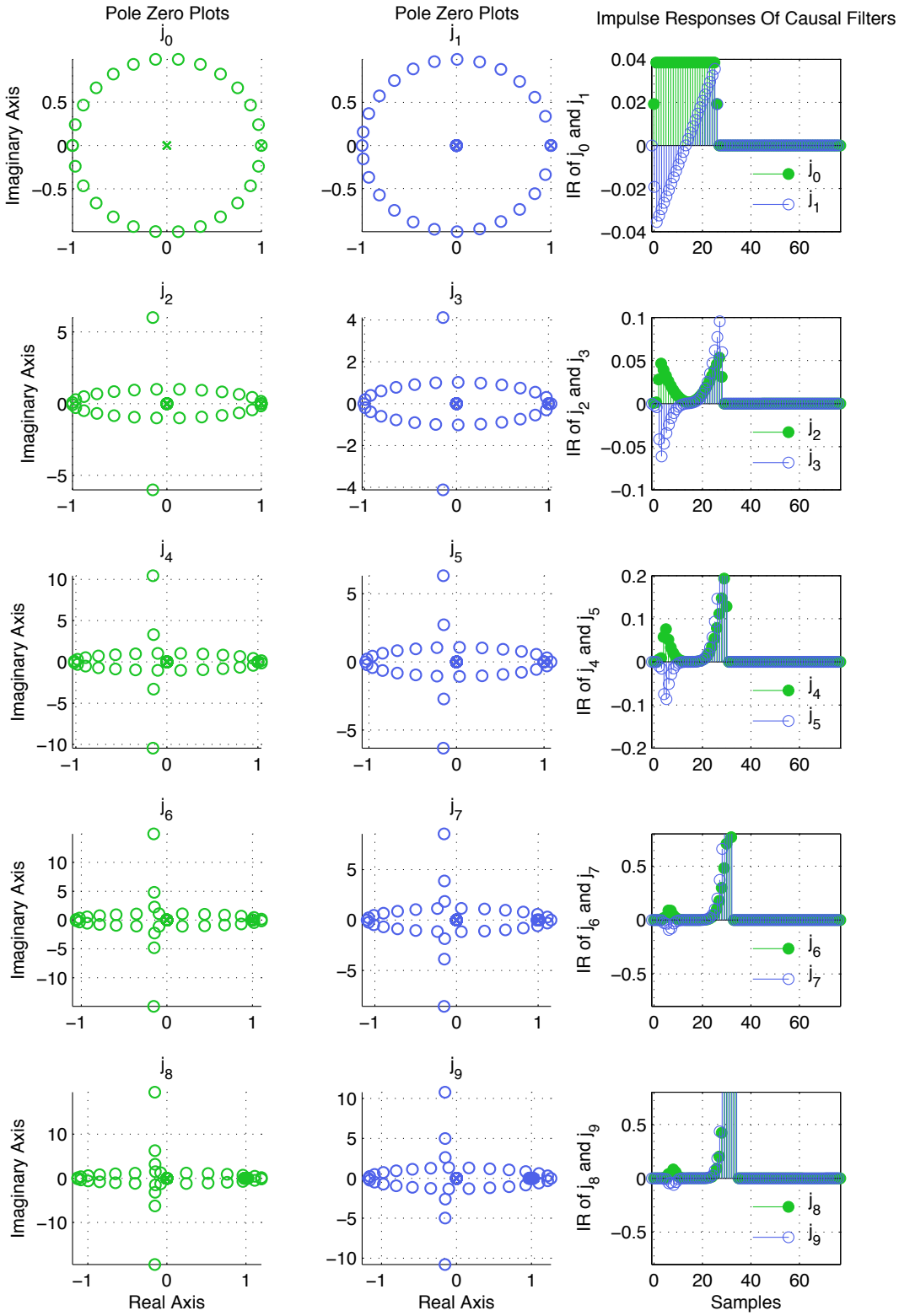

Figure 37 – Impulse responses and corresponding pole zero plots of spherical Bessel filters of different orders calculated by the second recurrence relation (2.22) and a translation distance of $r_{ct} \approx 0.1m$ respectively $\Delta n = 13[sam]$.

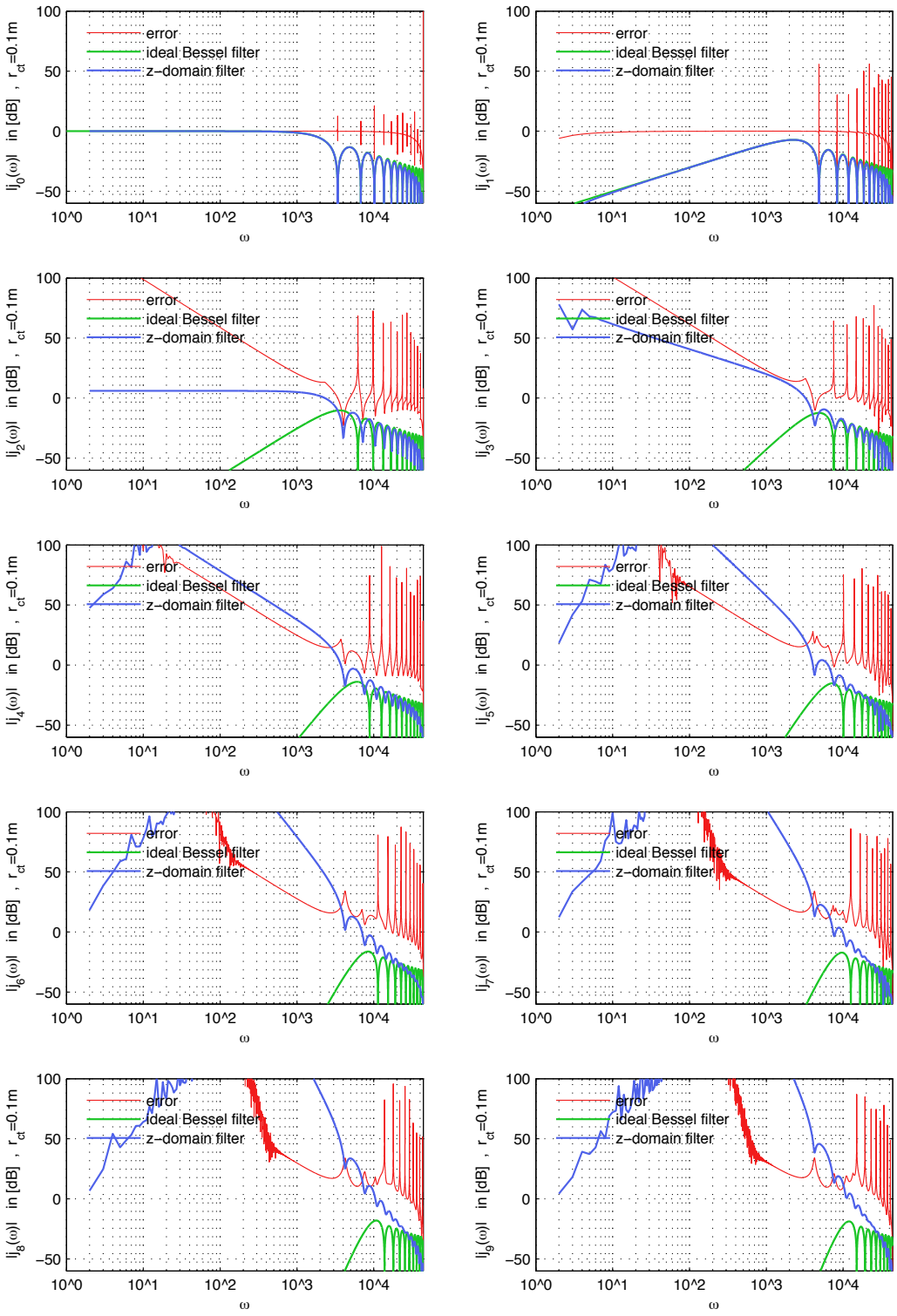

Figure 38 – Frequency responses of spherical Bessel filters of different orders calculated by the third recurrence relation (2.22) and a translation distance of $r_{ct} \approx 0.1m$ respectively $\Delta n = 13[sam]$.

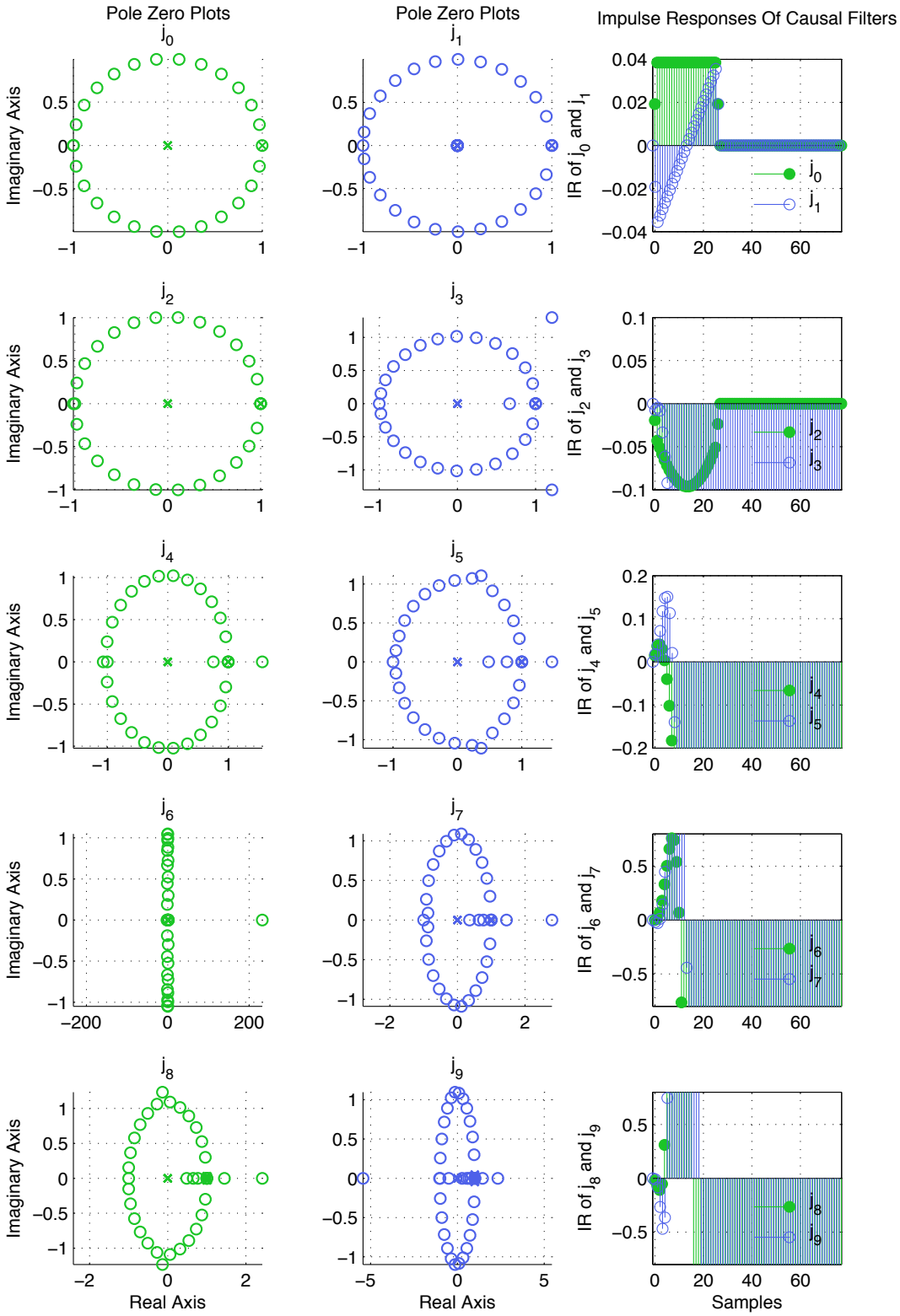

Figure 39 – Impulse responses and corresponding pole zero plots of spherical Bessel filters of different orders calculated by the third recurrence relation (2.23) and a translation distance of $r_{ct} \approx 0.1m$ respectively $\Delta n = 13[sam]$.

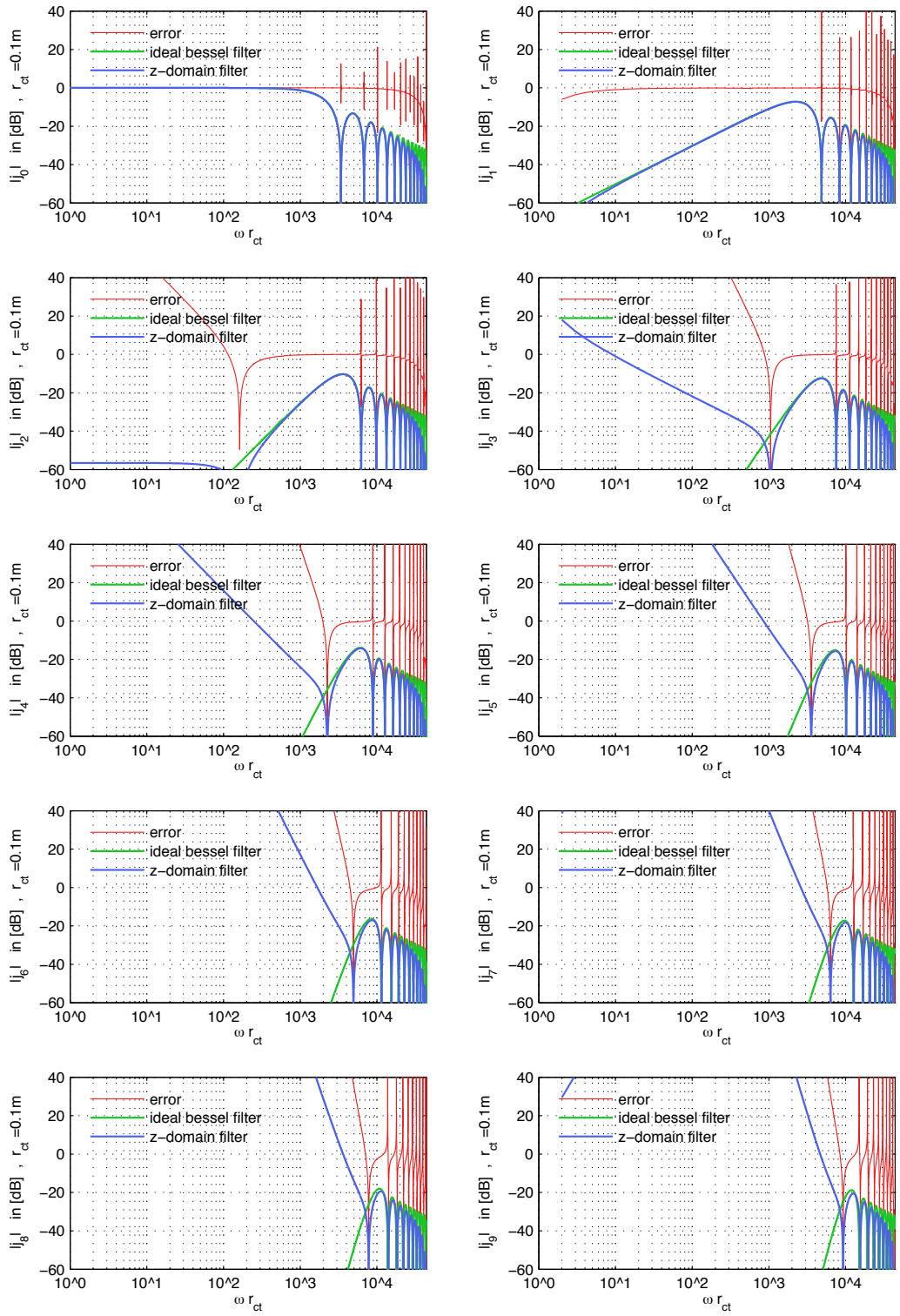

Figure 40 – Frequency responses of spherical Bessel filters of different orders calculated with usage of the time reversal approach. The translation distance is $r_{ct} \approx 0.1m$ respectively $\Delta n = 13[sam]$.

C Corrected Impulse Invariance Method Applied on Hankel Filters

To transform

$$h_n(s\Delta t) = -i^n e^{-s\Delta t}\frac{1}{s\Delta t}\Big(\frac{s-\alpha_r}{s}\Big)^{mod(n,2)} \cdot \prod_{l=1}^{div(n,2)} \frac{(s-\alpha_l)^2+\omega_l^2}{s^2} \tag{C.1}$$

by CIIM (cf. [Pom08]), $h_n(s\Delta t)$ can be split up in single poles and first order sections, whose transforms can stated as follows.

Transformation:

Single Pole

$$\begin{aligned} G(s) &= \frac{1}{s} \\ &\updownarrow \mathcal{L}^{-1} \\ g(t) &= u(t) \\ g[n] &= Tu[n] - \frac{T}{2}\delta[n] \\ &\updownarrow \mathcal{Z} \\ G(z) &= \frac{T}{1-z^{-1}} - \frac{T}{2} \\ &= \frac{T}{2}\cdot\frac{1+z^{-1}}{1-z^{-1}} \end{aligned} \tag{C.2}$$

First Order Section

$$\begin{aligned} G_{fos}(s) &= \frac{s-b_r}{s} = 1 - \frac{b_r}{s} \\ &\updownarrow \mathcal{L}^{-1} \\ g_{fos}(t) &= \delta(t) - b_r u(t) \\ g_{fos}[n] &= \delta[n] - Tb_r\Big(u[n] - \frac{1}{2}\delta[n]\Big) \\ g_{fos}[n] &= \Big(1+\frac{1}{2}Tb_r\Big)\delta(t) - Tb_r u(t) \\ &\updownarrow \mathcal{Z} \\ G_{fos}(z) &= 1 + \frac{T}{2}b_r - \frac{Tb_r}{1-z^{-1}} \\ &= \frac{(1+\frac{T}{2}b_r)(1-z^{-1}) - Tb_r}{1-z^{-1}} \\ &= \frac{1+\frac{T}{2}b_r - z^{-1} - \frac{T}{2}b_r z^{-1} - Tb_r}{1-z^{-1}} \end{aligned}$$

$$= \frac{1 - \frac{T}{2}b_r - (1 + \frac{T}{2}b_r)z^{-1}}{1 - z^{-1}} \tag{C.3}$$

This yields:

$$\begin{aligned} h_n(z) =& \mathcal{Z}\{h_n(s\Delta t)\} \\ =& \mathcal{Z}\left\{ \frac{-i^n}{\Delta t} \underbrace{e^{-s\Delta t}}_{\text{time shift}} \underbrace{\left(\frac{1}{s}\right)}_{\text{single pole}} \underbrace{\left(\frac{s-\alpha_r}{s}\right)^{mod(n,2)}}_{\text{first order section}} \cdot \prod_{l=1}^{div(n,2)} \left(\underbrace{\left(\frac{s-\alpha_l}{s}\right)^2}_{\text{first order section}} + \underbrace{\left(\frac{\omega_l}{s}\right)^2}_{\text{single pole}} \right) \right\} \end{aligned} \tag{C.4}$$

$$\begin{aligned} =& \frac{-i^n}{\Delta n} z^{-\Delta n} \Big(\frac{T}{2} \cdot \frac{1+z^{-1}}{1-z^{-1}}\Big) \Big(\frac{1 - \frac{T}{2}\alpha_r - (1+\frac{T}{2}\alpha_r)z^{-1}}{1-z^{-1}}\Big)^{mod(n,2)} \\ & \cdot \prod_{l=1}^{div(n,2)} \left(\Big(\frac{1 - \frac{T}{2}\alpha_l - (1+\frac{T}{2}\alpha_l)z^{-1}}{1-z^{-1}}\Big)^2 + \Big(\omega_l \cdot \frac{T}{2} \cdot \frac{1+z^{-1}}{1-z^{-1}}\Big)^2 \right) \end{aligned}$$

$$\begin{aligned} =& \frac{-i^n}{\Delta n} z^{-\Delta n} \Big(\frac{T}{2} \cdot \frac{1+z^{-1}}{1-z^{-1}}\Big) \Big(\frac{1 - \frac{T}{2}\alpha_r - (1+\frac{T}{2}\alpha_r)z^{-1}}{1-z^{-1}}\Big)^{mod(n,2)} \cdot \\ & \cdot \prod_{l=1}^{div(n,2)} \left(\frac{\frac{T^2}{4}(\omega_l^2 + \alpha_l^2) - T\alpha_l + 1}{(1-z^{-1})^2} + \frac{(\frac{T^2}{2}(\omega^2 + \alpha_l^2) - 2)z^{-1}}{(1-z^{-1})^2} + \frac{(\frac{T^2}{4}(\omega_l^2 + \alpha_l^2) + T\alpha_l + 1)z^{-2}}{(1-z^{-1})^2} \right) \end{aligned} \tag{C.5}$$

$$= - i^n z^{-\Delta n} \frac{T}{2\Delta n} \Big(\frac{b_0 + b_1 z^{-1}}{1 + a_1 z^{-1}}\Big) \Big(\frac{b_{0,r} + b_{1,r} z^{-1}}{1 + a_{1,r} z^{-1}}\Big)^{mod(n,2)} \cdot \prod_{l=1}^{div(n,2)} \left(\frac{b_{0,l} + b_{1,l} z^{-1} + b_{2,l} z^{-2}}{1 + a_{1,l} z^{-1} + a_{2,l} z^{-2}} \right) \tag{C.6}$$

Overview of filter coefficients according to eq. (C.5)

$b_0 = 1$	$b_1 = 1$
$a_1 = -1$	
$b_{0,r} = 1 - \frac{T}{2}\alpha_r$	$b_{1,r} = -(1 + \frac{T}{2}\alpha_r)$
$a_{1,r} = -1$	
$b_{0,l} = \frac{T^2}{4}(\omega_l^2 + \alpha_l^2) - T\alpha_l + 1$	$b_{1,l} = \frac{T^2}{2}(\omega^2 + \alpha_l^2) - 2$
$b_{2,l} = \frac{T^2}{4}(\omega_l^2 + \alpha_l^2) + T\alpha_l + 1$	
$a_{1,l} = -2$	$a_{2,l} = 1$

with α and ω denoting the scaled roots. Generalized versions can be obtained with a multiplication by the delay time Δn, so that $\tilde{\alpha} = \alpha\Delta n$ and $\tilde{\omega} = \omega\Delta n$.

D Spherical Bessel Filter in z-Domain

The derived z-transform $h_n(z)$ (cf. C) can be written as

$$\begin{aligned} h_n(z) =& \frac{-i^n}{\Delta n} z^{-\Delta n} \Big(\frac{T}{2} \cdot \frac{1+z^{-1}}{1-z^{-1}}\Big) \Big(\frac{1-\frac{T}{2}\alpha_r - (1+\frac{T}{2}\alpha_r)z^{-1}}{1-z^{-1}}\Big)^{mod(n,2)} \cdot \\ & \cdot \prod_{l=1}^{div(n,2)} \left(\frac{\frac{T^2}{4}(\omega_l^2+\alpha_l^2) - T\alpha_l + 1}{(1-z^{-1})^2} + \frac{(\frac{T^2}{2}(\omega^2+\alpha_l^2)-2)z^{-1}}{(1-z^{-1})^2} + \frac{(\frac{T^2}{4}(\omega_l^2+\alpha_l^2)+T\alpha_l+1)z^{-2}}{(1-z^{-1})^2} \right). \end{aligned} \tag{D.1}$$

Thus the z-transform $j_n(z)$ can be stated as

$$\begin{aligned} j_n(z) =& \frac{1}{2}(h_n(z) + h_n^*(z)) \\ =& \frac{1}{2}\Bigg[\frac{-i^n}{\Delta n} z^{-\Delta n} \Big(\frac{T}{2} \cdot \frac{1+z^{-1}}{1-z^{-1}}\Big) \Big(\frac{1-\frac{T}{2}\alpha_r - (1+\frac{T}{2}\alpha_r)z^{-1}}{1-z^{-1}}\Big)^{mod(n,2)} \cdot \\ & \cdot \prod_{l=1}^{div(n,2)} \Big(\frac{\frac{T^2}{4}(\omega_l^2+\alpha_l^2) - T\alpha_l + 1}{(1-z^{-1})^2} + \frac{(\frac{T^2}{2}(\omega^2+\alpha_l^2)-2)z^{-1}}{(1-z^{-1})^2} + \frac{(\frac{T^2}{4}(\omega_l^2+\alpha_l^2)+T\alpha_l+1)z^{-2}}{(1-z^{-1})^2} \Big) \\ & + \frac{-i^n(-1)^n}{\Delta n} z^{\Delta n} \Big(\frac{T}{2} \cdot \frac{1+z}{1-z}\Big) \Big(\frac{1-\frac{T}{2}\alpha_r - (1+\frac{T}{2}\alpha_r)z}{1-z}\Big)^{mod(n,2)} \cdot \\ & \cdot \prod_{l=1}^{div(n,2)} \Big(\frac{\frac{T^2}{4}(\omega_l^2+\alpha_l^2) - T\alpha_l + 1}{(1-z)^2} + \frac{(\frac{T^2}{2}(\omega^2+\alpha_l^2)-2)z}{(1-z)^2} + \frac{(\frac{T^2}{4}(\omega_l^2+\alpha_l^2)+T\alpha_l+1)z^2}{(1-z)^2} \Big) \Bigg] \end{aligned}$$

time shifted by $z^{-\Delta n}$

$$\begin{aligned} =& \frac{T}{4\Delta n} - i^n \Big(\frac{1+z^{-1}}{1-z^{-1}}\Big) \Bigg[z^{-2\Delta n} \Big(\frac{1-\frac{T}{2}\alpha_r - (1+\frac{T}{2}\alpha_r)z^{-1}}{1-z^{-1}}\Big)^{mod(n,2)} \\ & \cdot \prod_{l=1}^{div(n,2)} \Big(\frac{\frac{T^2}{4}(\omega_l^2+\alpha_l^2) - T\alpha_l + 1}{(1-z^{-1})^2} + \frac{(\frac{T^2}{2}(\omega^2+\alpha_l^2)-2)z^{-1}}{(1-z^{-1})^2} + \frac{(\frac{T^2}{4}(\omega_l^2+\alpha_l^2)+T\alpha_l+1)z^{-2}}{(1-z^{-1})^2} \Big) \\ & + (-1)^n \Big(\frac{1+\frac{T}{2}\alpha_r - (1-\frac{T}{2}\alpha_r)z^{-1}}{1-z^{-1}}\Big)^{mod(n,2)} \cdot \\ & \cdot \prod_{l=1}^{div(n,2)} \Big(\frac{\frac{T^2}{4}(\omega_l^2+\alpha_l^2) + T\alpha_l + 1}{(1-z^{-1})^2} + \frac{(\frac{T^2}{2}(\omega^2+\alpha_l^2)-2)z^{-1}}{(1-z^{-1})^2} + \frac{(\frac{T^2}{4}(\omega_l^2+\alpha_l^2)-T\alpha_l+1)z^{-2}}{(1-z^{-1})^2} \Big) \Bigg] \end{aligned} \tag{D.2}$$

References

[Baer06] G. Bärwolff, "Höhere Mathematik Mathematik für Naturwissenschaftler und Ingenieure", Spektrum Akademischer Verlag, 2006

[Bar07] H.-J. Bartsch, "Taschenbuch Mathematischer Formeln", Fachbuchverlag Leipzig, 2004

[Cav96] T. J. Cavicchi, "Impulse Invariance and Multiple-Order Poles", IEEE Trans. Signal Processing, Vol. 44, 1996

[Deb10] D. Deboy, "Acoustic Centering and Rotational Tracking in Surrounding Spherical Microphone Arrays", Diploma Thesis, Institute of Electronic Music and Acoustics, University of Music and Performing Arts Graz, 2010

[DZG07] R. Duraiswami and D. N. Zotkin and N. Gumerov, "Fast Evaluation of the Room Transfer Function Using Multipole Expansion", IEEE Trans. on Audio Speech and Language Processing, Vol. 15, No.2, 2007

[Foe07] O. Föllinger, "Laplace-, Fourier- und z-Transformation", Hüthig, 2007

[GD04] N. Gumerov and R. Duraiswami, "Fast Multipole Methods for the Helmhotz Equation in Three Dimensions", Elsevier Science, 2005

[Hoh09] F. Hohl, "Kugelmikrofonarray zur Abstrahlungsmessung von Musikinstrumenten", Master Thesis, Institute of Electronic Music and Acoustics, University of Music and Performing Arts Graz, 2009

[Ker10] M. Kerscher, "Compact Spherical Loudspeaker Array for Variable Sound-Radiation", Master's Thesis, Institute of Electronic Music and Acoustics, University of Music and Performing Arts Graz, 2010

[Men07] D. Menzies and M. Al-Akaidi, "Ambisonic Synthesis of Complex Sources", J. Audio Eng. Soc. October 2007

[MN02] P. Majdak and M. Noisternig, "Implementation kopfbezogener Binauraltechnik", Diploma Thesis, Institute of Electronic Music and Acoustics, University of Music and Performing Arts Graz, 2002

[Nic10] R. Nicol, "Sound Spatialization by Higher Order Ambisonics: Encoding and Decoding a Sound Scene in Practice from a Theoretical Point of View...", Proc. of 2nd Intern. Symp. on Ambisonics and Spherical Acoustics, 2010

[OSB04] A. V. Oppenheimer, R.W. Schafer and J. R. Buck, "Zeitdiskrete Signalverarbeitung", Pearson Studium, 2004

[Ple10] P. Plessas, "Rigid Sphere Microphone Arrays for Spatial Recording and Holography", Master's Thesis, Institute of Electronic Music and Acoustics, University of Music and Performing Arts Graz, 2010

[Pol07] M. Pollow, "Variable directivity of dodecahedron loudspeakers", Master's Thesis, Institute for technical acoustics Aachen, 2007

[Pom08] H. Pomberger, "Angular and Radial Directivity Control for Spherical Loudspeaker Arrays", Diploma Thesis, Institute of Electronic Music and Acoustics, University of Music and Performing Arts Graz, 2008

[PZ09] H. Pomberger and F. Zotter, "An Ambisonics Format for Felxible Playback Layouts", Proc. of Ambisonics Symposium Graz, 2009

[Son03] A. Sontacchi,"Dreidimensionale Schallfeldreproduktion für Lautsprecher- und Kopfhöreranwendungen", PhD Thesis, Graz University of Technology, 2003

[Wil99] E. Williams, "Fourier Acoustics: Sound Radiation and Nearfield Acoustical Holography", Academic Press, 1999

[Zmo00] J. Zmölnig, "Entwurf und Implementierung einer Mehrkanal-Beschallungsanlage", Diploma Thesis, Institute of Electronic Music and Acoustics, University of Music and Performing Arts Graz, 2000

[ZN07] F. Zotter and M. Noisternig, "Near- and Farfield Beamforming Using Spherical Loudspeaker Arrays", 3^{rd} Congress of the Alps Adria Acoustics Association Graz, 2007

[Zot09] F. Zotter, "Analysis and Synthesis of Sound-Radiation with Spherical Arrays", PhD Thesis, Institute of Electronic Music and Acoustics, University of Music and Performing Arts Graz, 2009

[ZP11] F. Zotter and H. Pomberger, "Akustische Holofonie und Holografie", Lecture Note, Institute of Electronic Music and Acoustics, University of Music and Performing Arts Graz, 2011

[ZPF09] F. Zotter and H. Pomberger and M. Frank, "An Alternative Ambisonics Formulation: Modal Source Strength Matching and the Effect of Spatial Aliasing", AES 126^{th} Convention Paper Munich, 2009

[ZPN10] F. Zotter and H. Pomberger and M. Noisternig, "Ambisonic Decoding with and without Mode-Matching: A Case Study Using the Hemisphere", Proc. of 2nd Intern. Symp. on Ambisonics and Spherical Acoustics, 2010

EIDESSTATTLICHE ERKLÄRUNG

Ich erkläre an Eides statt, dass ich die vorliegende Arbeit selbstständig verfasst, andere als die angegebenen Quellen und Hilfsmittel nicht benutzt und die den benutzten Quellen wörtlich und inhaltlich entnommenen Stellen als solche kenntlich gemacht habe.

Datum ..... Unterschrift .....

STATUTORY DECLARATION

I declare that I have authored this thesis independently, that I have not used other than the declared sources / resources, and that I have explicitly marked all material which has been quoted either literally or by content from the used sources.

date ..... signature .....